D.5.7. Test procedure proposals for Euro NCAP

Primary Author(s)	Núria Parera | Applus IDIADA
Related Work Package	WP5
Version/Status	1.0 | Final
Issue date	31/05/23
Deliverable type	R
Dissemination Level	PU

Project Acronym	SAFE-UP
Project Title	proactive SAFEty systems and tools for a constantly UPgrading road environment
Project Website	www.safe-up.eu
Project Coordinator	Núria Parera | Applus IDIADA
Grant Agreement No.	861570

INTERNAL

Co-Authors

Name	Organisation
Jacint Castells	Applus+ IDIADA
Pablo Lozano	Applus+ IDIADA
Simona Roka	Applus+ IDIADA
Christian Löffler	Robert Bosch GmbH
Carina Vogl	CARIAD SE
Johann Stoll	CARIAD SE
Kristin Blum	CARIAD SE
Volker Labenski	AUDI AG
Alessandro Zimmer	THI
Joed Lopes da Silva	THI
Jorge Lorente Mallada	TME
Juan Alamo	TME

Reviewers

Version	Date	Reviewer (Name/Organisation)	Action (Checked/Approved)
0.2	24.05.23	Christian Birkner (THI)	Checked
0.3	26-05-23	Adriano Palao (Euro NCAP)	Checked

Document Distribution

Version	Date	Distributed to
0.3	26-05-23	Coordination Team
1.0	31-05-23	Submission in the EC System
		Approved by the EC

Copyright statement

The work described in this document has been conducted within the SAFE-UP project. This document reflects only the views of the SAFE-UP Consortium. The European Union is not responsible for any use that may be made of the information it contains.

This document and its content are the property of the SAFE-UP Consortium. All rights relevant to this document are determined by the applicable laws. Access to this document does not grant any right or license on the document or its contents. This document or its contents are not to be used or treated in any manner inconsistent with the rights or interests of the SAFE-UP Consortium or the Partners detriment and are not to be disclosed externally without prior written consent from the SAFE-UP Partners.

Each SAFE-UP Partner may use this document in conformity with the SAFE-UP Consortium Grant Agreement provisions.

Executive summary

This report aims to give guidelines on test procedure, requirements and lessons learned obtained from the physical testing and virtual validation done in WP5 and WP4 to the working groups or for testing proposals for Euro NCAP.

In the SAFE-UP project a study of the current status of the accidentology in EU was carried out. The study included accident data, naturalistic data. The results obtained were used to define the baseline for the impact assessment, the baseline for the traffic simulation and the definition of use cases for the demo cases in each work package. The results of this study also were used for training material and e-learning courses. The accidentology activity and its mains results that could be useful input for Euro NCAP are summarized in this report.

The occupant monitoring system (OMS) (Demo 1) offers the potential to improve occupant safety by adapting the restraint system according to the features and conditions of each vehicle occupant. For that, the OMS must be able to provide the restraint system with a set of useful measurements about the occupants: anthropometry classification (body height and mass) position (occupied seat), seated posture, seat belt state, and the activity in which the occupant is currently engaged (e.g., drinking, eating, sleeping, holding an object). An OMS should be able to provide all this information at high-performance rates of accuracy and speed. The methodology, the work done and main results are briefly explained aiming the Euro NCAP interests.

Within the SAFE-UP EU Project, the different research studies that have been performed using HBMs regarding pre-crash low acceleration maneuvers or reclined postures. Based on the deliverable outcomes and generated knowledge, some conclusions and recommendations for Euro NCAP can be drafted. They will be divided into three main topics: pre-crash influence over occupant posture, novel postures and new interiors in frontal collisions, and HBM vs ATD.

From the performed test campaigns and simulations for Demo 2 In-vehicle system for enhanced VRU DETECTION in bad weather conditions, in this report is explained the scenario selection and specification for adverse weather conditions and provides an overview of the main results. It concludes with a summary of the main challenges and guidelines for further work. An overview of scenarios for passenger cars in conflicts with pedestrians and bicyclists is provided. They are derived based on crash data analysis and specified in terms of vehicle speeds by occurrence in accident situations, Euro NCAP test setups and based on Demo 2 results.

The scope of Demo 3 is to develop advanced vehicle dynamics intervention functions to avoid or mitigate critical events. More specifically, the main goal is the development of advanced active safety systems including autonomous emergency steering (AES) as a novelty. Therefore, special focus is given not only in the development of a fully-functional demonstrator, but also in understanding the potential field of effect of such a system, especially in comparison to current state-of-the-art active safety systems. The goal of the following Demo 3 scenario selection process is to identify scenarios that cannot be avoided by state-of-the-art active safety systems and have the theoretical potential to be avoided by

AES. These scenarios are then used to steer Demo 3 development towards a real-world safety benefit by directly addressing accident types that are not yet covered by any active safety system. Two simulation analyses were performed throughout the project with the goal of quantifying a potential AES field of effect in the relevant VRU accident scenarios.

Demo 4 in SAFE-UP project implements communication of V2X messages, in order to enhance the perception of traffic actors about their surroundings, with main objective to detect possible collision situations between vehicles and VRUs and timely present a warning to the user, so that he can react to avoid the accident, or in the case of the vehicle to also trigger an automated function like the vehicle's AEB system. Demo 4 is dealing with three kind of human traffic participants: drivers of vehicles, riders of bicycles (cyclists) and pedestrians. These are the intended recipients of warnings emitted by the "safety application" within each corresponding individual system.

The scenarios selected focused first on crashes with high KSI relevance, in urban areas and related to VRU's, especially non-designated pedestrian crossings and cyclist crossings. Besides this, since the developed system aims not only at providing timely warnings but also at triggering an active safety system (e.g. AEB), scenarios that are aimed by these systems by state-of-the-art technology (SOTA), were considered.

Detailed conclusions and next steps can be found in section 8 of this deliverables.

Table of contents

List of figures

List of tables

List of abbreviations

Abbreviation	Meaning
AV	Autonomous Vehicles
AD	Autonomous Driving
CA	Consortium Agreement
CAV	Connected Automated Vehicles
D	Deliverable
EC	European Commission
GA	Grant Agreement
MaaS	Mobility as a Service
OEM	Original Equipment Manufacturer
PM	Person Month
R&D	Research and Development
SC	Steering Committee
SotA	State-of-the-Art
T	Task
VRU	Vulnerable road user
WP	Work Package

1. Introduction

This report aims to give guidelines on test procedure, requirements and lessons learned obtained from the physical testing and virtual validation done in WP5 and WP4. The main results from each WP of the SAFE-UP project are explained in this report trying to give input to the main topics related to the road map of Euro NCAP and share the challenges and lessons learned from the experienced gained during the project to the working groups with the aim to improve the Euro NCAP testing procedures.

The main topics that will be summarized ins this report are a summary of the accidentology study on the current status in EU that has been done for use cases definition, The occupant monitoring system (OMS) (Demo 1), The HBMs activity : pre-crash influence over occupant posture, novel postures and new interiors in frontal collisions. The performed test campaigns and simulations for Demo 2 In-vehicle system for VRU DETECTION in bad weather conditions The Demo 3 on the development of advanced vehicle dynamics intervention functions to avoid or mitigate critical events. More specifically, the development of advanced active safety systems including autonomous emergency steering (AES) as a novelty by any active safety system.

And lastly, the Demo 4 which implements communication of V2X messages, in order to enhance the perception of traffic actors about their surroundings, with main objective to detect possible collision situations between vehicles and VRUs and timely present a warning to the user, so that he can react to avoid the accident, or in the case of the vehicle to also trigger an automated function like the vehicle's AEB system. Demo 4 is dealing with three kind of human traffic participants: drivers of vehicles, riders of bicycles (cyclists) and pedestrians. These are the intended recipients of warnings emitted by the "safety application" within each corresponding individual system.

2. Accidentology

In the SAFE-UP project a study of the current status of the accidentology in EU was carried out. The study included accident data, naturalistic data. The results obtained were used to define the baseline for the impact assessment, the baseline for the traffic simulation and the definition of use cases for the demo cases in each work package. The results of this study also were used for training material and e-learning courses. This section summarizes the key results of D2.6 [19].

2.1 PC in conflict with VRU

Pedestrians

The data clustering yielded a set of 3 420 pedestrian crash cases of which 1 541 were classified as killed or severely injured (KSI). About 97% of the filtered conflict scenarios were crashes in urban areas; however, 39.5% of all longitudinal cases took place in rural areas.

It is notable that in both conflict scenarios related to pedestrians crossing from the left while PC moves forward, namely, "crossing left without sight obstruction" (15.3% of all cases) and "crossing left with sight obstruction" (12.4%), had a substantially larger share among KSI cases compared to cases of all injury severities (P-CLwoSO: 19.5% of KSI cases, and P-CLwSO: 14.0% of KSI cases). Furthermore, the conflict scenarios with pedestrians crossing from the right, i.e., "crossing right without sight obstruction" (22.8% all / 23.2% KSI) and "crossing right with sight obstruction" (17.2% all / 18.8% KSI) had slightly higher shares in KSI. All the other scenarios had lower shares in KSI cases compared to crash cases overall. Figure 1 shows an overview of results for car-to-pedestrian (C2P) crashes.
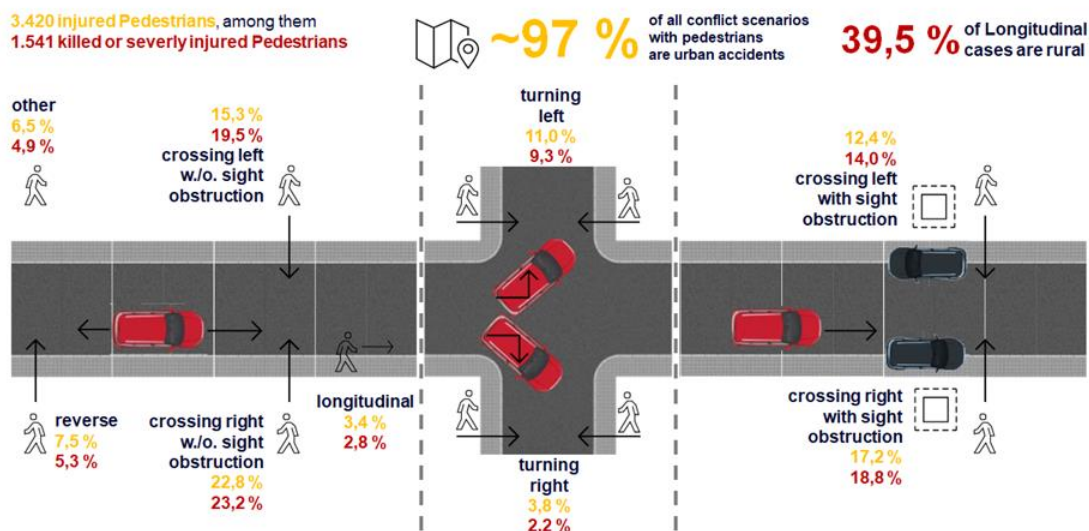
Figure 1: Overview of conflict scenarios for C2P crashes – schematic representation.

Cyclists

The clustered data results in a set of 7 660 cyclists in the 9 scenarios, of which 1 567 got killed or severely injured (KSI). About 98% of the filtered conflict scenarios are crashes in urban areas; however, notably, about 20% of all longitudinal cases take place in rural areas. Approximately 58% of the injured cyclists are involved in crossing crashes. Regarding KSI cyclists, the share increases to approximately 63%. It is notable that both crossing scenarios, i.e., 'crossing left' (22.4% of all cases) and 'crossing right' (35.2%) had a larger percentage when considering only cyclists with the injury severity KSI (25.5% B-CL and 37.8% B-CR). The scenarios 'longitudinal same direction' (5.4% / 6.2% KSI) 'turning left' (9.3% / 10% KSI) had a slightly higher share within the KSI dataset while all the other scenarios have a lower KSI percentage compared to their overall prevalence. Figure 2 shows an overview of results for car-to-bicyclist (C2B) crashes.
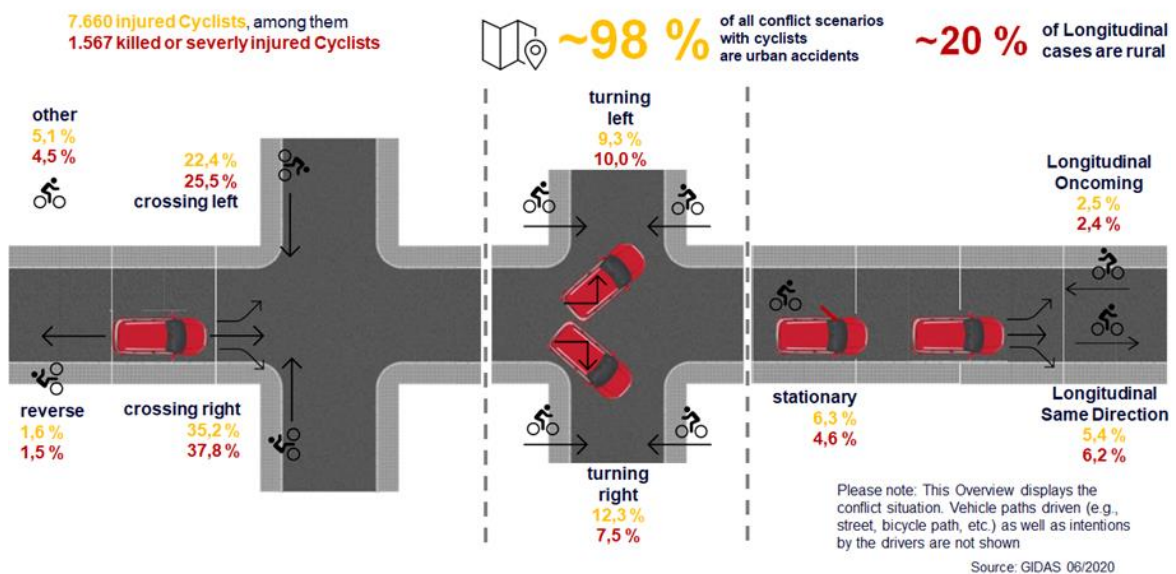
Figure 2: Overview of conflict scenarios for C2B crashes – schematic representation.

2.2 PC in conflicts with HGV

The overall result for head-on situations is summarized in Table 1 to generate input for further simulations based on in-depth data.

Table 1: Distributions of crash configuration parameters for passenger car-to-HGV>3.5t head-on collisions in GIDAS.

Variable	Q25	Q50	Q75
Overlap [%]	Up to 25%	50%	80%
Vc-PC [km/h]	24	39	56
Vc-HGV3.5 [km/h]	27	36	53
Vrel [km/h]	57	72	92
Impact Angle [°]	Up to ±5°	±10°	>10°
Contact/ Hit point [%]	Up to 20%	Up to 40%	80%
Weight PC [t]		1.5	2.5
Weight HGV3.5 [t]		Up to 10t	Up to 18t
Dimensions PC (W/L/H)	Basic car shape		
Dimensions HGV3.5	Basic HGV shape		

For the overview in Table 1, all results are described based on distribution percentiles for every parameter. Three quartiles of the distributions are given, namely Q25, where 25% of the values are below that value, the Q50, where 50% of the values are below that value and 50% are greater and the Q75, where 75% of the values are below that value. The abbreviations Vc and Vrel stand for collision speed and relative speed, respectively. Figure 3 below illustrates the collision configuration based on the values given within the Q50 column in Table 1.
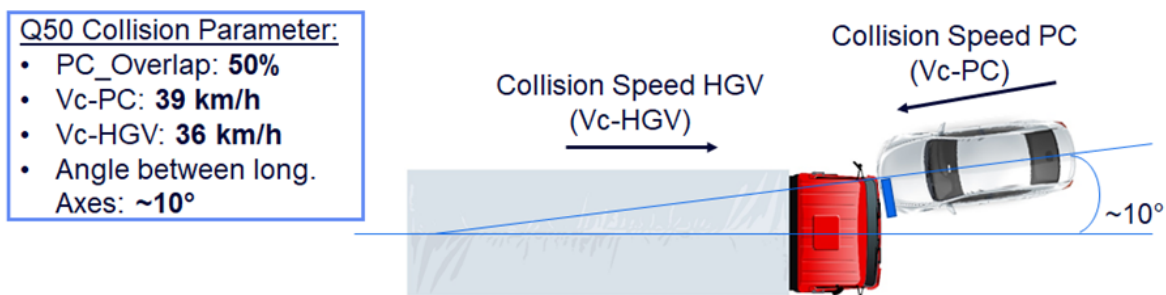
Figure 3: Illustration of Q50 passenger car vs. HGV3.5 head-on crash configuration.

The overall result for rear-end situations is summarized in Table 2 to generate input for further simulations based on in-depth data, in the same way as the results given for head-on collisions

Table 2. Distributions of crash configuration parameters for passenger car vs. HGV3.5 rear-end collisions in GIDAS.

Variable	Q25	Q50	Q75
Overlap [%]	50%	100%	100%
Vc-PC [km/h]	0	0	7
Vc-HGV3.5 [km/h]	18	29	42
Vrel [km/h]	16	25	35
Impact Angle [°]	Up to ±5°	Up to ±5°	Up to ±5°
Contact/ Hit point [%]	50%	50%	75%
Weight PC [t]	-	1.5	2.5
Weight HGV3.5 [t]	-	Up to 10t	Up to 18t
Dimensions PC (W/L/H)	Basic car shape		
Dimensions HGV3.5	Basic HGV shape		

Figure 4 illustrates the collision configuration based of the values given within the Q50 column Table 2 for rear-end collisions.
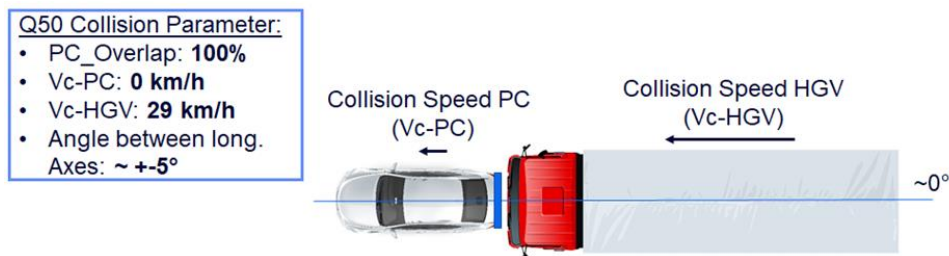
Figure 4. Illustration of Q50 passenger car vs. HGV3.5 rear-end crash configuration.

3. Occupant Monitoring

The occupant monitoring system (OMS) offers the potential to improve occupant safety by adapting the restraint system according to the features and conditions of each vehicle occupant. For that, the OMS must be able to provide the restraint system with a set of useful measurements about the occupants: anthropometry classification (body height and mass) position (occupied seat), seated posture, seat belt state, and the activity in which the occupant is currently engaged (e.g., drinking, eating, sleeping, holding an object). An OMS should be able to provide all this information at high-performance rates of accuracy and speed. In Figure 5 the relation between the OMS and other vehicle components is illustrated.
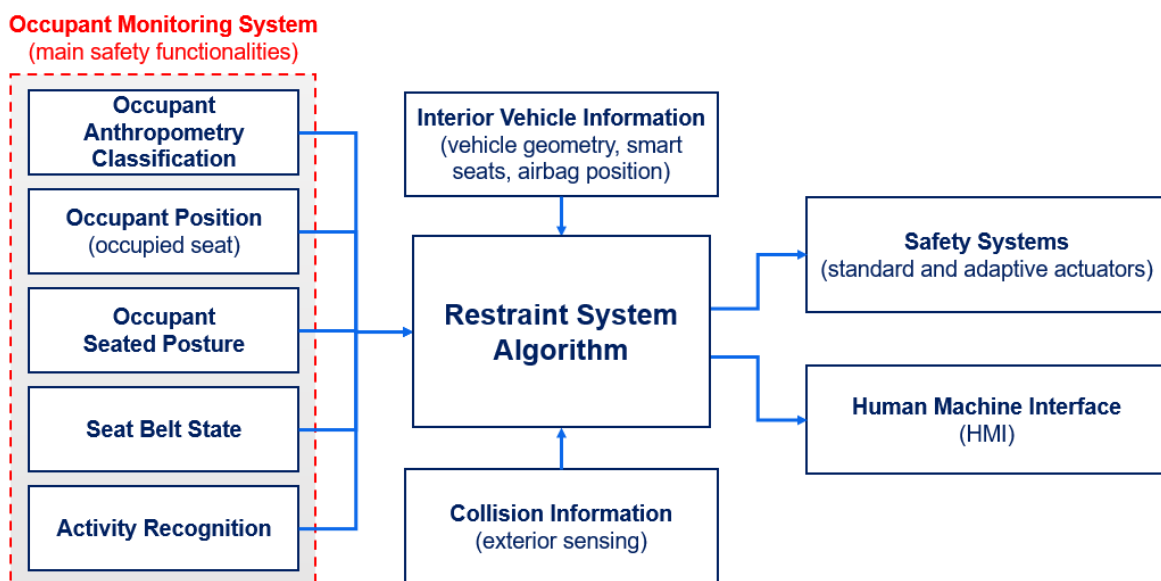
Figure 5: Diagram of Occupant Monitoring System Outputs and relation with other safety components

3.1 Occupant Monitoring System Functionalities

The main functionalities regarding the occupant monitoring system and the occupant safety are described as follows.

3.1.1 Occupant Anthropometry Classification:

An important factor for adapting the restraint system, especially the parameters for airbag deployment, is the occupant's mass and height. The OMS can infer it by using sensors, or this information can be previously provided to the system and retrieved by a person recognition module (e.g., biometrics). In Figure 6 is shown anthropometry distribution between female and male collected in SAFE-UP. One main requirement for developing and testing an OMS platform is to cover the high variability of gender diversity, stature, and mass.

The system must be able to generalize the target population and reduce any bias regarding that as much as possible.
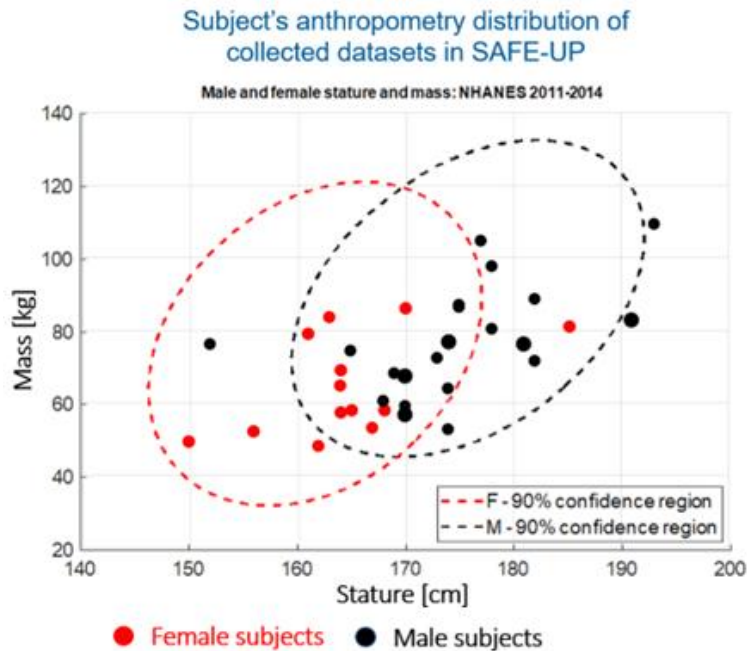
Figure 6: Anthropometry distribution of the collected dataset SAFE-UP with the Male and Female stature and mass of females and males based on the U.S. National Health and Nutrition Examination Survey (NHANES) data from 2011-2014 [100]

3.1.2 Detection of Occupant Seat Position

Restraint systems are developed and positioned according to position and geometry of each passenger seat. Therefore, the OMS should be able to inform each position the occupant is currently sitting. In Figure 7 is depicted the possible seat positions of a passenger vehicle. This information is useful to inform the restraint system, it tells when the airbag must be deployed and when it should not, for example.

Figure 7: Seat Positions for a passenger vehicle

3.1.3 Detection of occupant seated posture

The seated posture is an essential factor to perform the adaptation of the restraint system. If the occupant is too close to the airbag, its deployment should be suppressed. Or, if the occupant is too far from the airbag, the airbag can be deployed in two stages, for example. In Figure 8, different seat postures are depicted. Today, most of the human pose estimation (including the state-of-the-art methods) are based on computer vision, which relies on the use of cameras and deep neural network models.

Figure 8: Different seated postures

In Figure 9 is illustrated the output representation for output for pose estimation, the body key points. The position of each in point in the spatial space (three-dimensional) can be used to compute the distances of body parts (e.g., head and torso) to an airbag or other restraint system to perform the adaptation.

Figure 9: Output representation for pose estimation: body key points (blue circles)

3.1.4 Detection of Seat Configuration

The seat longitudinal displacement and back angle information in addition to the occupant data (classification, position, and posture), can provide useful information about how the occupant is seated and the possible postures. Therefore, it should be used to adapt parameters of the restraint system. In Figure 10 is shown examples of variations for seat configuration.
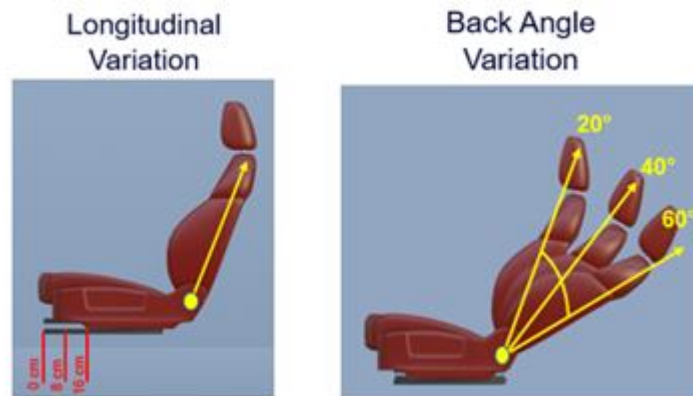
Figure 10: Seat configuration (left) longitudinal displacement and (right) back rest angle

3.1.5 Detection of Seat Belt State

Seat belt is one of the most important safety devices in a vehicle, and the way it is fitted is important. If the seat belt state is not used properly, it can change the body accelerations during a crash, and significantly increase the injuries. For the adaptation, the information of seat belt state can be used to improve safety.

3.1.6 Activity Recognition

In highly automated vehicles the occupants can engage in another tasks than driving, for example, sleeping, using a notebook, reading, etc. Depending on the task, for instance, handling an object (glass bottle of water) between the airbag and the hand can lead to dangerous injures. Therefore, this information could be useful for the adaptation. In Figure 11, some activities are presented.

Figure 11: Samples of activities: drinking and cell phone talking

3.2 Data collection baseline

To cover all scenarios, conditions, and reduce bias as much as possible, in SAFE-UP Task 4.4 [101], a baseline for data collection was designed and carried out. It includes a set of anthropometry groups, seat configurations, sequences of body movements, activities, and variations.

3.2.1 Anthropometry groups

The defined anthropometry groups for female and male subjects are presented in Table 1 and Table 4, respectively. The range values for mass and height were defined with basis on the target population (for Europe), and according to the adaptation parameters proposed in SAFE-UP Task 4.2 [102] of and algorithm developed in Task 4.4 of SAFE-UP [101].

Table 3: Anthropometry Groups for Female Subjects

Group	Mass Range [kg]	Height Range [meters]
Type 1	40 - 60	1.50 - 1.55
Type 2	60 - 100	1.5 - 1.55
Type 3	55 - 80	1.55 - 1.80
Type 4	80 - 100	1.55 - 1.80

Table 4: Anthropometry Groups for Male Subjects

Group	Mass Range [kg]	Height Range [meters]
Type 1	55 - 70	1.60 - 1.70
Type 2	60 - 90	1.70 - 1.85
Type 3	90 - 110	1.70 - 1.95

3.2.2 Seat configuration and sequence of body movement

To test and develop human posture estimation algorithm, which is a core function for the OMS, a set of samples of occupants performing different body movements and seated in different positions is required. Figure 12 illustrates the seat variations (longitudinal variation and the backrest angle) and the sequence of body movements to be performed. Depending on the body posture and field of view of sensors, some body parts may be partially or fully occluded, thus the necessity of performing these set of body movements to evaluate and create strategies for these conditions.
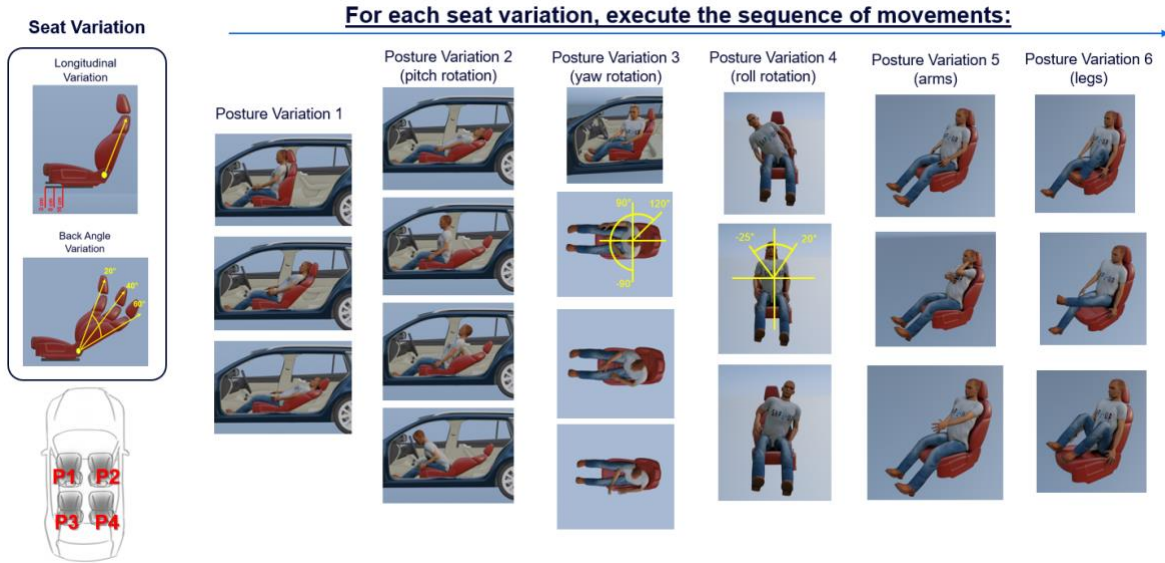
Figure 12: Seat variations and sequences of body movements

3.2.3 Activities

A set of activities that generates partial and full occlusion of body were proposed: (1) Smartphone texting, (2) smartphone talking, (3) newspaper writing, (4) using notebook, (5) drinking, and (6) eating.

3.2.4 Seat belt state

For testing the seat belt state detection, a set of test cases safe (properly belted) and dangerous (incorrectly belted) are proposed, some samples are shown in Figure 13.

| Properly belted | Shoulder belt under the shoulder | Shoulder belt behind the back | Shoulder belt wrong side of the head |

Figure 13: Samples of the seat belt state

3.2.5 Variations

In addition to the previously presented test cases, some variations on the conditions of the data collection can also be performed:

- **Garments:** when the occupants are wearing accessories (e.g., earrings, pendants, hats) or clothes (e.g., winter jackets, scarfs) that significantly changes the body silhouette, the captured data and detection system may be prone to failure. Therefore, additional data collection can be carried out to verify the system performance regarding it.

- **Ambient illumination:** for image-based sensors, the ambient illumination can be an issue. For example, if it is too dark or there is a dynamic light variation (tunnels), depending on the sensor technology it may lead to failures on the detection system.

3.2.6 Evaluation methodology

This two-step evaluation methodology is effective because the advantages and drawbacks of the system platform can be analysed in detail, and improvements and strategies can be made based on it. For example, in the cases of occlusion by objects (newspaper – Table 6) or self-occlusions by posture (yaw body rotation – Table 7), the system is not able to fully detect the occupant keypoints (especially the head), and the results are reflected on the analysis. The first step of the evaluation is a Global Analysis, where the system is evaluated completely for all testing database and all functions. It helps in the comparison between different platforms, for example, the use and combination of different detection algorithms (e.g., human pose estimation), sensor technologies (e.g., camera types), and placement of sensors, and vehicle interior and models.

Table 5: Detection Rate by Seat Configuration

Occupant Seat	Seat Longitudinal Position	Seat Back Angle	Occupant Detection Rate [%]
Front Row Left (Driver)	00cm	20deg	92.03
		40deg	97.29
		60deg	93.29
	08cm	20deg	95.58
		40deg	92.01
		60deg	88.96
	16cm	20deg	94.63
		40deg	93.10
		60deg	88.34
Front Row Right (Passenger)	00cm	20deg	87.13
		40deg	93.50
		60deg	88.39
	08cm	20deg	93.79
		40deg	93.09
		60deg	85.33
	16cm	20deg	95.77
		40deg	94.99
		60deg	84.22

Table 6: Detection rate according to the activities

Activity		Detection Rate [%]
Smartphone Texting		92.16
Smartphone Talking		97.49
Newspaper		83.45
Notebook		97.13
Drinking		96.54
Eating		99.72

Table 7: Detection rate according to the postures

Posture	Detection Rate [%]
Static along the seat	98.59
Pitch Movement	90.23
Yaw Rotation	86.04
Yaw Full Body	90.33
Roll Rotation	96.71
Arms	92.64
Legs (dashboard-crossed)	97.2

4. Human Body models

In recent years, the use of Human Body Models (HBMs) has become increasingly important in the field of crash safety research, especially when it comes to studying pre-crash scenarios or novel seating postures, fields of research for which ATDs are not designed. With the help of advanced computer-aided design software and biomechanical data, researchers are able to create virtual representations of the human body that accurately simulate the way the body responds to different types of impacts or low acceleration maneuvers.

This has allowed researchers to study the effects of different reclined postures on the human body during a crash, and to develop new safety measures that can reduce the risk of injury or death in such scenarios. By using these models, researchers are able to predict the impact of reclined postures on the spine, head, or neck, and to design safer seatbelt systems and other safety features that can protect passengers in the event of a crash.

Overall, human body models have revolutionized the way we approach crash safety research, providing researchers with powerful tools that enable them to better understand the complex biomechanics of the human body, and to develop safer vehicles and safety features that can save lives.

Within the SAFE-UP EU Project, the Deliverable 4.4 shows the different research studies that have been performed using HBMs regarding pre-crash low acceleration maneuvers or reclined postures. Based on the deliverable outcomes and generated knowledge, some conclusions and recommendations for Euro NCAP can be drafted. They will be divided into three main topics: pre-crash influence over occupant posture, novel postures and new interiors in frontal collisions, and HBM vs ATD.

4.1 HBM vs ATD

Future traffic scenarios, in 5 to 10 years, will most likely include mixed traffic (vehicle fleets composed of both traditional vehicles and vehicles with a high level of automation) or automated ones. Based on this information, Level 3 [1] vehicles are considered in the study. Level 3 vehicles represent "conditional automation" meaning that a human driver will respond appropriately to a request if needed. This level of automation allows the driver to be seated in a more relaxed, reclined position.

A current state-of-the-art frontal restraint system, i.e., a 3-point seat belt with B-pillar mounted belt guide, driver airbag in the steering wheel and knee bolster in the instrument panel, has limited protection functionality in the new proposed seating positions in which seatback angles are further from nowadays regulations' seatback angles. In particular, a reclined occupant posture may increase the risk of submarining [2] [3] [4], which is where the lap belt translates over the anterior superior iliac spines (ASIS) to load the abdomen directly and can result in injuries to the lumbar spine and hollow organs of the lower digestive system.

To assess in detail the injuries that may result from a crash, the injury output from a HBM or ATD is needed. The injury criteria output from an ATD is generally limited to specific scenarios (one specific ATD for one specific type of crash test) and limited by the mechanical elements that form the surrogate. Therefore, some of the measurements that can be done with these ATDs, like the chest displacement, are limited to four specific measurement points in the case of the THOR dummy (Upper Left, Upper Right, Lower Left, and Lower Right) or even one single measurement point for the Hybrid III dummy. HBMs, however, can measure the strain of every point of the rib cage, measuring all the circumference of the body and estimating the probability of 2, 3, 4, or 5 rib fractures depending on the age of the occupant. They can even be used to calculate if the structural integrity of the rib cage is in danger. Nevertheless, it is important to understand the variation of the outputs of both technologies, HBMs and ATD.

In the literature, most of the virtual reclined posture analysis has been performed using Human Body Models (HBMs) which are increasingly used to assess vehicle safety and injury risk, as currently regulated ATDs (Anthropomorphic Test Devices) are neither designed nor validated for reclined seating configurations. Nevertheless, these HBM simulation studies need to be correlated against repeatable physical tests that allow future cars to be rated according to regulation and consumer testing protocols. New options for crash dummies such as the THOR-Reclined kit from CELLBOND; which allows adapting the THOR ATD for these new reclined seating postures, are being developed and may enable the performance of physical tests in reclined occupant positions. However, the question of whether its performance is comparable to that of an HBM remains unanswered. The purpose of this study was to compare the outputs of a HBM and an ATD.

4.2 METHODOLOGY

Two simulation models (one HBM -THUMS- and one ATD -THOR-Reclined-) were compared by means of kinematics, injury criteria, and injury risk prediction in a generic frontal simulation environment [5] with a semi-rigid seat[1] during a frontal crash simulation. This semi-rigid seat was proposed by Uriot et al. [6] in 2015 and consists of two plates attached to a set of strings that can be changed to adjust the stiffness of the seat. The plate in the front recreates the anti-submarining foam of a standard seat and the second plate recreates the seat pan. This allows recreating a foam seat in a repeatable way while being a simple seat to model for simulation. The simulation model used in this study is shown in Figure 14.
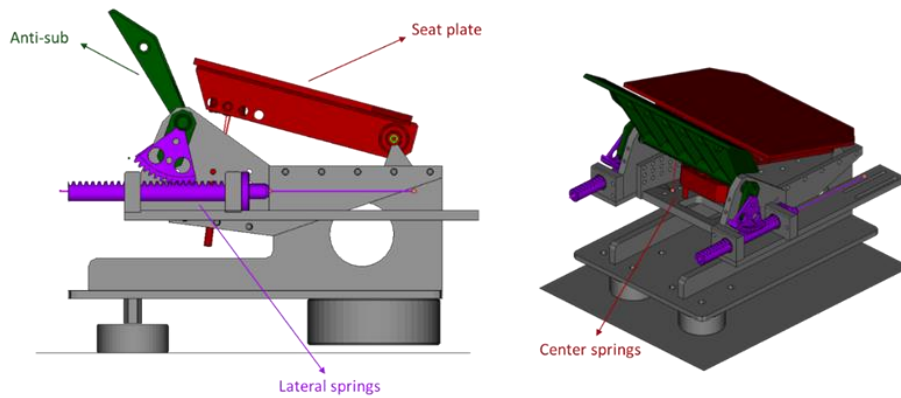
Figure 14 LAB CEESAR Semi-Rigid seat simulation model in the frontal configuration

Two impact simulations were performed using LS-DYNA MPP R9.3.1 (ANSYS/LST, Livermore, CA, USA) as solver and the Total HUman Model for Safety (THUMS, version 4.1) AM50 Occupant model (Toyota Motor Corporation, Japan) and the ATD-TH50R-D00.17_R00.06 model (ATD-MODELS GmbH, Weißwasser, Germany) as surrogates for the study. These two models are presented in Figure 15.
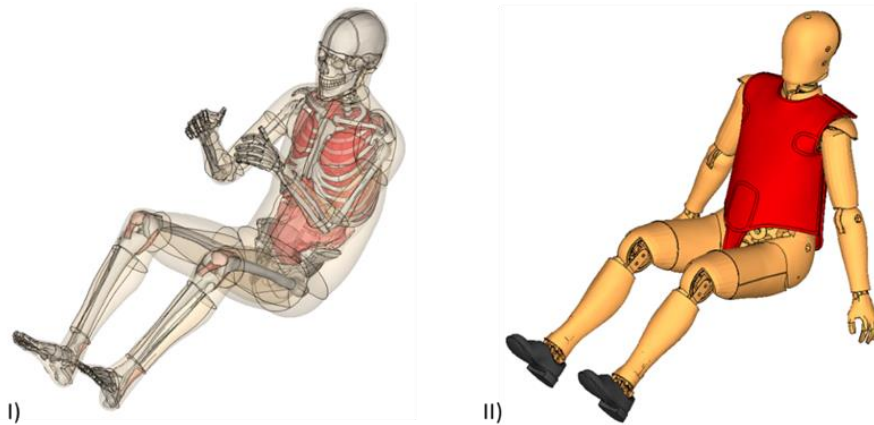
Figure 15: THUMS (Left, I) and THOR-Reclined (Right, II) simulation models in their original postures

4.3 Simulation Environment

The simulation environment used for this study is an adaptation of the generic frontal simulation environment used in the SAFE-UP project [5] (Figure 16). This environment consisted of a generic floor geometry and foot support, a semi-rigid seat, a generic seatback, a generic knee bolster, a State-Of-The-Art (SOTA) belt system installed in the seat, a simplified retractor with pre-tensioning and load limiting capabilities, a buckle with a crash locking tongue, an end bracket with pre-tensioner, a simplified belt webbing (defined using *MAT_SEATBELT card from LS-DYNA), a generic steering column (SC) with a production steering wheel, and a generic driver airbag (DAB). This generic environment model was validated by Autoliv.
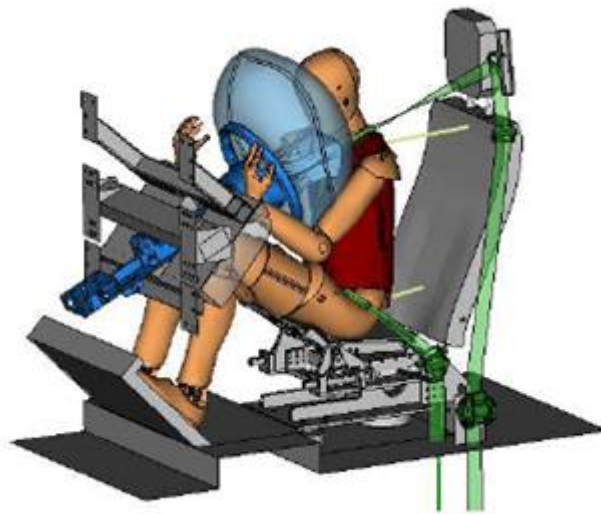
Figure 16: SAFE-UP Generic environment simulation model [5]

Some modifications were made to adapt the proposed environment to the IDIADA's sled testing facilities and to be able to reproduce it physically. The semi-rigid seat was used in the frontal configuration proposed by Richardson in 2020 [3] using 128N/mm seat pan lateral springs, a 379N/mm seat pan center spring, and 132 N/mm anti-submarining springs.

The seatback was simplified for easier construction as a physical part. The adapted model consisted of a rigid steel plate with foam on top to protect the dummy on the rebound phase for future sled tests. This foam was modeled as Ethafoam 220 and had no specific function during the crash phase. The dynamic model of this foam was provided by Autoliv for the SAFE-UP project. The seatback was positioned at a 45-degree angle according to the SAE standard [7] [8].

Regarding the footrest, an expanded polypropylene (EPP) foam with a density of 30g/l was used to reduce tibia loads and stabilize the contacts between the surrogates and the floor. The material characterization was done internally in IDIADA.

The geometry of the knee bolster was maintained from the original model. However, the foam material was changed to an EPP of 60g/l to recreate a stiffer dashboard that can apply higher loads to the occupant's femurs.

The belt system elements were adapted to the new seatback configuration. The D-ring was positioned close to the seatback, simulating a belt-in-seat mount. The retractor was positioned right below the D-ring to emulate a physical testing routing. The firing parameters of the belt remained the same as in the original model. The 3-point belt system consisted of a shoulder belt retractor with two load limiters (3.5 kN and 10 kN) and 2 kN pre-tensioners, a 2 kN lap belt pre-tensioners, and a crash locking tongue.

The steering column and the belt system remained unchanged from the original model. The collapsible column had a force level of 4.5kN with 100mm of maximum stroke. The updated environment model is presented in Figure 17.
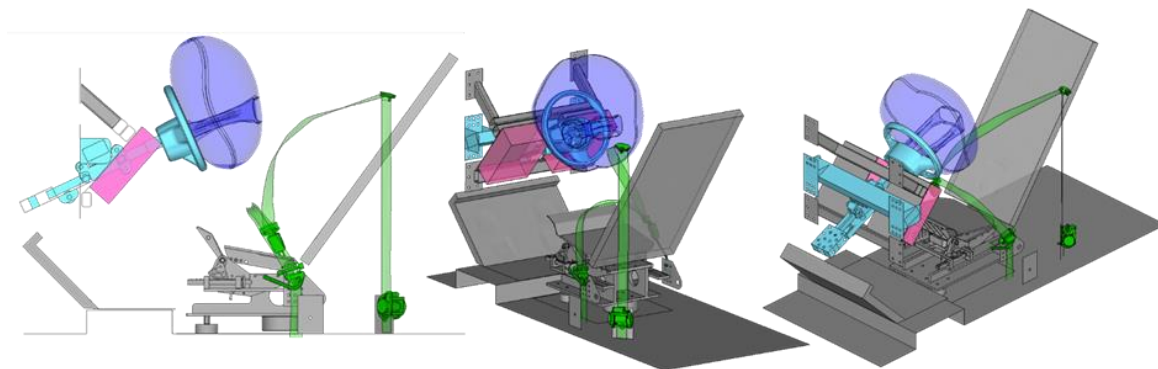
Figure 17: Adapted generic frontal model used in the study. In grey: the semi-rigid seat, seatback, foot support, and structures. In light blue: collapsible steering column and steering wheel. In dark blue: driver airbag. In pink: knee bolster. In green: seatbelt system.

4.4 Occupant Positioning and Belt Routing

The study used the THUMS model as the main finite element HBM. This model represents a 50th-percentile male with a stature of 178.6 cm and a weight of 78.5 kg and was used as the baseline model. THUMS was positioned via a (pre)simulation and the THOR-Reclined ATD was positioned based on the achieved posture of the FE HBM. The two models were positioned in a reduced environment with just the semi-rigid seat plates (which were considered rigid), the seatback, and the foot support.

First, the final posture was estimated based on the UMTRI 2018 study [9]. The anatomical landmarks (ankle joint, knee joint, acetabulum joint, L5/S1 joint, T12/L1 joint, C7/T1, Head/C1 joint, head and center of the eye) were calculated using the complete regression model including the anthropometric predictors using Python v3.10.6 (Python Software Foundation, Beaverton, USA). The values used for the posture estimation and the obtained landmarks are shown in Figure 18.

Variable	Value
Stature (mm)	1786
Weight (kg)	78,5
Erect sitting heihgt (mm)	893
Seatback angle (deg)	45
Presence of headrest (-)	0

I)

Letter	Anatomical landmark
A	Center of eye
B	Head/C1
C	C7/T1
D	T12/L1
E	L5/S1
F	Acetabulum joint
G	Knee
H	Ankle

II)
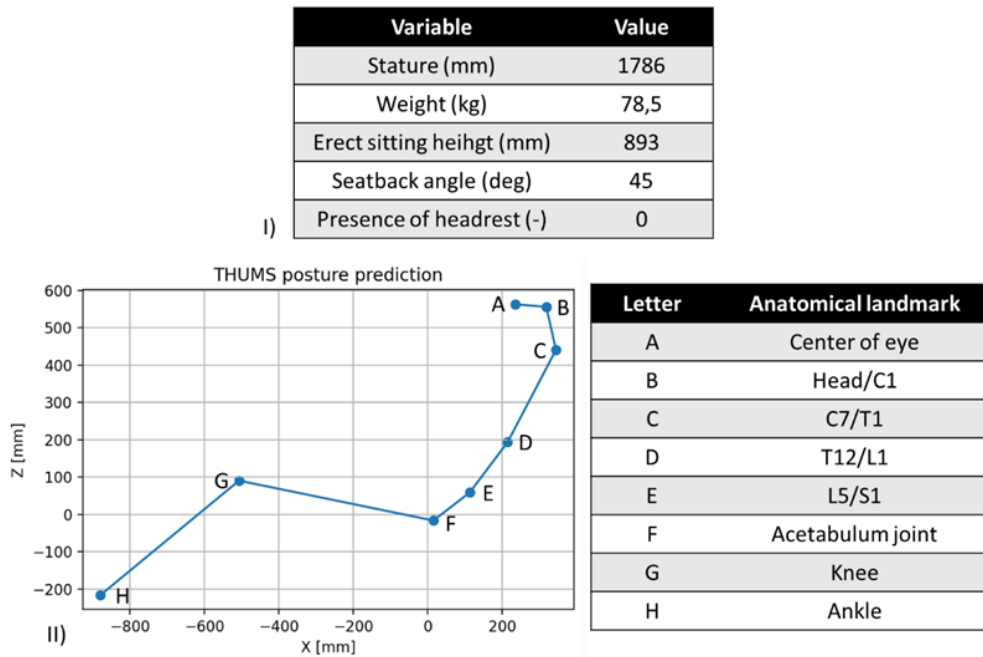
Figure 18: I) Variable values used for the posture estimation, and II) coordinates of the anatomical landmarks obtained if the seat H-point was placed in the (0,0)

To position the occupant model, a (pre)simulation was run using the marionette method [10]. The previously mentioned anatomical landmarks were used as targets to achieve the desired pre-impact posture. The knee and ankle landmarks were modified so the leg's posture fitted the simulation model used for this study. Regarding the arms, they were placed in line with the torso and the hands were placed in contact with the seat to obtain an achievable posture for the THOR-Reclined dummy model. The THUMS nodes used for this (pre)simulation are shown in the following Table.

Table 8. Node IDs used for each anatomical landmark

Anatomical Landmarks	NODE ID	Anatomical Landmarks	NODE ID
Left Ankle	82002574	C7/T1 joint	89000708
Right Ankle	81002574	Left Shoulder	86007088
Left Knee	82074216	Right Shoulder	85007088
Right Knee	81074216	Left Elbow	86006275
Left Acetabulum	83001318	Right Elbow	85006275
Right Acetabulum	83501318	Left Wrist	86003794
L5/S1 joint	89066294	Right Wrist	85003794
T12/L1 joint	89065464	Head/C1 joint	87000782

The positioning was performed based on the work presented by Alexandros Leledakis et al. [11]. A two-step (pre)simulation was used to position the model. The first stage had a duration of 450 ms. During the first phase, one-dimensional elements were used, applying a force from 0 to 500 N to position the model. Simultaneously, the geometrical constraints of the generic environment that had contact with the HBM were moved to their original position. These surfaces (the anti-submarining plate and seat plate of the semi-rigid seat, the footrest, and the seatback) were originally moved 150 mm away from their original position in X and Z directions. The second stage had a duration of 300 ms. In this phase, the one-dimensional elements force was set to 0 and the model was allowed to reach equilibrium. Gravity was activated throughout the complete simulation and a global damping of 0.15 was used. This process is illustrated in Figure 19.
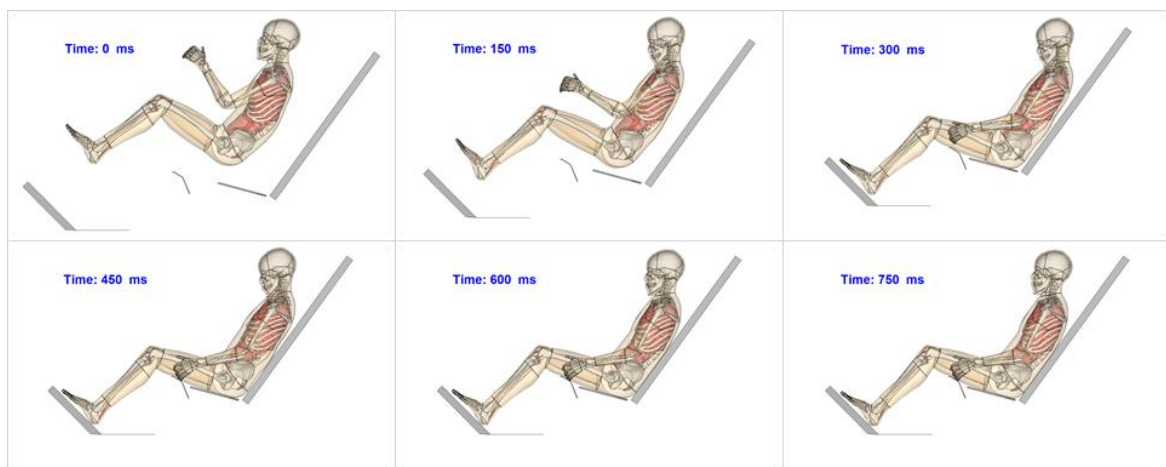
Figure 19: HBM positioning (pre)simulation. The environment elements (in grey) start 150 mm away from their original position and are repositioned during the first stage of the simulation. The last 300 ms are used to reach equilibrium in the model.

The position of the nodes of the HBM, the footrest foam, and the seatback foam were retained for the impact simulation. Foam and internal HBM stresses were not retained.

The same procedure was applied to the THOR-Reclined dummy model. In this case, the reference was the achieved posture of the HBM, so the dummy was positioned as close as possible to the THUMS. Due to the differences between both models, priority was given to the similar positioning of the internal structure of the dummy and the HBM skeleton, starting from the iliac spines. The dummy was (pre)simulated using the same simulation process of the HBM as can be seen in Figure 20.
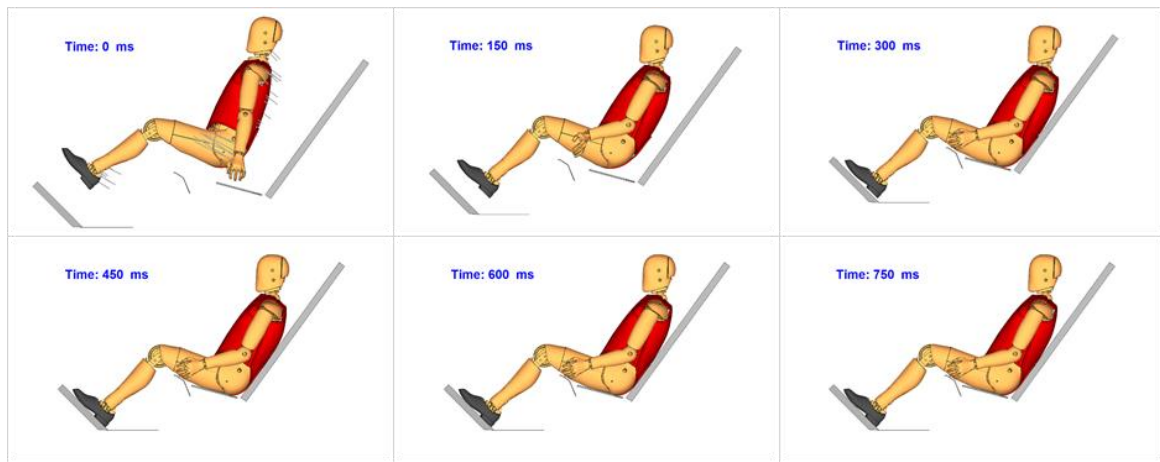
Figure 20: ATD positioning (pre)simulation. The environment elements (in grey) start 150 mm away from their original position and are repositioned during the first stage of the simulation. The last 300 ms are used to reach equilibrium in the model.

Following this method, a comparable posture of the ATD was obtained. A comparison between the posture achieved with each model is shown in Figure 21.
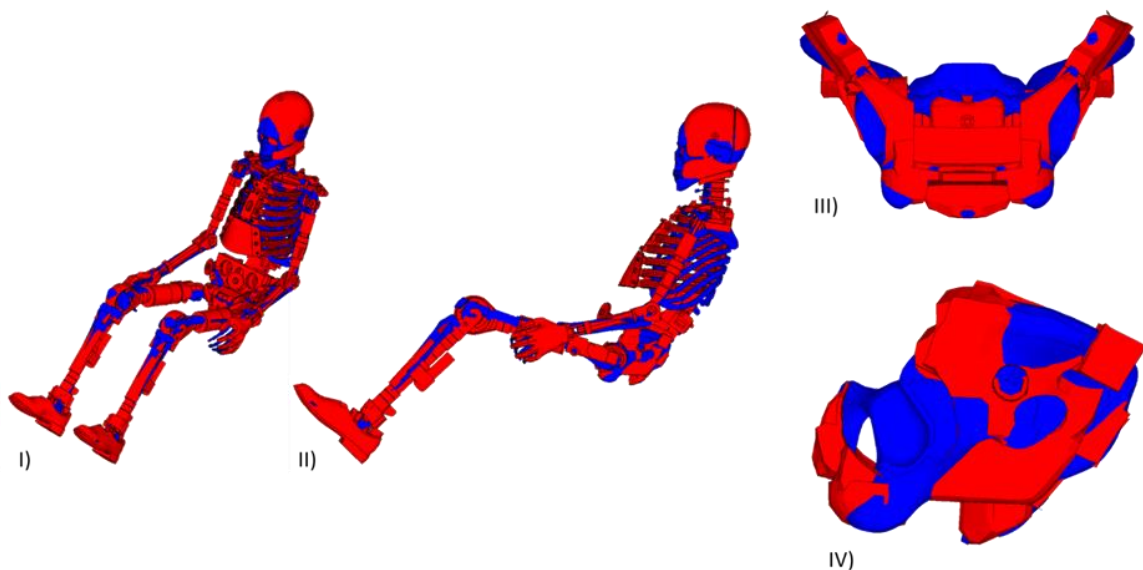
Figure 21. Comparison of the achieved postures of the HBM (blue) and the ATD (red). I) Isometric perspective. II) Lateral view. III) Frontal view of the pelvis of both models. IV) Lateral view of the pelvis of both models.

Regarding the belt routing, in both cases the shoulder belt was positioned following a straight line between the D-ring and the belt tongue, using the shortest path possible that allowed the belt to pass through the middle part of the collarbone of each model. The lap belt was positioned following a straight line between the buckle and the end bracket of the belt, placing the webbing in the lowest part of the abdomen possible for each model (Figure 22). No initial pretension was given to the belt.
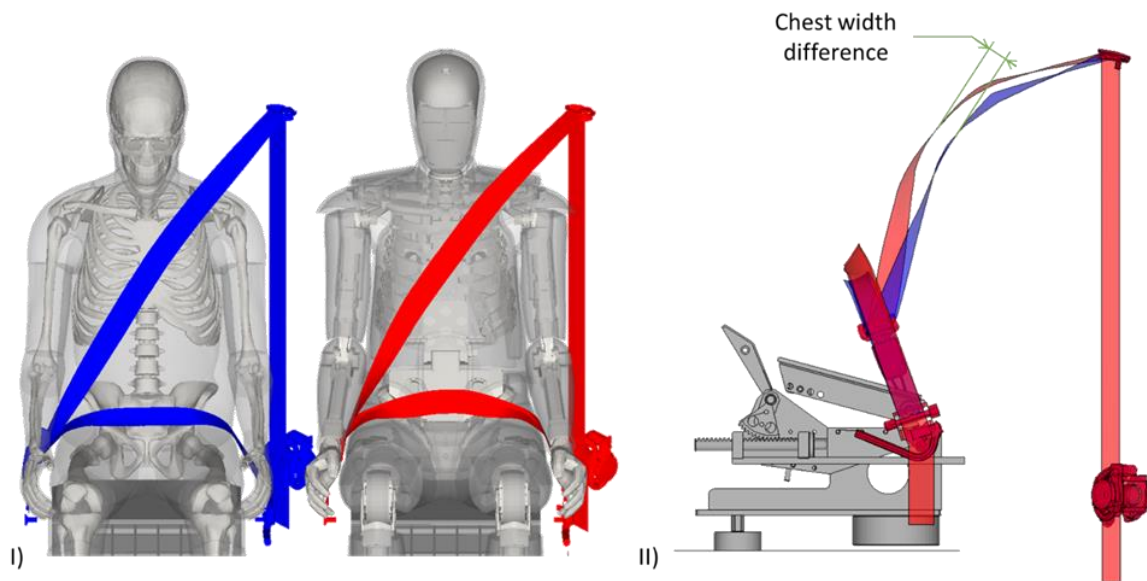
Figure 22: Belt fit comparison of both models. The THUMS belt is presented in blue and the THOR-Reclined belt is presented in red. I) Side-by-side comparison of belt fit over each surrogate. II) Lateral view of the belt and the semi-rigid seat. A gap between both belt models can be observed due to the difference in the chest width of both models.

4.5 Crash configuration

The full frontal 56km/h Car-to-Car (C2C) crash pulse from EU project OSCCAR [12] was used for this analysis. The characteristics of this pulse are presented in Figure 23. The pulse was chosen due to its high severity, as this would highlight the similarities and differences that may exist between the HBM and the ATD.
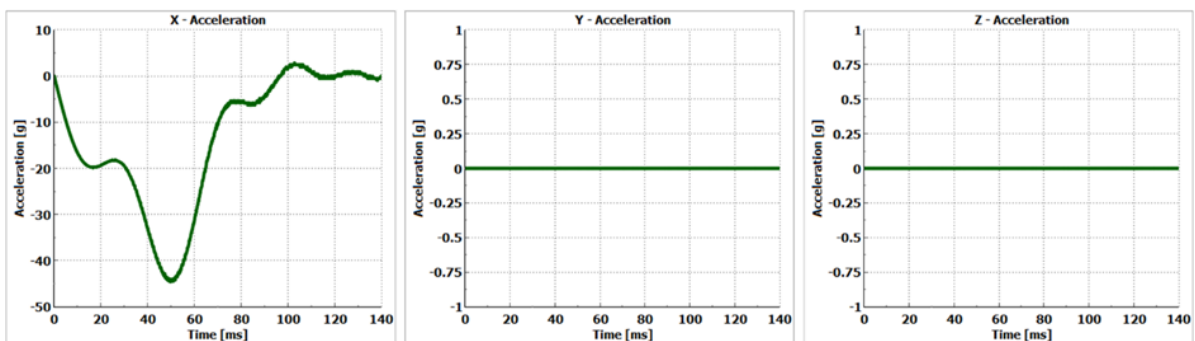
Figure 23: Full frontal 56 km/h C2C crash pulse from EU project OSCCAR

4.6 Analysis methods

Both simulation models were compared using surrogate kinematics, restraint system outputs, injury risk prediction, and visual inspection.

Regarding kinematics, the head centre of gravity (CG), T1, T4, T12, and pelvis Anterior Superior Iliac Spine (ASIS) kinematics were compared between both models.

Seat belt forces, webbing pay-outs at the retractor, belt tongue slip, webbing pay-ins at the end bracket pre-tensioner, DAB pressures and volume changes, steering column strokes and forces, and rotations of anti-submarining and seat pan plates were chosen as the main restraint system outputs to use for the comparison.

To evaluate the injury risk, outputs were defined for the HBM following the recommendations of the OSCCAR deliverable D3.3 [13]. Regarding the ATD, the standard outputs were used for the analysis, and injury risk criteria was evaluated based on [14]. For the head, HIC and BrIC injury risks were evaluated according to [14]. DAMAGE was as well evaluated based on [15]. Regarding the neck, cross sections were defined in the cervical vertebrae of the HBM (C1-C7) to analyse axial loading through cortical and spongy bones, left and right transverse processes, spinous process, and the ligaments connected to the respective vertebrae according to [13]. The maximum values of forces from all the vertebrae were then compared with the maximum loads measured by the load cells of the upper and lower sections of the neck of the ATD. Regarding the thorax, rib fracture risk was assessed according to [13] [16] for the HBM using cortical bone maximum principal strain. This risk of rib fracture was then compared to the peak resultant chest deflection injury criterion for the ATD [14]. The anterior superior iliac spine (ASIS) peak force was also measured in the HBM by cross sections through cortical and spongy bone to assess iliac wing fracture risk. This load was then compared to the one measured in the THOR-Reclined ASIS load cells. The leg injury was assessed by femur force measurement. A comparison between the recorded values of the ATD's load cells and the HBM cross sections was made.

Submarining and overall behaviour of both models in the generic frontal environment simulation model were assessed based on visual inspection.

5. Demo 2 In-vehicle system for VRU DETECTION in bad weather conditions

This section details the scenario selection and specification for adverse weather conditions and provides an overview of the main results from the performed test campaigns and simulations for Demo 2 In-vehicle system for VRU DETECTION in bad weather conditions. It concludes with a summary of the main challenges and guidelines for further work.

5.1 Scenario selection and specification

This chapter provides an overview of scenarios for passenger cars in conflicts with pedestrians and bicyclists. They are derived based on crash data analysis and specified in terms of vehicle speeds by occurrence in accident situations, Euro NCAP test setups and based on Demo 2 results.

5.1.1 VRU accident analysis

With the focus on adverse weather conditions (AWC) the following results of the crash data analysis are summarized here:

5.1.1.1 Pedestrian crossing left without sight obstruction (P-CLwoSO)
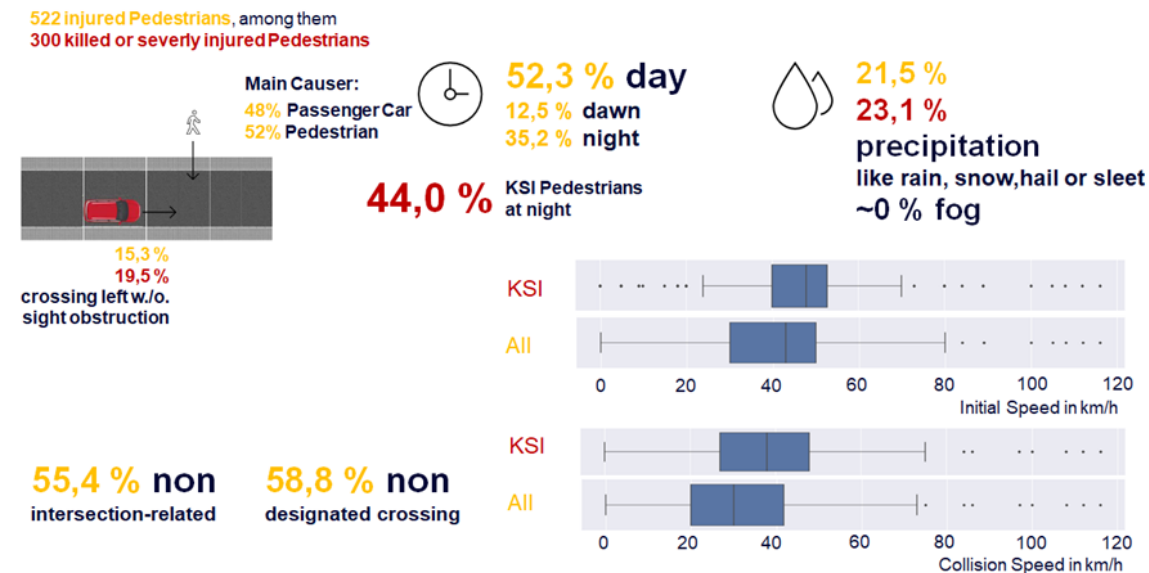
Figure 24. Results summary for C2P conflict scenario 1: P-CLwoSO.

In 21.5% of all cases and in 23.1% of KSI cases, precipitation is present. Precipitation aggregates the following weather conditions: rain, snow, hail and sleet. Close to 0% of the crashes foggy conditions had been recorded.

5.1.1.2 Pedestrian - Passenger car turning left (P-PCTurnL)

In 25.3% of all cases and in 23.2% of KSI cases, precipitation is present. Precipitation aggregates the following weather conditions: rain, snow, hail and sleet.
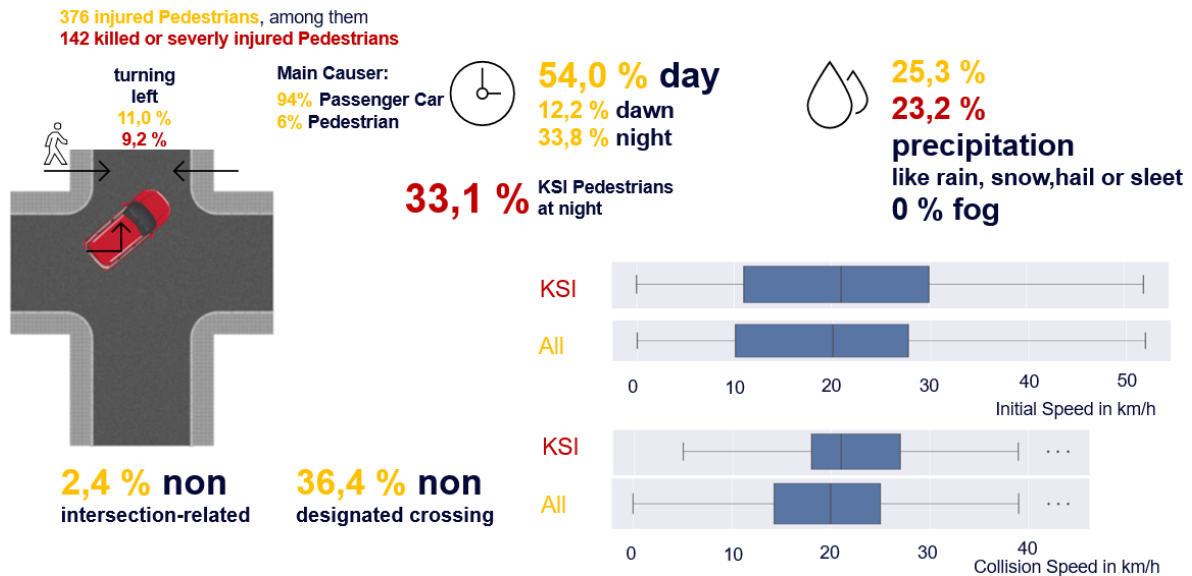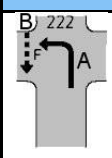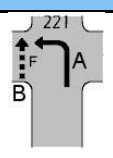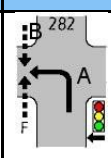
Figure 25. Results summary for C2P conflict scenario 7: P-PCTurnL.

The following table divides the P-PCTurnL scenario by the walking direction of the pedestrian: Same direction as the turning passenger car (UTYP 221) or the opposite direction of the turning passenger car (UTYP 222) and gives an overview of the share of crashes where precipitation was present.

Table 9. Classification by crash type within P-PCTurnL.

	UTYP 222	UTYP 221	UTYP 282
Pictogram			
All injury severities	53.7%	43.6%	1.1%
All injury severities % with precipitation	17,7%	34,1%	Low sample size
KSI	50.0%	45.1%	2.8%
KSI % with precipitation	13,9%	32,8%	Low sample size

5.1.1.3 Cyclist crossing from right (B-CrR)

In 7.2% of all cases and in 7.7% of KSI cases, precipitation is present. Precipitation aggregates the following weather conditions: rain, snow, hail and sleet.
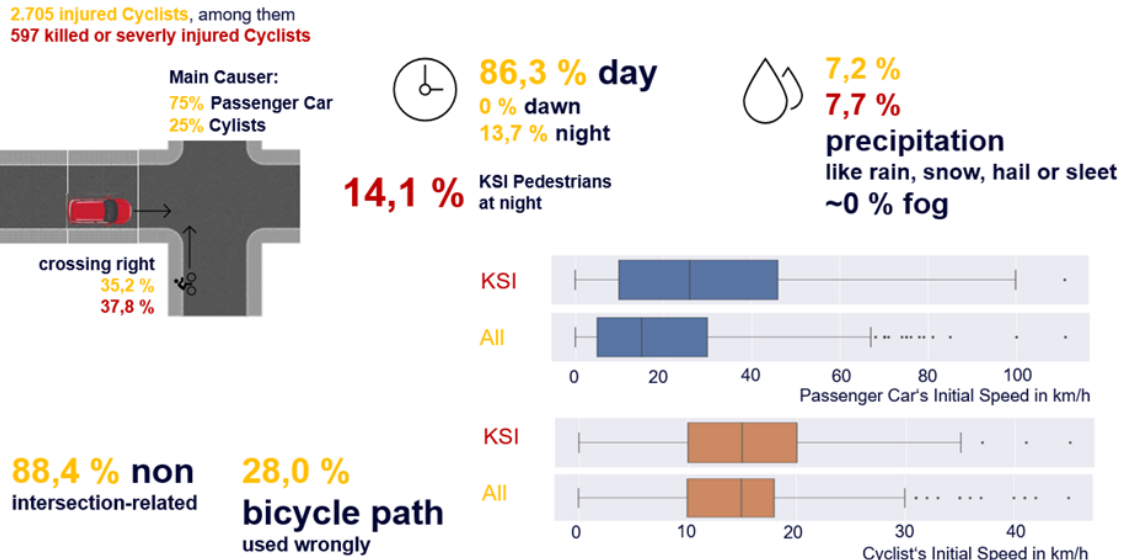
Figure 26. Results summary for C2B conflict scenario 1: B-CR.

5.1.1.4 Cyclist – PC turning left (B-PCTurnL)

In 12.8% of all cases and in 11.8% of KSI cases, precipitation is present. Precipitation aggregates the following weather conditions: rain, snow, hail and sleet.
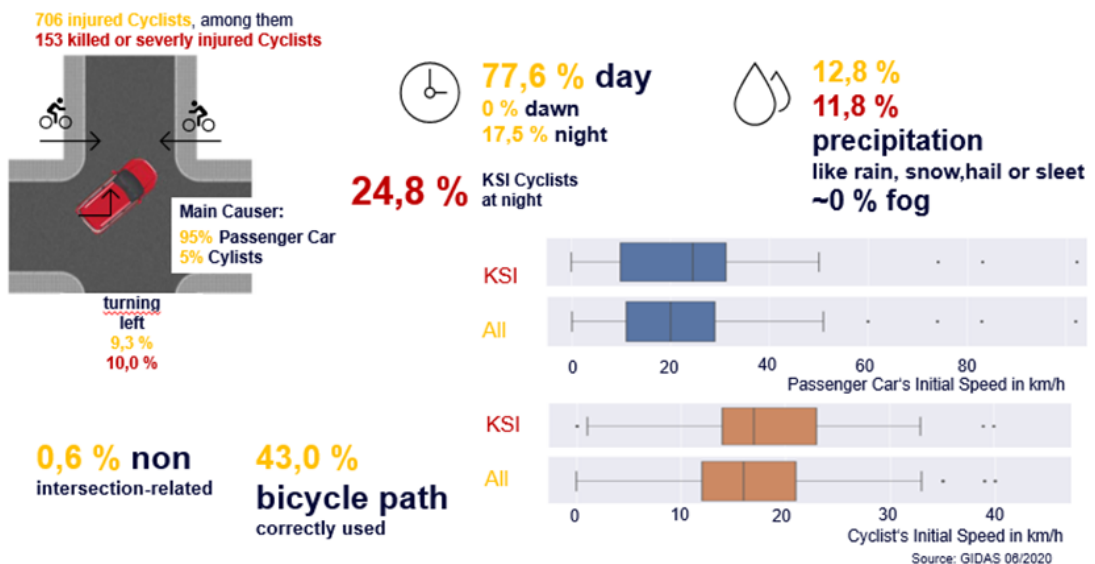
Figure 27. Results summary for C2B conflict scenario 7: B-PCTurnL.
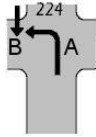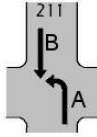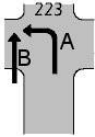
The following table divides the B-PCTurnL scenario by the travelling direction of the cyclist: Same direction as the turning passenger car (UTYP 223) or the opposite direction of the

turning passenger car (UTYP 211, 224) and gives an overview of the share of crashes where precipitation was present.

Table 10. Classification by crash type within B-PCTurnL.

UTYP	UTYP 224	UTYP 211	UTYP 223
UTYP			
All injury severities	41.2%	34.8%	16.6%
All injury severities % with precipitation	14,8%	8,5%	18,1%
KSI	39.9%	35.9%	17%
KSI % with precipitation	11,5%	3,6%	32,0%

5.1.2 Use cases for adverse weather

The use cases for car-to-VRU crashes in adverse weather conditions (AWC) are those scenarios with a larger-than-average prevalence of precipitation like rain, snow, hail or sleet. Fog was found to be less relevant as it is present in 0-1% of crashes. The use cases that are recommended to be addressed by safety systems with improved performance in weather conditions that could adversely affect sensor performance include the following scenarios:

The use cases selected for car-to-pedestrian crashes in bad weather are the conflict scenarios P-CLwoSO (Pedestrian crossing left without sight obstruction) and P-PCTurnL (Passenger car turning left). The results show that the highest absolute occurrence of crashes with precipitation is in the conflict scenario P-CLwoSO for the group of injured (3.3%) as well as for the group of killed and severely injured pedestrians (4.6%). The highest relative share of precipitation within one conflict scenario is in the conflict scenario P-PCTurnL, where 25.3% of the crashes in the group of injured pedestrians are with precipitation. A detailed analysis shows that the conflict where the pedestrian walks in same direction (UTYP 221) as the passenger car has the highest relevance within the P-PCTurnL scenario.

For the car-to-bicycle crashes in bad weather, the conflict scenarios B-CR (Cyclist crossing from right while PC moves forward) and B-PCTurnL (Cyclist in conflict with PC turning left) are selected as use cases. The results show that the highest absolute occurrence of crashes with precipitation is in conflict scenario B-CR for killed and severely injured cyclists (2.9%) and in conflict scenario B-CL for the group of all injured cyclists (2.9%). As the conflict scenario B-CR also has a relatively high share of all injured cyclists (2.5%), it is chosen as a use case. The highest relative share of precipitation within one conflict scenario is in

conflict scenario B-PCTurnL, where 12.8% of the injured cyclist cases are with precipitation. A detailed analysis shows that the conflict where the cyclist drives in the opposite direction (UTYP 221) as the passenger car has a high relevance within the B-PCTurnL scenario. Taking into account the overall higher occurrence of cyclists approaching from the opposite direction, this B-PCTurnL scenario has the highest relevance for precipitation.
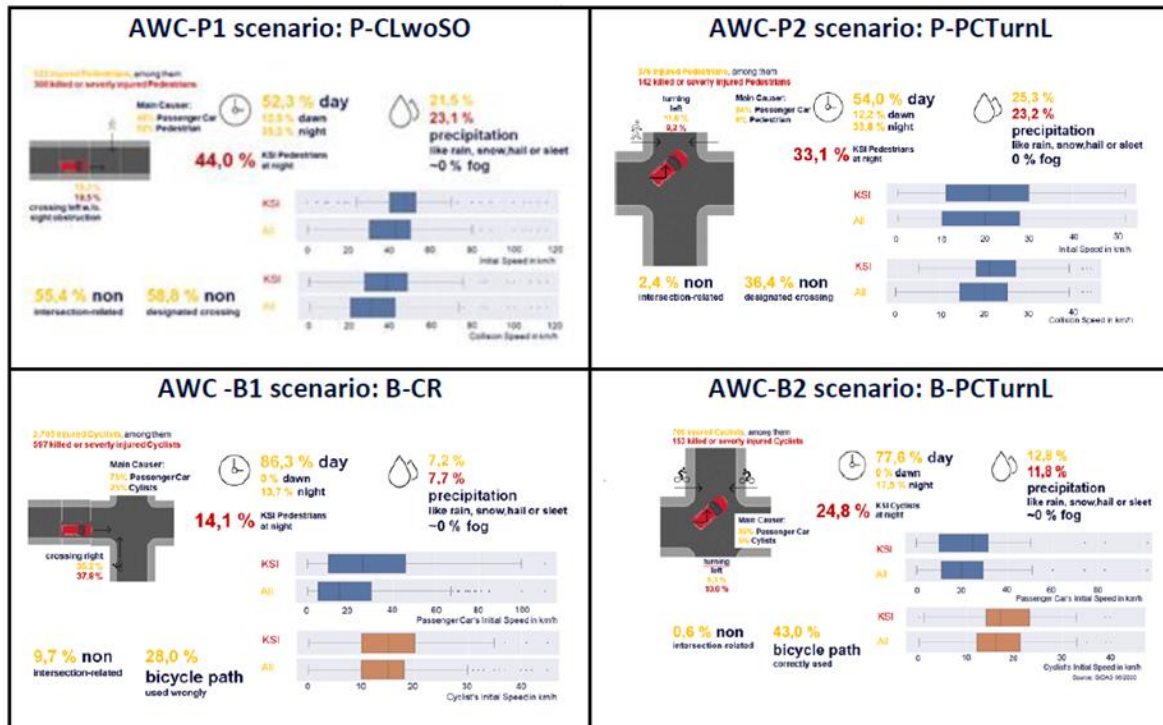
Figure 28: Car-to-VRU scenarios recommended for consideration for safety systems under adverse weather.

5.1.3 Rain amount analysis

For defining scenarios under adverse weather conditions, the type and intensity of adverse weather must be concretized. The crash analysis showed that precipitation as an adverse weather condition is significantly more prevalent than fog for VRU crashes. Therefore, in Deliverable D2.6 [19] GIDAS data was linked to weather stations of the "Deutscher Wetterdienst" (DWD) to estimate for the given subjective intensity labels light, moderate, and heavy, which precipitation rates in mm/h likely occurred during the analyzed crashes. Table 11 gives the resulting values from the linkage of data (median, mean, and 90th percentile) as well as the general ranges defined by the DWD for the labels.

Table 11: Mapping of the intensity labels of GIDAS accidents to the ranges defined by the DWD and to the precipitation amounts from the nearest DWD weather station [19].

Rain intensity (i) label	Range by DWD [mm/h]	Median in GIDAS crashes [mm/h]	Mean in GIDAS crashes [mm/h]	90th percentile in GIDAS crashes [mm/h]
Light	i < 2.5	0.54	0.87	1.7
Moderate	2.5 ≤ i < 10	0.96	2.7	3.6
Heavy	i ≥ 10	1.1	3.1	5.7

5.1.4 Specification of scenarios
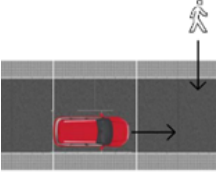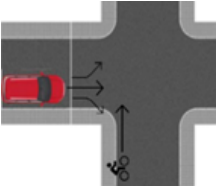
Four use cases of car-to-VRU accidents under adverse weather conditions were defined for the Demo 2 investigation, which are summarized in Chapter 5.1.2. Even though from a technical perspective also the conflict clusters with high relative shares of precipitation are interesting, the focus for generating test scenarios is on conflict clusters with the highest relevance in the crash statistics. Therefore, the conflicts with the highest absolute number of crashes with precipitation for pedestrians and bicyclists are selected and hence, test specifications are defined for the crossing scenario from left without sight obstruction for the pedestrian (AWC-P1: CLwoSO) and for the crossing scenario from right for the bicyclist (AWC-B1: B-CR).

To leverage synergies between test cases and to keep future testing effort manageable, the test scenarios are defined in correspondence to the existing structure and parameters of the Euro NCAP specification. Table 12 shows the linkage of the test cases under precipitation to the test cases with the corresponding setup from the Euro NCAP protocol [22]. The cluster CLwoSO corresponds to the Car-to-Pedestrian Farside Adult (CPFA) test case of Euro NCAP and the cluster B-CR corresponds to the Car-to-Bicyclist Nearside Adult (CBNA) test case. In the following, the selected scenarios are investigated in more detail.

Table 12. Linkage of SAFE-UP use cases for adverse weather to Euro NCAP Scenarios.

Schematic illustration of the conflict situation	Scenario / Description	ENCAP Description	VUT Speed	Target Speed	Impac location
	AWC-P1: CLwoSO Adverse weather condition P1 Pedestrian crossing from right while Vehicle moves forward	CPFA Car-To-Pedestrian Target is coming from Farside no obstruction	10-60 kph	8 kph	50 %
	AWC-B1: B-CR Adverse weather condition B1 Bicyclist crossing from right while PC moves forward	CBNA Car-to-Cyclist Target is coming from nearside, no obstruction	10-60 kph	15 kph	50 %

5.1.4.1 AWC-P1 scenario: P-CLwoSO

In the CPNA scenario, an adult pedestrian is tested who crosses the road from the left with 8 kph and has the virtual hit point at 50 %. The vehicle speed ranges from 10 kph to 60 kph in these tests. The pedestrian target stands at the roadside with a distance of 6 m to the virtual hit point (see Figure 29) and accelerates within 1.5 m to a running speed of 8 kph. The acceleration takes 1.4 s and for the remaining distance of 4.5 m the target needs a time of 2.2 s. The result is a moving time of the pedestrian target of 3.6 s, after starting the acceleration.

Since Euro NCAP test cases generally have a test duration of 4 s, this time is used to calculate the length of the rain area. At the highest vehicle speed of 60 kph, which corresponds to 16.6 m/s, the vehicle drives a distance of about 67 m, which represents the highest dimensions of the rain area. When considering the vehicle length of 5 m and a buffer of 1 m each to ensure that the objects are fully in the rain area, the length of the rain area adds up to 74 m. Consequently, the width of the rain area should be 9 m in total, which includes the 6 m distance between the dummy and the hit point, as well as additionally half the vehicle width of approximately 1 m and again a buffer of 1 m to each side. This results in a maximal rain area dimension of 74 m length and 9 m width.
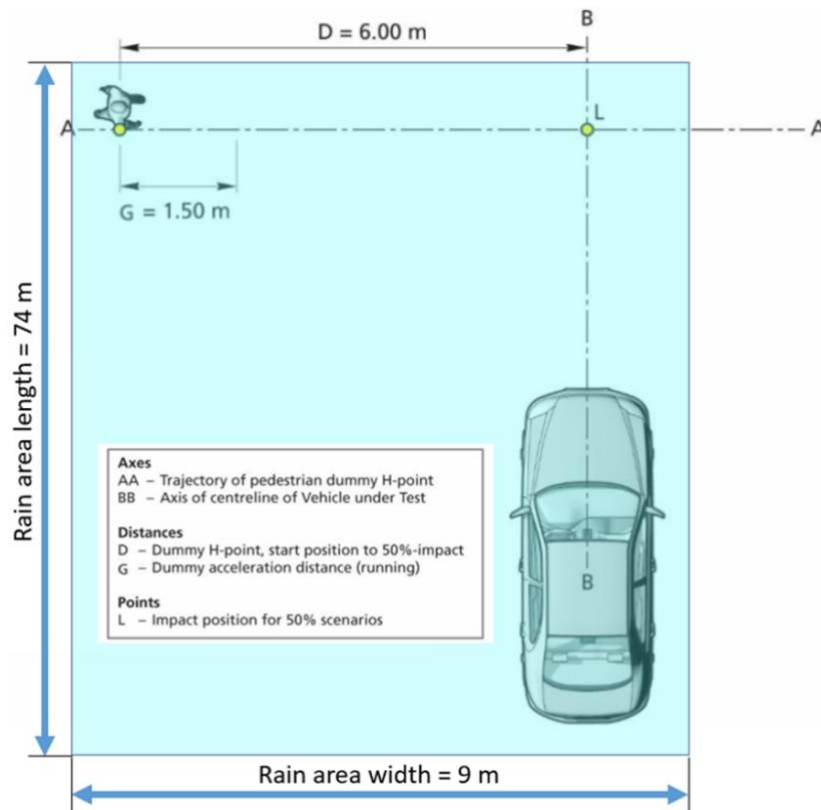
Figure 29. CPNA scenario and required rain area (without acceleration distance of vehicle in the rain area). Adapted from Euro NCAP [22].

5.1.4.2   AWC-B1 scenario: B-CR

In the CBNA scenario, an adult bicyclist is tested who crosses the road from the right with 15 kph and has the virtual hit point at 50 %. The vehicle speed ranges from 10 kph to 60 kph in these tests. The bicyclist target starts the acceleration behind parked vehicles (see Figure 30). However, since the bicyclist moves with 15 kph 16.6 m (rounded 17 m) in the testing time of 4 s, this test case is classified as unobstructed. When the bicyclist accelerates behind the parked vehicles, the rain area must not cover the bicyclist as the prerequisite is that it is not in the visible field of the sensors there.

Since Euro NCAP test cases generally have a test duration of 4 s, this time is used to calculate the length of the rain area. At the highest vehicle speed of 60 kph, which corresponds to 16.6 m/s, the vehicle covers a distance of about 67 m, which represents the highest dimensions of the rain area. When considering the vehicle length of 5 m and a buffer of 1 m each to ensure that the objects are fully in the rain area, the length of the rain area adds up to 74 m. The width of the rain area with 20 m is calculated from the 17 m for the visible distance between the dummy and the hit point, half a vehicle width of 1 m, and additional a buffer of 1 m to each side. This results in a total area with a length of 74 m and a width of 20 m.
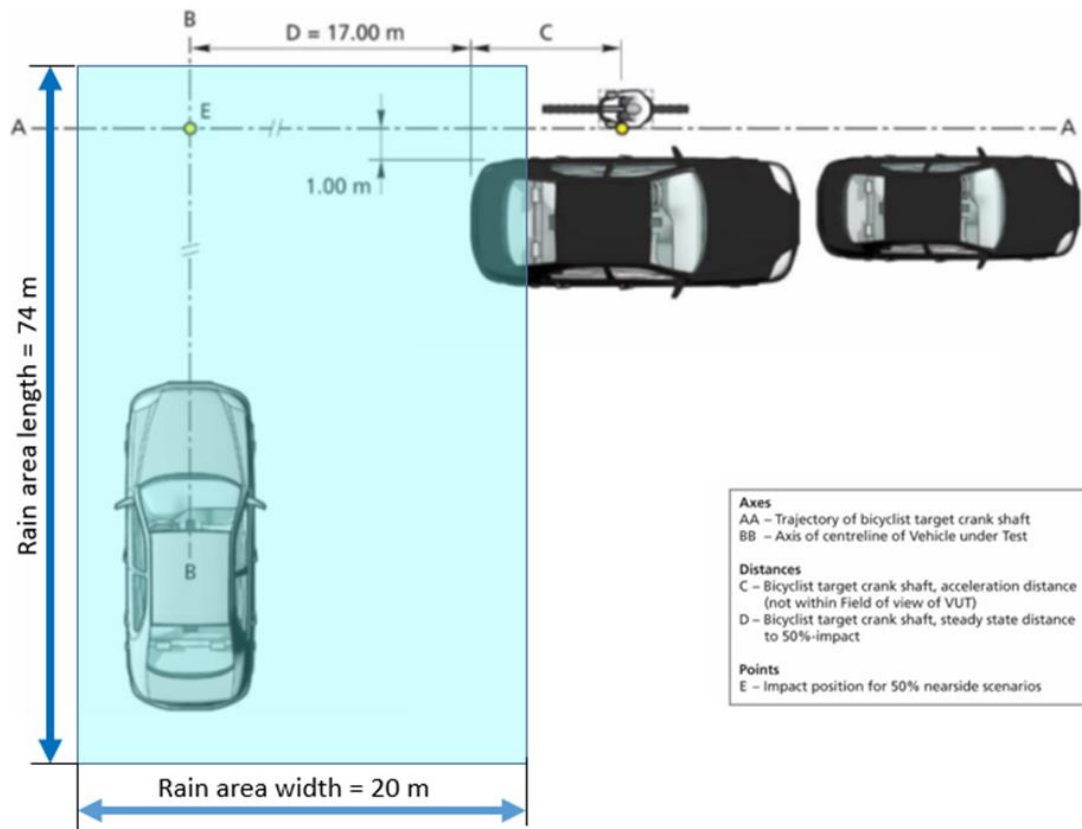
Figure 30. CBNA scenario and required rain area (without acceleration distance of vehicle in the rain area). Adapted from Euro NCAP [22].

For the calculation of the required rain areas to test the selected scenarios with vehicle speeds up to 60 kph, the acceleration distance of the vehicle is not considered. If the acceleration distance should also be within the rain area, it must be correspondingly larger.
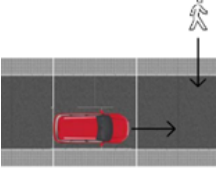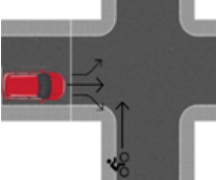
Table 13 summarizes the additional parameters for the scenario in terms of adverse weather conditions, where the rain intensity is taken from the ranges defined in Chapter 5.1.3 and the friction coefficients from [23].

Table 13. Linkage of SAFE-UP use cases for adverse weather to Euro NCAP Scenarios with additional defined adverse weather conditions.

Schematic illustration of the conflict situation	SAFE-UP Scenario	ENCAP Scenario	Rain area (without vehicle acceleration)	Rain intensity	Friction coefficient
	AWC-P1: CLwoSO	CPFA	74 m x 9 m	0 – 6 mm/h	0.9 – 0.7
	AWC-B1: B-CR	CBNA	74 m x 20 m	0 – 6 mm/h	0.9 – 0.7

5.2 Testing and simulation analysis and results

This chapter provides an overview of the main results from the performed test campaigns and simulations for Demo 2.

5.2.1 Second measurement campaign (static)

This chapter details the setup and the evaluation of the second measurement campaign, which was performed in a static setting.

5.2.1.1 Measurement campaign setup

The second measurement campaign was conducted to estimate the fields of view (FoV) of the radar and the camera sensors of the SAFE-UP Demo 3 vehicle under different adverse weather conditions, so that these results can be integrated into simulations (see Deliverable D3.5 [20] for more details). A second motivation was the improvement of today's sensor models, which are mostly only defined by a range and an aperture angle and do not take into account general real existing effects in the sensors.

As accident statistics showed the importance of crossing scenarios under adverse weather conditions, the focus of this measurement was on an angle setting, which is representative for crossing object scenarios. A grid of static measurement locations was defined, where the VRU dummies were placed in different distances and angles to the vehicle.

Due to the limitation of the rain area in the test hall to 50 m x 4 m, the setup is rotated such that the vehicle's investigated sensors as well as the dummies are always fully within the rain area. Also, the targets are rotated at these locations such that the angle between the vehicle and the target direction always maintains 90°, which is realistic for crossing scenarios. Figure 31 shows the grid of static measurement locations as well as how the rotation is realized on the example of the 33° positions.

Following configurations in all combinations were tested in the second measurement campaign:

- Targets: Pedestrian (moving legs), bicyclist (static), powered two-wheeler (static)

- Weather settings: Dry, rain 16 mm/h, rain 66 mm/h, rain 98 mm/h, fog 25 – 35 m visual range, fog with <10 m visual range

- Angle between vehicle's forward direction and target position: 0°, 16°, 33°, 50°

- Radial distances from vehicle's front to target position: 7.33 m, 14.7 m, 22.0 m, 29.3 m, 36.7 m, 44.0 m
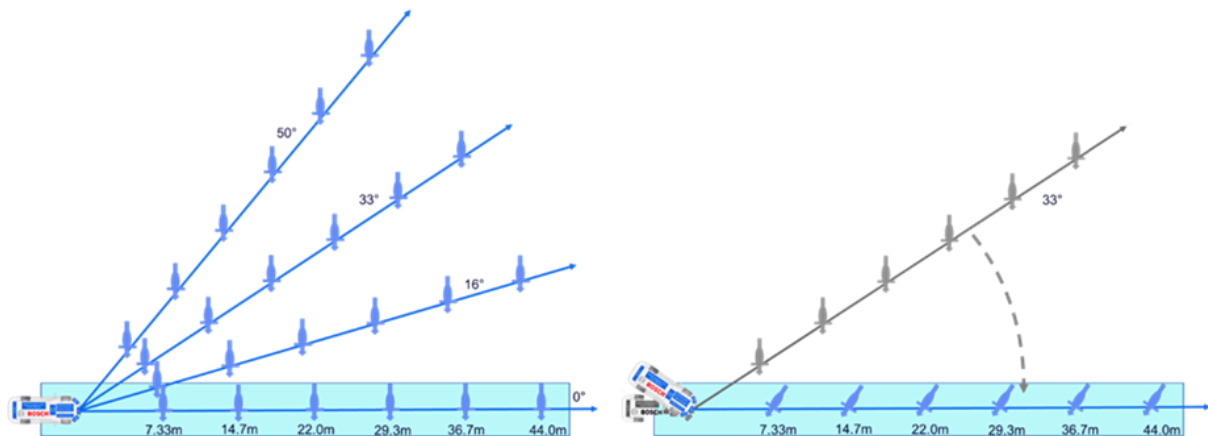
Figure 31. Test grid of the second measurement campaign (static measurement) inside the CARISSMA test hall [20].

5.2.1.2 Measurement campaign evaluation

For each measurement location, it was evaluated with the methodology described in more detail in Deliverable D3.5 [20], if the dummy is detected by the investigated sensors or not. As the angular positioning of the vehicle was performed by manually parking the vehicle guided by a laser and small angle errors can already lead to a large offset at positions with higher distance, systematic errors needed to be identified first in the data post-processing.

To decide in a threshold-based approach if a target is detected or not, a bounding box for the pedestrian is used around the corrected reference position.

The radar locations (estimated reflection points of the radar) within the bounding boxes are filtered by their quality estimates. Therefore, all radar locations are discarded, when their estimated azimuthal position quality is below 0.75 or when their estimated radar cross section (RCS) is below or equal to -20 dBm², to ensure that only reflections possibly originating from a VRU are considered. If at least one radar location meets all criteria, the pedestrian is classified as detected at this position.

For the front camera sensor, a detection algorithm which returns object lists was running. These lists can be used to decide if the pedestrian target was detected or not detected. If the error in the y-coordinate direction is smaller or equal to 0.60 m and the error in the x-coordinate direction is smaller or equal to 3.0 m, the pedestrian is classified as detected at this position. The reason why the acceptable error in the x-coordinate direction is chosen significantly larger is that the camera has difficulties in estimating the distance for stationary tests.

To generate FoVs for integrating sensors into simulations, which are continuous and not limited to the testable area from the test hall, theoretical characteristics of the radar and camera sensor are combined with the results from the measurement campaign as described in Deliverable D3.5 [20]. Therefore, the theoretical shape of the FoV for the radar and camera sensor is used and scaled such that it matches the measured values categorized in detected or not detected as closely as possible. The resulting FoVs from this methodology are shown in Figure 32 for the investigated radar and camera sensor, where a detection of the pedestrian dummy is assumed to be possible for the different rain amounts. The radar sensor FoVs can be integrated into simulations for 0 mm/h, 16 mm/h, 66 mm/h and 98 mm/h and the camera sensor FoVs for 0 mm/h, 16 mm/h and 66 mm/h. For 98 mm/h no reliable prediction was ensured in a defined area with the camera sensor.
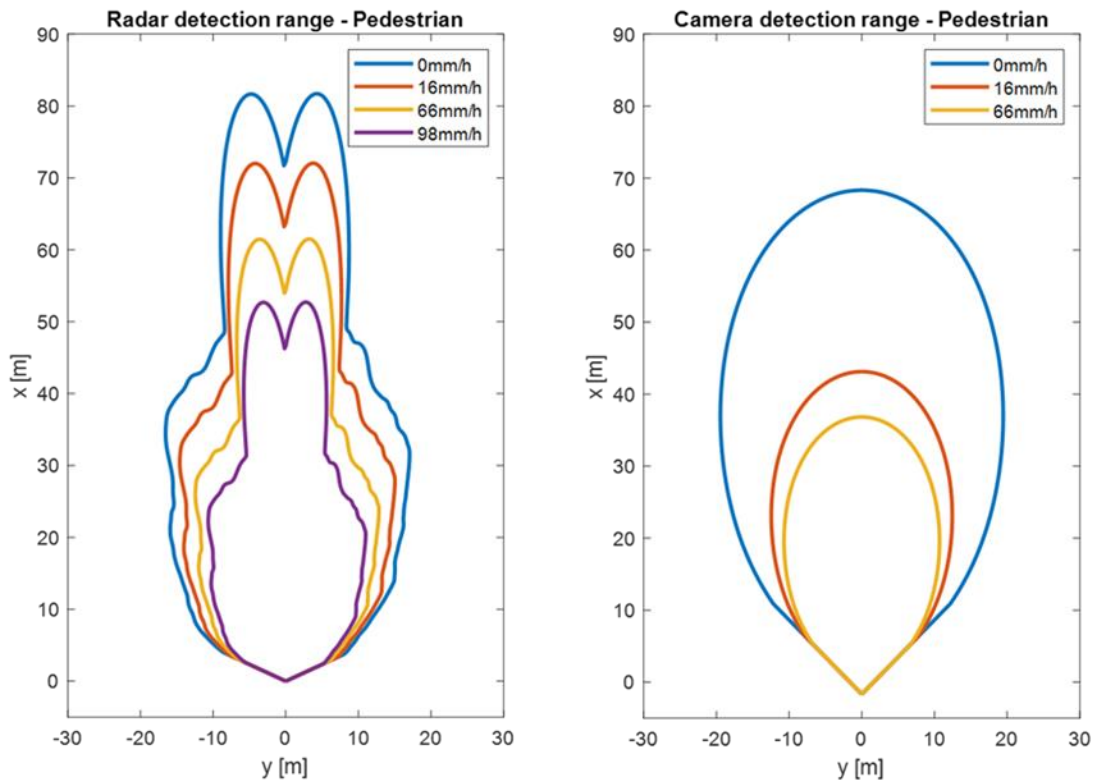
Figure 32. Resulting FoVs from the second measurement campaign, which are sensor-specific and depend on the methodology from [20].

5.2.2 Simulation analysis

This chapter details the scenario selection for simulation, the setup of the simulations, and the results thereof, which are summarized from Deliverable D3.6 [21].

5.2.2.1 Simulated scenarios

The basis for the simulation scenario selection are the identified conflict scenarios between passenger cars and pedestrians from Deliverable D2.6 [19] summarized in Figure 1. Due to the low velocities in the reversing cluster (90th percentile at 9.5 km/h for the passenger car) and a precipitation share significantly below the baseline precipitation share, the reversing cluster is disregarded for simulations.

For each of the selected scenario clusters, up to 3 simulation configurations with different velocity values are defined. One configuration is simulated with the median velocity values of the passenger car and the pedestrian in the respective cluster at a TTC of 2.5 s. In addition, up to two configurations are simulated with sensor critical velocity values of the cluster at a TTC of 2.5 s.

For the crossing scenarios one sensor critical configuration focuses on the range limitation and one on the opening angle limitation of a sensor. For the configuration focusing on range, the 90th percentile of the passenger car velocity distribution and the 10th percentile of the

pedestrian velocity distribution of the cluster at a TTC of 2.5 s is chosen. For the configuration focusing on the opening angle, the 10th percentile of the passenger car velocity distribution and the 90th percentile of the pedestrian velocity distribution of the cluster at a TTC of 2.5 s is chosen.

For the longitudinal cluster, besides the configuration with median velocities one configuration represents the worst case and one the best case in terms of range. To simulate the worst case, the 90th percentile of the passenger car as well as pedestrian velocity distribution is selected, and the pedestrian is chosen to run in oncoming direction. To simulate the best case, the 10th percentile of the passenger car as well as pedestrian velocity distribution is selected, and the pedestrian is chosen to head in the same direction as the passenger car.

The goal for the simulation is to provide a representative excerpt from the accident events including pedestrians, while limiting the simulation effort for this large database. The selected scenarios are structured in such a way that they can be compared with existing results from other projects. As the scenarios have also been used by Euro NCAP over the last years, it is reasonable to harmonize the test cases with the test matrix from Euro NCAP for vehicle to pedestrian crashes.

In Table 14, the defined configurations for the simulations including the corresponding Euro NCAP scenario, the velocities, the virtual hit points and the layouts are summarized. The selected velocities are marked in each line in bold.

Table 14. Simulated passenger car to pedestrian configurations, which are harmonized with Euro NCAP test cases.

Safe-UP ID.Number	Cluster	Category	EuroNCAP Scenario	Simulation Scenario	v_ego kph	v_ego kph2	v_traget kph	Virtual Hitpoint	Obstruction
					All injury severities	KSI	All injury severities		
1a	P-CLwoSO	Median	CPFA	CPFA	45	48 (V0)	5	50% (ENCAP)	no
1b	P-CLwoSO	Range	CPFA	CPFA	60	63 (V1)	2	50% (ENCAP)	no
1c	P-CLwoSO	Angle	CPFA	CPFA	21 (V2)	30	15	50% (ENCAP)	no
2a	P-CLwSO	Median	CPFA	CPFAO	35	40 (V0)	6	50% (ENCAP Nearside)	ENCAP modified
2b	P-CLwSO	Range	CPFA	CPFAO	50	52 (V1)	1	50% (ENCAP Nearside)	ENCAP modified
2c	P-CLwSO	Angle	CPFA	CPFAO	19 (V2)	24	16	50% (ENCAP Nearside)	ENCAP modified
3a	P-CRwoSO	Median	CPNA	CPNA	40	45 (V0)	5	25% (ENCAP, Sensor critical)	no
3b	P-CRwoSO	Range	CPNA	CPNA	54	58 (V1)	2	25% (ENCAP, Sensor critical)	no
3c	P-CRwoSO	Angle	CPNA	CPNA	14 (V2)	17	13	25% (ENCAP, Sensor critical)	no
4a	P-CRwSO	Median	CPNCO	CPNAO	35	40 (V0)	6	50% (ENCAP)	yes
4b	P-CRwSO	Range	CPNCO	CPNAO	51	55 (V1)	3	50% (ENCAP)	yes
4c	P-CRwSO	Angle	CPNCO	CPNAO	19 (V2)	24	15	50% (ENCAP)	yes
5a	P-Long	Median	CPLA	CPLA	50 (V0)		5	50% (ENCAP)	no
5b	P-Long	Range opposite dir.	CPLA	CPLA	79 (V1)		6	25% (ENCAP)	no
5c	P-Long	Range same dir.	CPLA	CPLA	20 (V2)		2	50% (ENCAP)	no
71a	P-PCTurnL-SD	Median	CPTA	CPTA-L	24 (V0)		5	50% (ENCAP)	no
72a	P-PcTurnL-OD	Median	CPTA	CPTA-L	20 (V1)		5	50% (ENCAP)	no
81a	P-PcTurnR-SD	Median	CPTA	CPTA-R	20 (V2)		4	50% (ENCAP)	no
82a	P-PCTurnR-OD	Median	CPTA	CPTA-R	17 (V3)		5	50% (ENCAP)	no

5.2.2.2 Description of simulation setup

Simulation setup - input

In order to obtain results from the simulation that are as reliable as possible and that meet the requirements of accident analysis, some parameters of the simulation setup must be defined in advance.

As the vehicle model, the standard IPG vehicle model from CarMaker is used, whereof all parameters and properties are predefined. Certain properties such as brake characteristics and steering characteristics are defined specifically in the project for simulation and can be requested from the CarMaker vehicle model. Within this framework, they follow the requested parameters and are limited only by the maximum ranges of the CarMaker model.

The different clusters from accident research are simulated both with the radar and with the camera sensor, which is why the position of the sensors must be taken into account. The simulations were performed individually for both sensors and no fusion system was considered. The installation location of both sensors is shown in Figure 33. The camera sensor is installed at 2.3 m and the radar sensor at 4.0 m distance starting from the vehicle's origin marked with a red cross at the back.
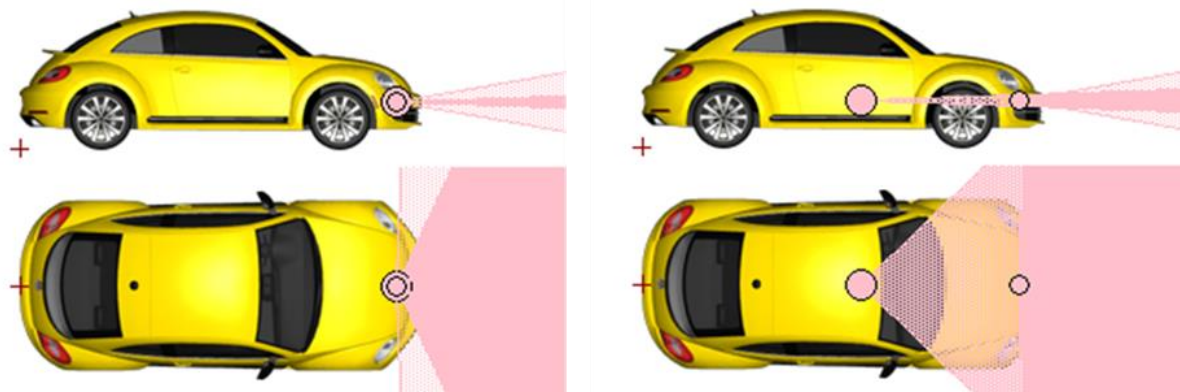
Figure 33. Positioning of the sensors in the IPG vehicle.

As described in Chapter 5.2.1.2, FoVs for the radar were generated for the rain intensities 0 mm/h, 16 mm/h, 66 mm/h, and 98 mm/h and for the camera sensor for 0 mm/h, 16 mm/h and 66 mm/h. The integration of the FoVs into simulations is shown in Figure 34, which is implemented with a script that can read in data in the format of opening angle and corresponding range values and that can display the sensors in the simulation based on this input. As rain affects besides the field of view also the friction coefficient, this value is as well adapted based on the values from Table 15 via the friction parameter in the IPG-Roadfile.
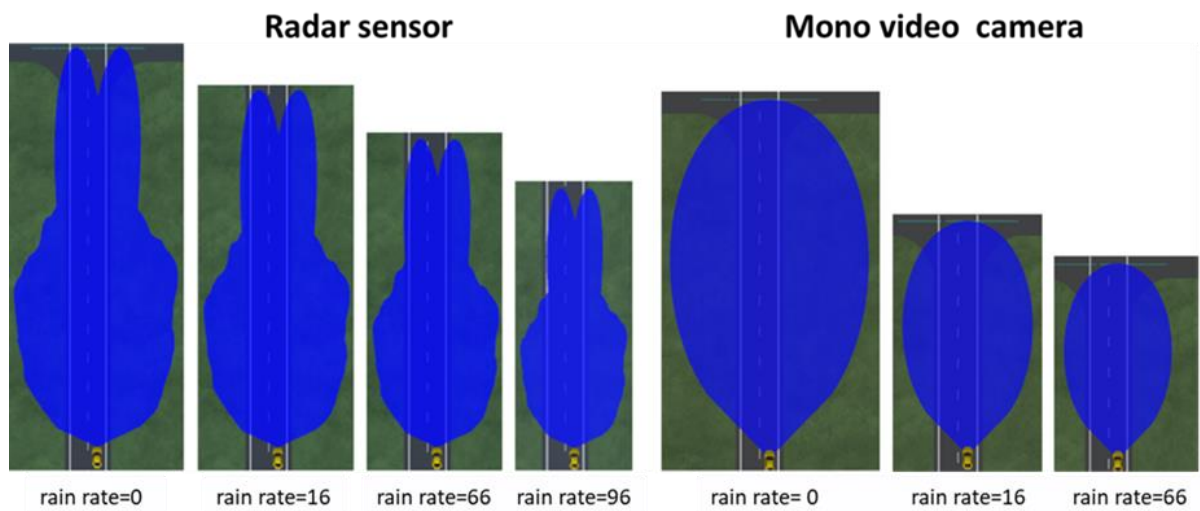
Figure 34. Adapted FoVs integrated into CarMaker.

Table 15. Selected friction coefficients for the tested rain intensities.

Rain intensity	Friction coefficient
0mm/h	0.9
16mm/h	0.8
66mm/h	0.6
96mm/h	0.4

As described in Chapter 5.2.2.1, occlusion scenarios are also required in the simulations. In harmonization with the test setup from Euro NCAP, the occlusions are generated with stationary vehicles. The distance between the driving and the parking vehicles is 1 m and the pedestrian moves past the vehicle at a distance of 1 m to the vehicle as illustrated in Figure 35 for the scenario CRwSO.
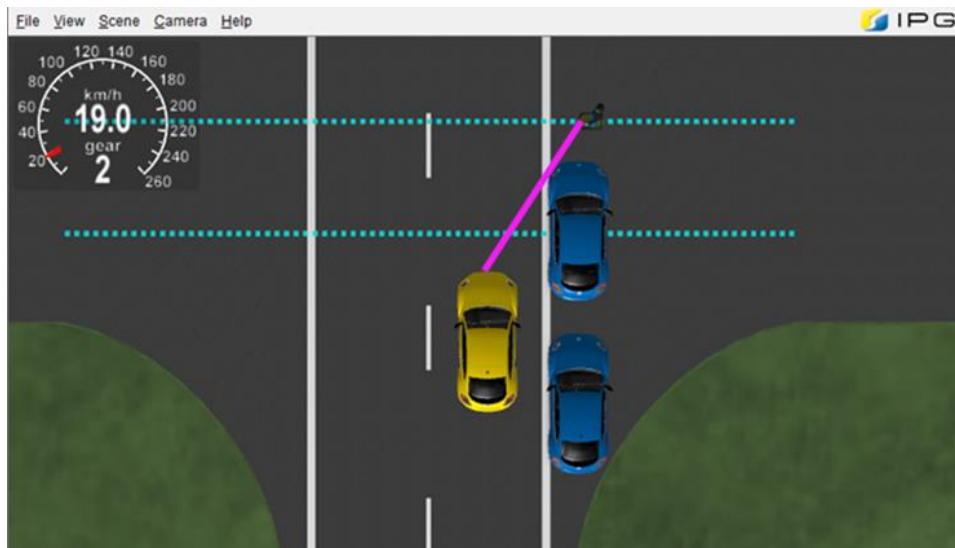
Figure 35. Setup how the occlusion scenarios are modelled in CarMaker.

The pedestrian coming from the right is hidden at larger distances and cannot be detected by the sensor. The earliest point at which the pedestrian can be theoretically detected is marked with a pink line in Figure 35. From this point, the object detection time of the sensor begins as soon as the pedestrian is 500 ms within the FoV of the sensor under investigation. For the scenario CLwSO, the distances are defined similarly, however, the parking vehicles are then on the left lane.

As also emergency steering is implemented as a possible intervention maneuver, the dimensions of the road width and the objects needed to be defined. The width of the lane including lane markings is defined as 3.9 m (lane width + lane markings: 3.5 m + 0.15 m + 0.25 m - maximum values from Euro NCAP [22]) the width of the vehicle as 2.1 m (width including the side mirrors: 1.8 m + 2*0.15 m - from IPG CarMaker vehicle specification), the width of the pedestrian as 0.33 m in the crossing scenarios (step width - from IPG CarMaker pedestrian specification), and the width of the pedestrian as 0.55 m in the longitudinal scenarios (shoulder width - from IPG CarMaker pedestrian specification) as shown in Figure 36 for a longitudinal scenario example. It is assumed that steering as an evasive maneuver is in general possible if the available space between the pedestrian and the left lane including the lane marking is larger than or equal to the vehicle width.

Figure 36. Definition of the different width, which are required for evasive steering.

Simulation setup - output

To evaluate the results of the simulations, several output parameters were extracted besides the parameters defining the simulation setup, which include the passenger car and pedestrian velocity, the virtual hit point in relation to the passenger car, the rain rate as well as the friction coefficient.

For each simulation, the time required for intervening with steering (T_{steer}) and braking (T_{brake}) is extracted. Thereby, the values under nominal conditions are estimated, which are used for the decision of the intervention type. The resulting intervention type is also extracted for each simulation such that it can be evaluated if braking or steering is preferable in certain scenario types.

In addition, the TTC at which the object is detected is extracted ($T_{detected}$), which is defined by the time at which the pedestrian is 500 ms in the FoV of the investigated sensor. It is assumed that 500 ms are required for the sensor detection and the signal transmission after the pedestrian initially enters (nearest point) the FoV. For each scenario the TTC at which the intervention is triggered ($T_{intevention}$) is stored. It is equal to the minimum of the variables $T_{detected}$, T_{brake}, and T_{steer}. The smaller T_{brake} or T_{steer} value decides the chosen intervention maneuver. If the pedestrian is detected sufficiently early, the intervention is triggered when the TTC value is equal to the time required for the braking or steering maneuver (case $T_{intevention}=T_{brake}$ or $T_{intevention}=T_{steer}$). If the pedestrian is detected later than the intervention maneuver would take, it is triggered as soon as the pedestrian is detected (case $T_{intevention}=T_{detected}$).

For the cases where the intervention function cannot avoid a collision, a parameter is used, which is set from 0 to 1 in the case of a collision (collision), and the collision speed ($v_{collision}$) is extracted, which indicates the residual speed of the passenger car with which it hits the pedestrian. In simulations where the selected intervention maneuver is braking but a collision cannot be avoided, the collision speed is correspondingly lower than the initial speed of the passenger car depending on the time of triggering. In simulations where the chosen intervention maneuver is steering but a crash cannot be avoided, the collision velocity is equal to the initial passenger car velocity as it is not combined with braking.

5.3 Results

Note

The simulated results are not considering or limited to generalization due to

- Impact of fusion logic between camera and radar detection with resulting limitations of FoV in terms of detection and functional performance

- Validation of theoretical results by real driving tests and quantification of a realistic avoidance and reduction potential

- Potential risk with weather-dependent design of emergency intervention in terms of type of intervention (braking, steering) and earlier intervention timing

- Confirmation of results and trends by further camera and radar sensors necessary, especially dynamic testing

- More performant AEB than the one theoretically calculated here holds less potential to adapt the braking timing in case of reduced friction coefficient.

5.3.1 Result overview

The number of simulated cases in the crossing and longitudinal scenarios is 21 each, consisting of nine cases with camera detection and 12 cases with radar detection (see Figure 37). The nine cases with camera detection result from three velocity configurations V0, V1 and V2, varied with three rain intensities (0 mm/h, 16 mm/h and 66 mm/h). The mapping from the velocity configurations Vx to the actual velocity values are given in Table 14 for all scenarios. The 12 cases with radar detection result from three velocity configurations V0, V1 and V2, varied with four rain intensities (0 mm/h, 16 mm/h, 66 mm/h, and 96 mm/h). The deviation results from the observation that camera detection is no longer possible at the highest rain rate and is therefore not simulated.
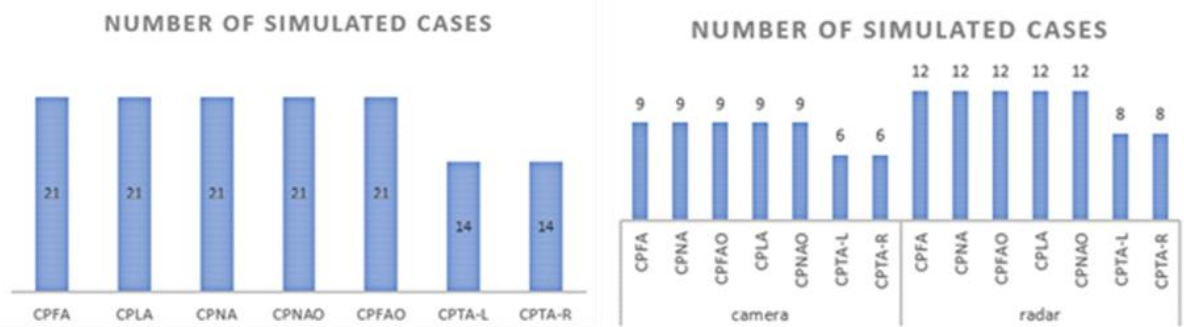
Figure 37. Numbers of simulated cases.

The number of turning scenarios to the left and to the right each consist of six cases with camera detection and eight cases with radar detection. These consist of two median velocities to the left (V0 and V1) and two median velocities to the right (V2 and V3) each with a same-directed and an oncoming target, varied with three or four rain intensities, respectively (see Figure 37).

Of the 21 cases in each of the longitudinal and crossing scenarios and the 14 cases in each of the turning scenarios, i.e. a total of 133 cases, braking intervention was preferred to steering intervention in 126 cases (see Figure 38). Steering intervention was the prevailing choice in only seven cases in the longitudinal scenario CPLA, where in three camera-based and four radar-based scenarios the steering time (T_{steer}) was smaller than the braking time (T_{brake}).
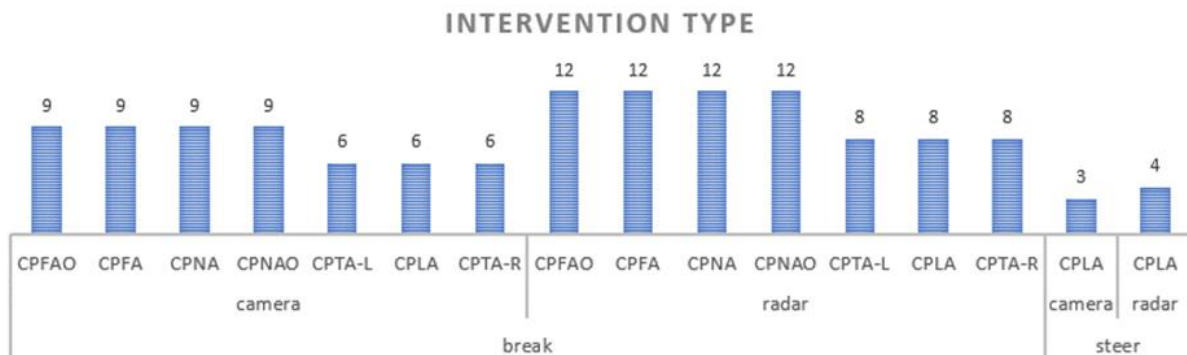
Figure 38. Intervention type per scenario.

The number of collisions shows that the proportion of collisions predominates in scenarios with obstruction (see Figure 39). The obstruction causes delayed detections, which lead to a significant limitation of the avoidance potential. The reason for the high number of collisions is especially that all rain rates from 0 mm/h to 96 mm/h are included in this evaluation. It can also be observed that for the nearside crossing pedestrian, CPNAO, the visual obstruction directly next to the driving trajectory leads to more collisions than for the farside crossing pedestrian, CPFAO. The ego velocities of both scenarios are comparable, which allows this conclusion.
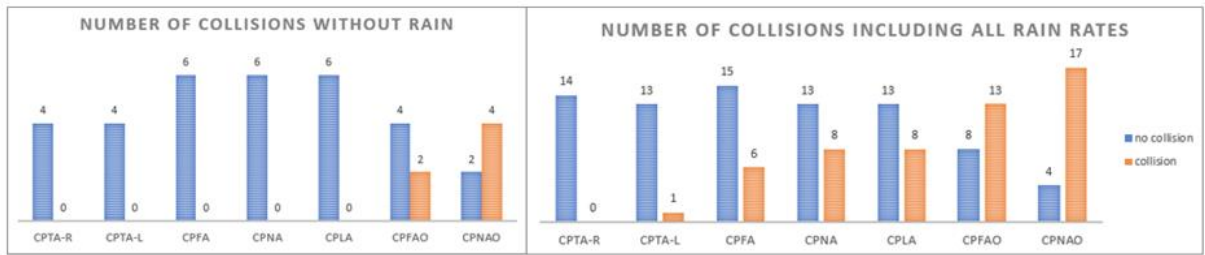
Figure 39. Number of collisions per scenario.

In general, it can be observed that collisions occur in almost every scenario. Turning right is the exception here with none and turning left with one collision. Both braking and steering intervention lead to collisions (see Figure 40).
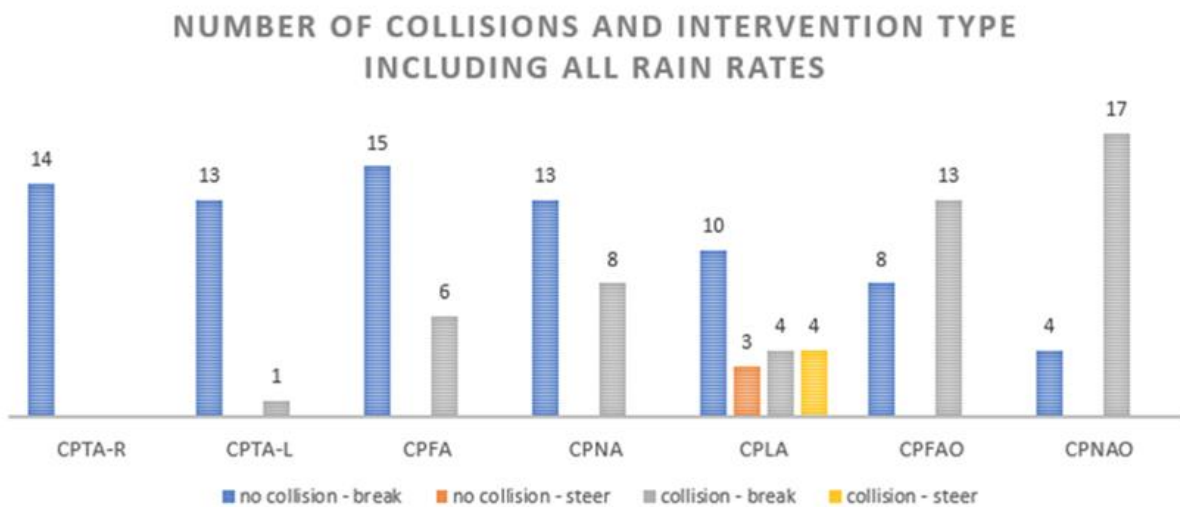
Figure 40. Number of collisions per scenario depending on intervention type.

The number of collisions, taking into account the rain rate, shows a clear trend (see Figure 41). Regardless of the detection type, camera or radar, the number of collisions increases with higher rain rates. If 16 % collisions occur with no precipitation, the proportion rises to 26 %/ 21 % at 16 mm/h. At 66 mm/h the proportion of collisions is then 63 % and at 96 mm/h (radar) 74 %.
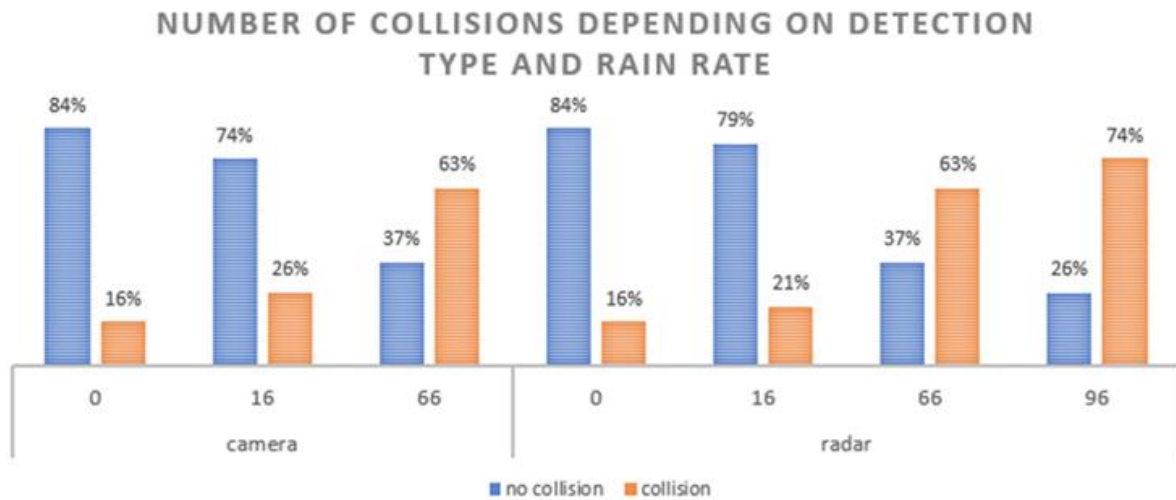
Figure 41. Number of collisions depending on rate rate (0 mm/h, 16 mm/h, 66 mm/h, 96 mm/h).

5.3.2 Result individual scenarios

The summary of the results of the individual scenarios focuses on the rain rates 0 to 66 mm/h. This is based on two factors: Firstly, rain rates lower than 16 mm/h usually occur, but this was the lowest measurable value in the test hall (see Deliverable D2.6 [19] for evaluation). On the other hand, the rain rate 66 mm/h takes into account a friction coefficient of 0.6, which can also occur at lower rain rates due to water accumulation caused by road irregularities. A rain rate of 96 mm/h, in contrast, is to be categorized as a locally occurring and very rare phenomenon.

Figure 42 shows an overview of the simulated scenarios at the rainfall rates 0 mm/h, 16 mm/h and 66 mm/h. For each scenario, the share of simulations with collisions, the influence of the detection type and the cause of the collision are evaluated.

scenario	1 CPFA	2 CPNA		3 CPLA		4 CPFAO	5 CPNAO	6 CPTA-R	7 CPTA-L
0mm/h & μ = 0,9									
collisions	0%	0%		0%		33%	67%	0%	0%
FoV	/	/		/		camera & radar	camera & radar	/	/
cause	/	/		/		obstruction: 2	obstruction: 4	/	/
16mm/h & μ = 0,8									
collisions	0%	33%		33%	0%	33%	67%	0%	0%
FoV	/	camera & radar		camera	radar	/	/	/	/
cause	/	friction: 2*		FoV: 1	/	/	/	/	/
66mm/h & μ = 0,6									
collisions	67%	67%		67%		100%	100%	0%	0%
FoV	camera & radar	camera	radar	camera & radar		camera & radar	camera & radar	/	/
cause	FoV: 1 friction: 3	FoV: 1* friction: 1	friction: 1	FoV: 1 friction: 2		friction: 2 obstruction: 2	friction: 2	/	/

* Cause changed from 16mm/h friction to 66mm/h FoV
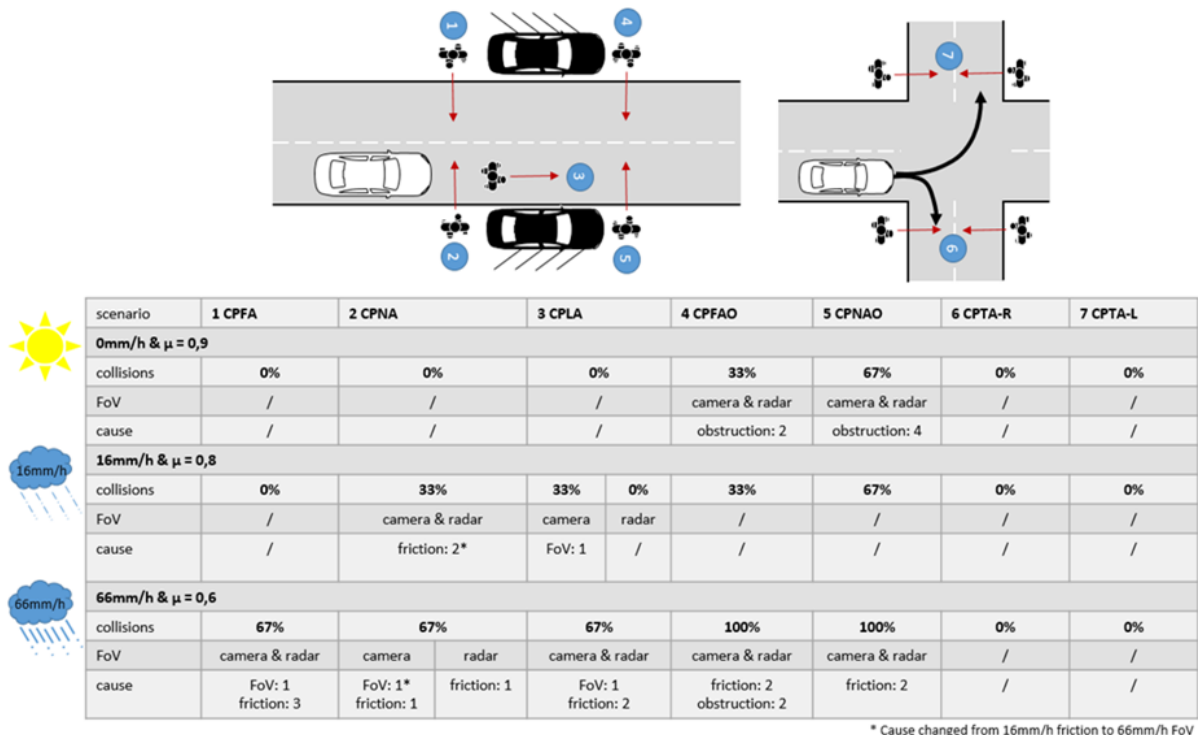
Figure 42. Scenario overview including rain rate, share of collisions, detection influence and causation (only additional causes in comparison to lower rain rates are given - except for *).

In the crossing scenario without obstruction CPNA, at 16 mm/h rain rate in 33 % of the simulated scenarios collisions occur compared to 0 % at 0 mm/h. These are due to the reduced friction. At 66 mm/h rain rate, the percentage then is 67 % for both crossing scenarios, CPNA and CPFA. The cause here is predominantly the reduced friction value, but also the limitation of FoV due to the rain rate.

In the longitudinal scenario (CPLA), collision occurs exclusively at the camera at 16 mm/h due to the reduced FoV caused by the rain rate. At 66 mm/h then 67 %, but here also due to the reduced friction.

The crossing scenarios with visual obstruction, CPFAO and CPNAO, show collisions even without the influence of rain. In 33 % of the simulated scenarios from CPFAO and in 67 % of the simulated scenarios from CPNAO collisions occur. The reason for this is the limitation of the FoV by the visual obstruction. At 66 mm/h, 100 % collisions then occur in both obstructed scenarios. In contrast to the lower rain rate with the cause of visual obstruction, the reason here is also the reduced coefficient of friction and in the case of CPFAO additional two cases due to visual obstruction.

In the turning scenarios to the left and right with oncoming pedestrians as well as pedestrians moving in the same direction, no influence is visible from 0 to 66 mm/h rain rate as no collisions occur.

5.3.2.1 Rain rate 0 mm/h

The simulations at 0 mm/h rain rate, i.e. without rain, serve as baseline and provide a possibility to compare which scenarios already show collisions without the influence of rain. This is the case for the two scenarios with visual obstruction, CPFAO (33 %) and CPNAO (67 %).

5.3.2.2 Rain rate 16 mm/h

In summary, at 16 mm/h it can be concluded that the **influence of the rain rate on the FoV** is very small in the scenarios considered. Only in the scenario CPLA the limitation of the camera FoV leads to a collision. This can be explained by the higher degradation of the camera FoV from 0 mm/h to 16 mm/h rain rate (ca. -40 %) compared to the radar FoV (ca. -15 %). However, this influence is only noticeable at the high ego speed (79 kph).

The **influence of the rain rate on the friction coefficient** at 16 mm/h and thus on the deceleration capabilities of the ego vehicle is evident in two cases, namely in the CPNA scenario with the high ego speed (52 kph).

The **influence of visual obstruction on the FoV** is not present in any additional scenario compared to 0 mm/h.

5.3.2.3 Rain rate 66 mm/h

It can be summarized that at 66 mm/h the **influence of the increased rain rate on the FoV** is higher than at 16 mm/h in the considered scenarios. A limited FoV due to the rain rate can be seen in further two cases in the CPFA, CPNA and CPLA scenarios. In the CPNA scenario, the cause changes from friction coefficient at 16 mm/h to FoV restriction (66 mm/h). All three cases involve the highest ego velocities, respectively: CPFA (63 kph), CPNA (68 kph) and CPLA (53 kph).

The **influence of rain rate on friction coefficient** at 66 mm/h is evident in all crossing and longitudinal scenarios. In additional 10 out of a total of 30 simulated cases collisions occur compared to 16 mm/h. Ego speeds are in both high and medium ranges: CPFA (48 kph and 63 kph), CPNA (45 kph), CPLA (50 kph), CPFAO (52 kph), CPNAO (55 kph).

An additional **influence of visual obstruction on the FoV** at 66 mm/h is present in the CPFAO scenario. Here, the lowest ego speed (19 kph) in combination with the highest target speed (16 kph) is affected.

5.3.3 Chosen intervention AEB or AES

Only in the **longitudinal scenarios** with a high ego velocity (79 kph) a decision was made to select an AES intervention over an AEB intervention. In this case, the difference was marginal. In all cases across nearly all rain rates (camera from 16 mm/h, radar from 66 mm/h), the FoV was limited by the rain rate such that a collision occurred.

5.3.4 Field-of-View analysis results

5.3.4.1 All P-CLwoSO Cases in TRAVIS

All accidents that are caused by the conflict P-CLwoSO can be analyzed with TRAVIS as shown in Figure 43 with approach trajectories of pedestrians relative to the passenger car. The environmental information of the accident (objects, road markings) is hidden. The approach trajectories of the pedestrians are given for this scenario for each of the accidents (n=298) from the GIDAS PCM. The trajectories are colored according to the relative approach speed (green = 0 km/h to red = 120 km/h). The maximum time range of the approach is TTC=5 s. The longer the relative approach trajectory, the more distance is covered within the 5 seconds and the faster the relative approach of the pedestrian. The reason for this is the higher speed of the passenger car, since the walking speed of the pedestrian must be assumed to be limited.
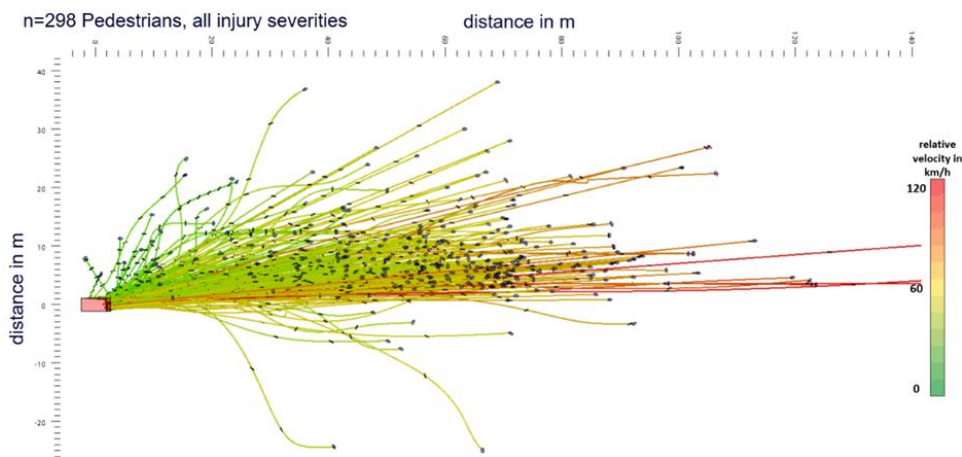
Figure 43. All cases of P-CLwoSO out of GIDAS in TRAVIS.

5.3.4.2 Analysis of Field-of-Views (FoV) of all P-CLwoSO Cases using TRAVIS

Different types of sensors can be added within TRAVIS. The range of a sensor is described as a function of the opening angle. Figure 44 shows the sensor range of the radar and the camera for the trajectories according to with a precipitation rate of 16 mm/h (Deliverable D3.5 [20]). On this basis, it can be evaluated at which TTC pedestrians involved come into the detection range of the radar or the camera. TRAVIS can be used to evaluate how high the proportion of pedestrians involved is in relation to the TTC in the detection range of the radar, the camera or the sensor set overall. A pedestrian is recognized by the sensor if half of the floor area is in the detection area. For a pedestrian to be detected in the sensor set, the pedestrian must be detected either by the camera or by the radar (or condition).
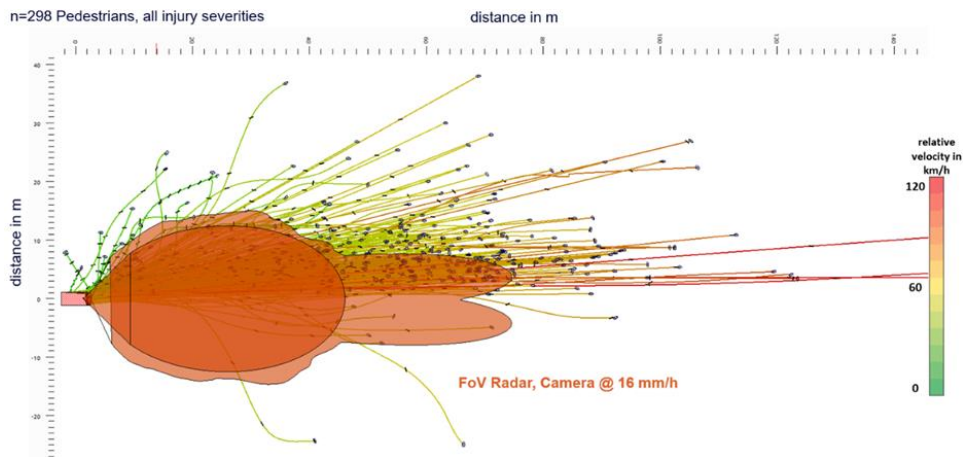
Figure 44. All cases of P-CLwoSO out of GIDAS in TRAVIS with Field of View (FoV) of Radar and Camera at 16 mm/h amount of rain.

Figure 45 shows the proportion of pedestrians in the P-CLwoSO scenario from TTC = 5s to TTC = 0s in the field of view of the sensor set for 0 mm /h precipitation (blue), 16 mm/h precipitation (orange) and 66 mm/h precipitation (yellow) are indicated. There are differences between 1.6 s and 5 s TTC for detected pedestrians. As the TTC increases, the differences in detected pedestrians become larger. Up to a TTC = 1.6 s, 95% of the pedestrians are recognized. The remaining pedestrians above 95% represent special cases.
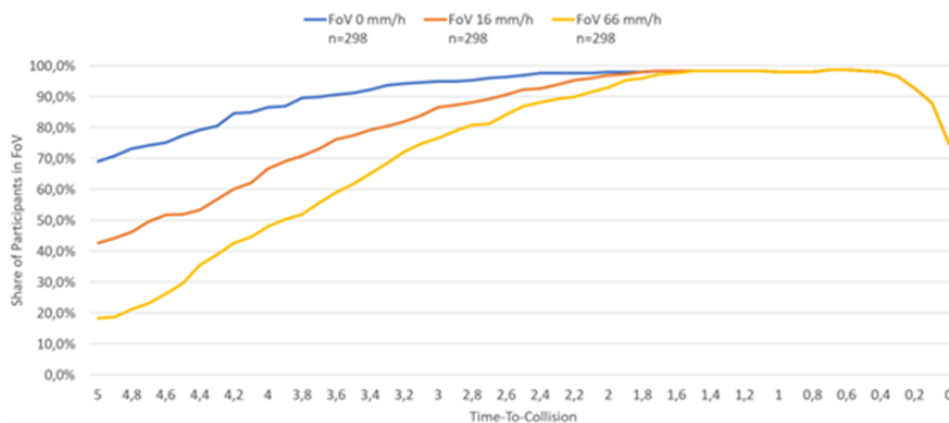
Figure 45. Proportion of Participants in FoV for Sensor Set for Scenario P-CLwoSO from TTC=5 s to TTC=0s.

Criticality of the situation over time based on data from the Traffic Accident Scenario Community of the Fraunhofer Institute for Transport and Infrastructure Systems

To determine the criticality of a driving situation, there is the data basis of the Traffic Accident Scenario Community (TASC) of the Fraunhofer Institute for Transport and Infrastructure Systems (IVI) [24]. This database contains natural driving data and accident data. Accident data is based on traffic accidents recorded by the police. The data is processed to also identify the pre-crash phase of the accidents. The pre-crash information are also available

in PCM format. It is thus possible to describe the pre-accident phase for many accidents and to calculate a TTC between the parties involved. Figure 46 (left) shows an example of a possible course of an accident with the P-CLwoSO scenario. Since the original case is an accident, the TTC drops to 0 s over time. This scenario is varied regarding the possible reaction of those involved to avoid the accident. If a possible reaction nevertheless leads to an accident, the TTC in the corresponding variation is also zero (see Figure 46 - right). However, if the attempt to avoid the accident is successful, then there is a minimum TTC for this variation. For each original case, a set of TTC is formed with the variations (Figure 46 - table on the right). An average minimum TTC is formed from the minimum TTC values for each accident.
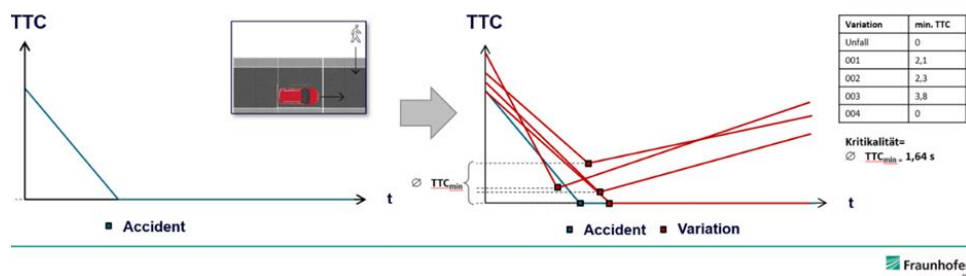
Figure 46. TTC of an accident and average minimum TTC of a maneuver.

The determined average minimum TTC can be used for a driving maneuver or summarized in a scenario and presented as a distribution as shown in Figure 47. The distribution of the minTTC can be divided into deciles and a criticality scale can be derived. Figure 47 on the right shows the violin diagram for the P-CLwoSO scenario based on n=295 cases. The distribution of the TTC shows that a large range of minimum TTC values from 0.5 s to 1.2 s can be found and that this scenario becomes critical in this time range. This shows that when accidents in this scenario are varied, the resulting critical situations reach low TTC values. Accordingly, this time range is also the field of action for safety functions, for which the pedestrians must also be recognized accordingly in this time range—plus any triggering times or reaction time for functions with a response request to the driver.
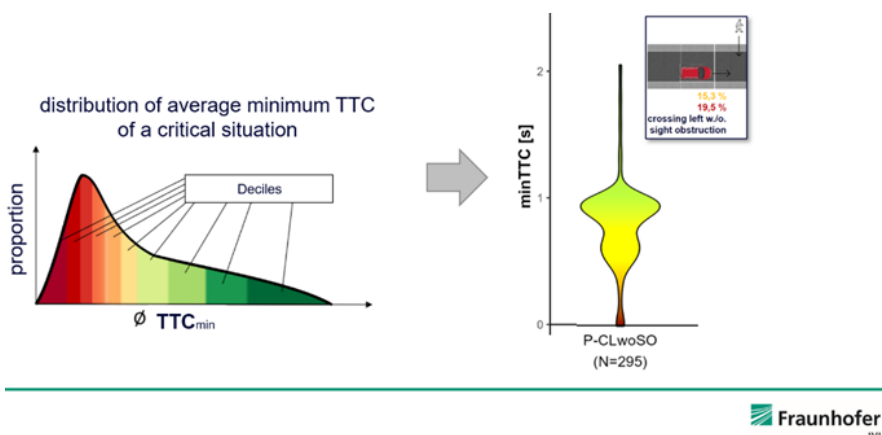
Figure 47. Distribution of average minimum TTC of a critical situation (left) and violin diagram for critical situation P-CLwoSO.

5.3.4.3   Result of Analysis of FoV in TRAVIS and TASC Data

As a result, the proportions of pedestrians detected in the P-CLwoSO scenario can be superimposed using the violin diagram from the analysis of the TASC data as given in Figure 48. The detection rates for the sensor set are very high for all levels of precipitation for the time range in which the respective minimum TTCs accumulate from the variation of the TASC cases. In this time range, a safety function has the option of avoiding impending accidents by intervening. This investigation shows the robustness of the sensor set with respect to precipitation amounts in the relevant time range of the selected scenario P-CLwoSO for the critical situation.
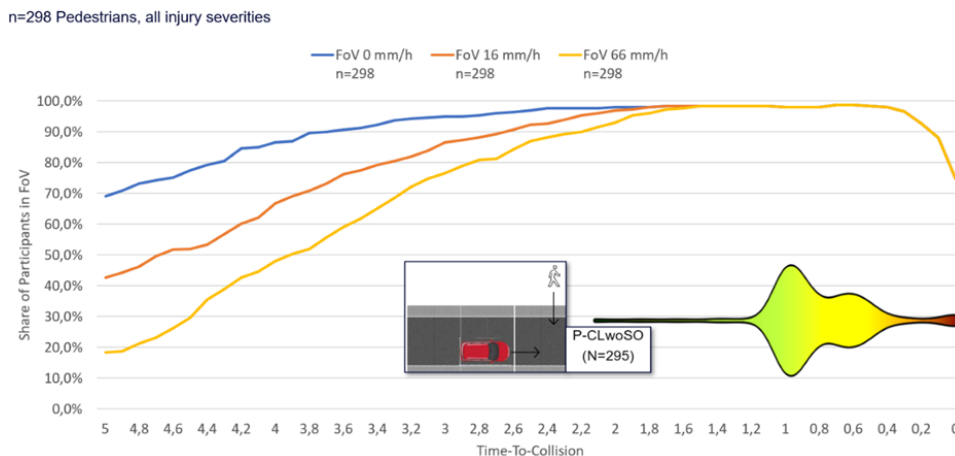
Figure 48. Share of pedestrians within FoV for different precipitation intensities and Violin-plot of the min. TTC based on accident variation.

5.3.5 Third measurement campaign (dynamic)

This chapter details the setup and the evaluation of the third measurement campaign, which was performed in a dynamic setting.

5.3.5.1   Measurement campaign setup

The goal of the third measurement campaign is to generate data to verify the simulative results with real world performances in adverse weather conditions by performing dynamic tests under rainy weather conditions. Therefore, scenarios are selected with possible TTC periods, which are testable in the rain area and are controllable for the test driver in the test hall. The measurement setup for one example is shown in Figure 49 and a more detailed description can be found in Deliverable D3.5 [20].

The following parameter are varied and tested leading to eight configurations, which are tested in the third measurement campaign and compared to simulations:

-    Targets: Pedestrian

-    Rain settings: 0 mm/h, 16 mm/h, 66 mm/h, 98 mm/h

- Vehicle velocity: 2 configurations between 15 kph – 35 kph, which were controllable

- Target velocity: 8 kph

The focus of the measurement campaign is on the perception performance of the radar and camera sensor of the Demo 3 vehicle. No AEB was triggered in the tests.
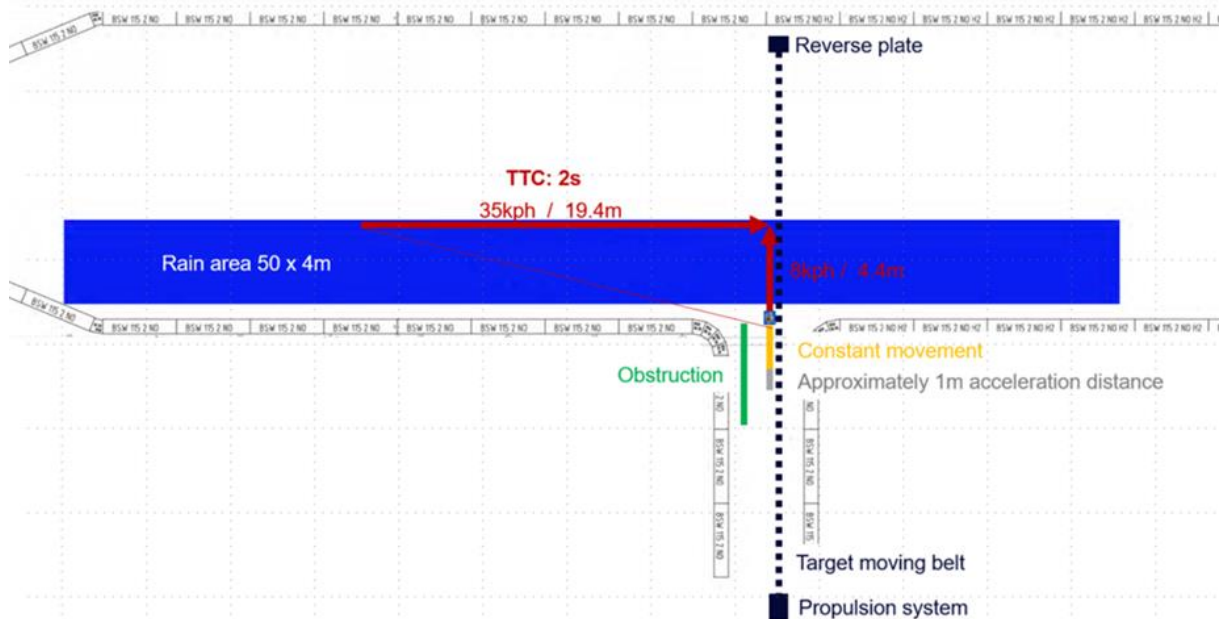
Figure 49. Measurement setup on the example of a mirrored scenario from cluster P-CLwoSO (35 kph vehicle velocity, 8 kph pedestrian velocits, and a TTC of 2 s) [20].

5.3.5.2   Measurement campaign evaluation

As the focus for the comparison to simulative results is on the perception performance of the radar and camera sensor of the Demo 3 vehicle, particularly interesting is the time information at which the pedestrian target was recorded in the object lists. There was one object list exclusively available for the camera sensor and one for the fused information of the radar and camera sensor. In case the radar has detected an object but the camera sensor not, the detection of the radar only can be extracted from the fused information.

Each test case is evaluated based on at which TTC values the pedestrian target is not obstructed by the wall and at which TTC values the target is first detected with the respective sensor. Additionally, the time passed between those two positions is calculated. The results are summarized in Table 16 and described in detail in Deliverable D3.8 (not yet published). The given vehicle velocity in Table 16 is the extracted velocity from the position, at which the radar sensor can theoretically first see the target. In the following, always this velocity is referenced, which is why sometimes for comparisons between the same desired velocity configuration two velocities are given. The pedestrian velocity given in Table 16 is the desired speed programmed into the target system, which is also not constant during the test runs due to readjustments from the light barriers.

Table 16: Summary of the key detection performance results of the third, dynamic measurement campaign (in the cases with * only radar detections are available).

Test case ID	Rain [mm/h]	Vehicle velocity [kph]	Target velocity [kph]	TTC [s] first not obstructed radar	TTC [s] first not obstructed camera	TTC [s] first detected testing fused	TTC [s] first detected testing camera	UTC time offset [s] not obstructed until detected radar/fused	UTC time offset [s] not obstructed until detected camera
1	0	15	8	2.75	2.67	1.82	2.38	0.82	0.26
2	0	35	8	1.97	1.96	1.12	1.57	0.92	0.42
3	16	16	8	2.55	2.46	1.75	2.30	0.68	0.18
4	16	32	8	2.39	2.37	0.53*		1.86*	
5	66	17	8	3.14	3.10				
6	66	33	8	2.25	2.23				
7	98	14	8	3.31	3.26				
8	98	32	8	2.46	2.46				

Only for test case ID 1, 2, and 3 the camera object list as well as the fused object list contains the pedestrian. For test case ID 4 only the radar sensor has detected the pedestrian, and at all other test cases, the pedestrian was neither detected by the camera sensor nor the radar sensor.

The results do not show a degradation of the detection performance due to adverse weather at the settings with 15/16 kph at 0 mm/h and 16 mm/h as the TTC values for first detected are similar and the UTC time offsets between not obstructed until detected are even shorter at 16 mm/h. However, the results show a degradation of the detection performance due to adverse weather at the settings with 35/32 kph at 0 mm/h and 16 mm/h as only the radar has detected the pedestrian at 16 mm/h and this also significantly delayed compared to 0 mm/h.

The results also indicate a degradation in detection performance due to higher vehicle velocities for the settings with 15 kph and 35 kph at 0 mm/h. The time passed between the pedestrian being not obstructed and being detected is higher for the vehicle velocity of 35 kph both for the fused sensors as well as the camera.

Based on these results, it can be assumed that vehicle velocities higher than 15 kph in combination with rain impede the detection performance and, contrary to the expectations from the static measurements, also the rain rate of 16 mm/h can be challenging for radar and camera sensors in dynamic settings for vehicle velocities higher than 15 kph. Even if a detection was possible here, it was with a high time delay.

5.3.5.3 Comparison to simulations

To be able to compare the dynamic test results to simulations, where FoVs from static measurements are integrated, all of the test cases are simulated according to the same methodology as described in Deliverable 3.6 [21] and parameters are extracted like the TTC values, where the object was detected with the video and radar sensor or where the intervention was triggered.

Table 17 summarizes the compared TTCs values from the third, dynamic measurements to the simulation results, where the FoV models derived from the second, static measurement are integrated. In addition, the TTCs at which the intervention was initiated in simulations is included, which shows that at 0 mm/h and 16 mm/h with the vehicle velocity of 35/32 kph,

the detection of the pedestrian with the fused sensors or the radar sensor in testing would have been later than when the generic AEB function has been triggered in simulations.

Table 17. Comparison of the results of the third, dynamic measurement campaign to simulations, where FoV models derived from the second, static measurement are integrated (in the cases with * only radar detections are available or only simulations with radar FoV models are integrated).

Test case ID	Rain [mm/h]	Vehicle velocity [kph]	Target velocity [kph]	TTC [s]						intervention simulation
				first not obstructed		first detected testing		first detected simulation		
				radar	camera	fused	camera	radar	camera	
1	0	15	8	2.75	2.67	1.82	2.38	1.89	1.85	0.95
2	0	35	8	1.97	1.96	1.12	1.57	1.73	1.73	1.26
3	16	16	8	2.55	2.46	1.75	2.30	1.88	1.84	0.96
4	16	32	8	2.39	2.37	0.53*		1.75	1.73	1.22
5	66	17	8	3.14	3.10			1.87	1.84	0.98
6	66	33	8	2.25	2.23			1.75	1.73	1.22
7	98	14	8	3.31	3.26			1.92		0.93*
8	98	32	8	2.46	2.46			1.74		1.21*

In conclusion, the detection performance in the dynamic measurement was considerable lower than to be expected from the results of the simulations, where the results of the static measurement are integrated, especially as no detection with any sensor at any distance was possible at 66 mm/h and 98 mm/h. Due to no detection degradation between 0 mm/h and 16 mm/h at the vehicle velocity configuration of 15/16 kph, but an obvious detection degradation between 0 mm/h and 16 mm/h at the vehicle velocity configuration of 35/32 kph, it is assumed that the influence of the rain rate on sensors should not be evaluated independent of the vehicle velocity.

Therefore, it must be assumed that the sensor models derived from static measurements in Deliverable D3.5 [20] (summary in Chapter 5.2.1) might lack the capability of being also applicable for dynamic scenario with vehicle velocities above 15 kph and that the perception performance at vehicle velocities above 15 kph as well as at rain intensities above 16 mm/h is probably overestimated in the simulations in Deliverable D3.6 [21] (summary in Chapter 5.2.2). However, these effect can also originate to some extent from other limitations, which are summarized in Chapter 5.4 and should be addressed in future work to develop reliable sensor models.

5.4 Challenges

This chapter summarizes the main challenges encountered during the Demo 2 development.

5.4.1 Perception dependency

All results of the measurement campaigns are **dependent on the methodology of the respective analysis** as well as on the **sensor hardware** and the **algorithms** for processing the raw sensor data and cannot be treated as generalizable results. For example, the camera data from the second and third measurement campaign was evaluated based on object lists, which were returned from the camera detection algorithm. For evaluating the returned radar locations from the first and second measurement campaign, different assumptions in the methodology were required to conclude whether the radar sensor detected an object.

Therefore, it is likely that other algorithms or other evaluation methodologies result in different degradations under rainy conditions even if the same hardware would be used, which makes it difficult to conclude generic results of perception under adverse weather conditions. It is necessary to consider the complete chain of hardware and software in a vehicle for assessing the perception performance, and re-evaluation is necessary for each change in the chain.

5.4.2 Virtual testing (difficult as result of demo 2 activities)

The weather filter of the first and second measurement campaign and the FoV models of the second measurement campaign give indications on the detection range of sensors under different adverse weather conditions. Both measurement campaigns were conducted in a static setup, where dummies were placed at a grid of locations to make full use of the testable rain area. The resulting FoV models for the radar and camera sensor were integrated into the simulations and evaluated for various car-to-pedestrian scenarios as described in Deliverable D3.6 [21]. To verify the approach, certain scenarios were simulated as well as tested dynamically in the test hall during the third measurement campaign. In this process, it became evident, even though only few test runs were performed, that **the results of the static measurements do not align with the dynamic tests** and that **the perception performance is not only affected by adverse weather but also by the ego vehicle velocity**. Up to now, there is no approach on how virtual testing can be realized, where sensor degradations of adverse weather conditions at different ego velocities are integrated.

5.4.3 Test equipment and rain system

In order to design various dynamic tests under rain conditions, **large rain areas with realistic rain amounts and friction conditions at the ground would have been required**, as shown in Chapter 5.1.4. In the tests performed in the SAFE-UP project, only a rain area with a size of 50 m x 4 m was available. Therefore, instead of the typical 4 s testing time,

only for example a time of 2 s could have been tested to ensure that the pedestrian dummy is in the rain area during the movement as shown in Figure 49. From the originally planned tests, therefore, only a few remained that could be carried out in the hall. Also, the evaluation of rain amounts at crashes showed that rain amounts up to 5.7 mm/h should be of focus for the investigation, but the lowest possible testable rain condition was 16 mm/h in the test hall. The performance evaluation of an AEB system at wet surfaces would have required realistic friction coefficients, which were above average in the test hall.

In addition, due to ensuring the controllability and safety in the test hall, only a **maximum speed of 35 kph** was possible for testing. Limiting factors were the acceleration and deceleration distance as well as the small distance to the lateral barriers. The poor visibility under the very high rainfall would not have allowed a further reduction of the distance between the vehicle and the barriers for the driver. Another difficulty in the test hall was the high time effort in carrying out the tests. The stronger the rain intensity was the greater the effort to remove the water from the track.

Another challenge was posed by the propulsion system for pedestrian and cyclist targets. While the targets themselves had no problem with the rain, **the used propulsion system has not yet been approved for rainy operation**. The structure had to be designed in such a way that the propulsion system as well as the reversing plate had the maximum possible distance to the rain area to limit the risk that water is dragged into the systems.

Normally, the test system is controlled via a GPS-based system such that the dummy is hit at the predefined hit point without executing an action such as AEB and AES. Since **no device to connect the propulsion system to the indoor positioning system in the hall was available**, it was necessary to switch to light barriers to trigger the target movement. However, these are limiting factors if the speed of the vehicle is not constant and additionally their operation is disturbed during the high rainfall intensities.

5.5 Guidelines/future work

This chapter identifies guidelines based on the insights from Demo 2 and potential further work.

5.5.1 Test equipment and rain system

Two key challenges in testing under rainy conditions were the available rain system and test equipment as described in 5.3.3. Therefore, future initiatives should focus on **developing rain generation systems** which **cover minimum the area of the scenarios described in Chapter 5.1.4** for a time of at least 4 s and which can produce **homogeneous rain with lower intensities**. It should also be ensured that the friction coefficient at the ground is realistic such that the AEB performance can be evaluated not only at different rain intensities, but also at different wetnesses of the road. Also, a **comparison between in-hall and outside tests under rainy conditions** would be beneficial to assess if the reflections inside a hall decrease the detection performance. Additional, future work should be done to

develop waterproof test equipment including propulsion systems, which can be used at rainy conditions and at wet grounds.

5.5.2 Further dynamic testing

As the FoVs generated from the static measurement campaigns could not have been verified with the results of the dynamic measurement campaign, further work should investigate the additional **influence of the vehicle velocity on the detection performance** with more dynamic tests. Due to the high test effort, tests with same specifications were only conducted once and variations would also be expected between different runs of one test case. Therefore, performing tests with same specifications several times would increase the confidence in the results. Additionally, a wider variation of test specifications especially in terms of vehicle velocities and realistic rain intensities would be required to assess the influence on the detection performance.

In addition, the results described in Chapter 5.2.2 showed that in simulations the reduced friction caused crashes. These results must be further analysed with **testing at rainy conditions and wet surfaces with realistic friction coefficients and state-of-the-art AEB systems**.

5.5.3 Reliable friction estimation

If testing at rainy conditions and wet surfaces with state-of-the-art AEB systems also shows a potential for improving emergency interventions with a weather-dependent design, it has to be analyzed **how the friction coefficient can be reliably estimated and predicted by the vehicle**. Currently known friction coefficient measurement options do not determine the friction coefficient in such a quality and continuity that it should be used for safety functions as by earlier triggering also the likelihood of false positives rises.

6. Demo 3 Vehicle integrated BRAKING & SWERVING FUNCTIONS to avoid collisions with other vehicles and VRUs

The scope of Demo 3 is to develop advanced vehicle dynamics intervention functions to avoid or mitigate critical events. More specifically, the main goal is the development of advanced active safety systems including autonomous emergency steering (AES) as a novelty. Therefore, special focus is given not only in the development of a fully-functional demonstrator, but also in understanding the potential field of effect of such a system, especially in comparison to current state-of-the-art active safety systems.

6.1 Scenario selection

The goal of the following Demo 3 scenario selection process is to identify scenarios that cannot be avoided by state-of-the-art active safety systems and have the theoretical potential to be avoided by AES. These scenarios are then used to steer Demo 3 development towards a real-world safety benefit by directly addressing accident types that are not yet covered by any active safety system. Two simulation analyses were performed throughout the project with to goal of quantifying a potential AES field of effect in the relevant VRU accident scenarios.

The first analysis is based on an exemplary GIDAS Pre-Crash-Matrix (PCM) accident data set [27] solely for crossing pedestrian cases and can be found in the deliverable report D3.3 [25]. As the PCM cases contain a high-fidelity reconstruction of the accidents, this analysis gives a very realistic insight into the real-world accident avoidance potential. The results show that 12% of additional accident cases could be avoided by AES. However, the representativeness of these results is limited, as PCM cases are only a subset of the German In-Depth Accident Study (GIDAS) dataset and no further weighting was performed.

Therefore, a second simulation analysis is used to match the overall project scope. It focuses on a holistic scenario selection process considering all relevant SAFE-UP scenario clusters identified in the deliverable report D2.6 [19]. To ensure that all potential cases are covered, a full-factorial simulation experiment serves as the basis for the scenario selection. The relevant Demo 3 scenarios are then selected based on a filtering process considering both accidentology relevance and technical feasibility. The following sections focus on this second simulation analysis. A detailed description of the approach can be found in the deliverable report D3.6 [21].

6.1.1 Scenario selection method

The scenario selection method is based on a simulation of generic implementations of Autonomous Emergency Braking (AEB) and Autonomous Emergency Steering (AES) systems. Those systems are simulated and applied to vehicles involved in synthetically generated accidents derived from the Virtual Vehicle co-simulation platform, described in the deliverable report D5.3 [18]. Based on an assessment of the accident avoidance potential, accident clusters are formed and specified by their parameter distributions. Figure 50 shows an overview of the simulation process.
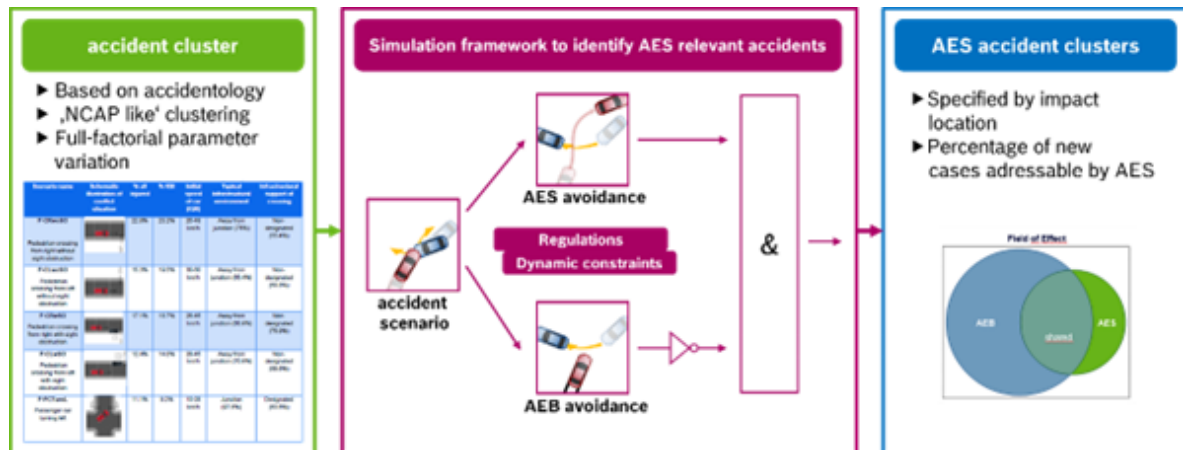
Figure 50. Scenario selection methodology overview.

Single accident scenarios are generated out of the full-factorial simulation experiment, based on the relevant accident scenarios defined in the deliverable report D2.6 [19]. These single accident scenarios are then simulated with the application of both an AEB and an AES maneuver. The respective maneuvers are applied separately, no combined AEB/AES maneuvers are considered. A case becomes relevant for AES only when AES accident avoidance is feasible while AEB accident avoidance is impossible.

To be able to generate useful and realistic simulation results, several assumptions must be made. A detailed description of these assumptions can be found in section 3.1.2 of the deliverable report D3.3 [25]. Figure 51 shows an overview of the general simulation assumptions.
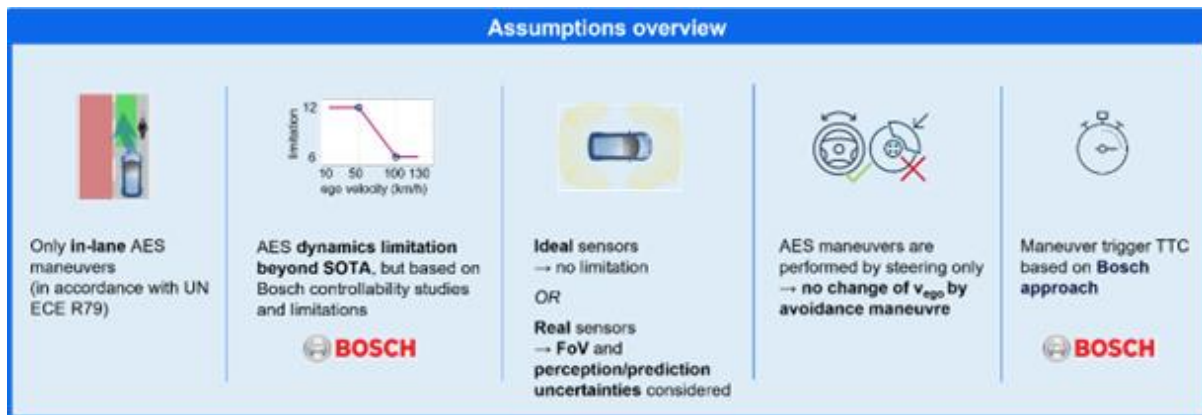
Figure 51. Simulation assumptions for the assessment of the accident avoidance potential of an AES maneuver.

Additionally, both Field-of-View limitations and perception and prediction uncertainties derived from sensor specifications or measurements are modeled.

The relevant AES scenarios are selected based on Ego vehicle and VRU velocity ranges which show a relevance according to accident analyses. The process of the velocity ranges definition can be found in the deliverable report D3.6 [21].

6.1.2 Selected Demo 3 AES accident clusters

The basis for the Demo 3 scenario selection process is formed by the most relevant accidents with killed or severely injured road users (KSI) identified in in the deliverable report D2.6 [19], which mainly are crossing pedestrian and bicyclist cases with and without sight obstruction:

- P-CRwoSO – Pedestrian crossing from right without sight obstruction
- P-CRwSO – Pedestrian crossing from right with sight obstruction
- P-CLwoSO – Pedestrian crossing from left without sight obstruction
- P-CLwSO – Pedestrian crossing from left with sight obstruction
- B-CRwoSO – Bicyclist crossing from right without sight obstruction
- B-CRwSO – Bicyclist crossing from right with sight obstruction
- B-CLwoSO – Bicyclist crossing from left without sight obstruction
- B-CLwSO – Bicyclist crossing from right with sight obstruction

For the definition of the AES accident clusters, only cases without sight obstruction are considered. For the obstruction cases, it is expected that the time for the perception algorithm to initially detect and spawn an object has a big influence on the performance. As it turned out to be rather complex to model these effects in a way that the simulation results can be used reliably for the scenario selection, the results without obstruction serve as the basis for the obstruction cases as well. The obstruction effect will then be assessed as part of the safety benefit assessment through simulative and physical testing.

The results are clustered based on the impact location. Frontal collisions are separated into close corner and distant corner, referring to the ego vehicle's corner in relation to the direction the VRU is coming from (see pictograms in the following tables). Side crashes form the third cluster.

For each of the clusters, parameter distributions for ego and VRU velocity, lateral or longitudinal impact location (lateral for frontal impact, longitudinal for side impact) and lane width are given as boxplots showing median and 25%/75% percentiles. Additionally, the complete range of the respective parameter is shown in the top of the table cell. Furthermore, the avoidance share compared to all simulated accidents of the respective cluster is given in the last column. For the lane width, a median value of 3.5m can be found in all of the identified clusters.
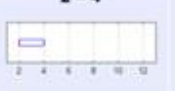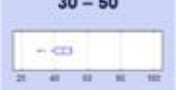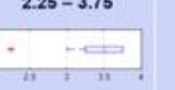
Table 18 and Table 19 contain the final scenarios for the pedestrian and bicyclist cases respectively. As different velocities for the bicyclist crossing from left and right are relevant according to accident analyses, the clusters are not identical, in contrast to the pedestrian cases.

6.1.2.1 Pedestrian

For the pedestrian cases, the avoidance shares for both clusters *frontal impact, close corner* cluster, where the AES maneuver would avoid the accident by steering *into* the walking direction of the pedestrian, and *frontal impact, distant corner*, an avoidance share of 3.7% respectively was identified. For both frontal impact clusters, ego velocities are close to the maximum values given by accidentology with median values around 50kph, whereas pedestrian velocities are rather low with median values around 2kph. Impact locations are mostly on the edge of the ego vehicle.

The side impact cases show a still quite high avoidance share of 37.7%. Ego velocities are comparable to the frontal impact cases, whereas pedestrian velocities are higher compared to the frontal impact cases with a median value around 4kph. Impact locations mainly distribute around the front half of the vehicle.

Table 18. AES relevant and feasible accident clusters: pedestrian.

Scenario	Impact location	Ego velocity [kph]	VRU velocity [kph]	Lat./Long. crash impact location [%]	Lane width [m]	Avoidance [%]
P-CRwoSO / P-CLwoSO Pedestrian crossing from right/left without sight obstruction	Frontal impact, close corner	40 – 50	2 – 8	-5% – 0%	3 – 3.75	3.7
P-CRwoSO / P-CLwoSO Pedestrian crossing from right/left without sight obstruction	Frontal impact, distant corner	40 – 50	2 – 4	90% – 105%	2.25 – 3.75	3.7
P-CRwoSO / P-CLwoSO Pedestrian crossing from right/left without sight obstruction	Side impact	30 – 50	2 – 10	-4.5% – 104.5%	2.25 – 3.75	37.7
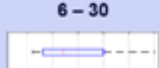
6.1.2.2 Bicyclist

For the bicyclist cases crossing from right, the avoidance shares for the *frontal impact, close corner* cluster, where the AES maneuver would avoid the accident by steering *into* the walking direction of the pedestrian, a neglectable avoidance share of 0.6% was identified, whereas the avoidance share of the *frontal impact, distant corner* cluster disappears completely. The ego velocities remain quite high with a median value of 70kph, whereas cyclist velocities are rather low with a median value of 2kph. Impact locations are mostly on the edge of the ego vehicle.

The side impact cases show a higher avoidance share of 35.2%. Ego velocities are comparable to the frontal impact cases with a slightly lower median value around 70kph, whereas cyclist velocities are higher compared to the frontal impact cases with a median value around 12kph. Impact locations mainly distribute around the front half of the vehicle.

For the bicyclist cases crossing from left, the avoidance shares for both the *frontal impact, close corner* cluster and the *frontal impact, distant corner* cluster disappear completely.

The side impact cases show a remaining avoidance share of 10.6%. Ego velocities are lower compared to the frontal impact cases with a median value of 45kph, whereas cyclist velocities are slightly lower compared to the frontal impact cases with a median value of 10kph. Impact locations also mainly distribute around the front half of the vehicle.

Table 19. AES relevant and feasible accident clusters: bicyclist.

Scenario	Impact location	Ego velocity [kph]	VRU velocity [kph]	Lat./Long. crash impact location [%]	Lane width [m]	Avoidance [%]
B-CRwoSO Bicyclist crossing from right without sight obstruction	Frontal impact, close corner	45 – 70	6 – 12	-45% – -20%	3 – 3.75	0.6
B-CRwoSO Bicyclist crossing from right without sight obstruction	Frontal impact, distant corner					0
B-CRwoSO Bicyclist crossing from right without sight obstruction	Side impact	25 – 70	6 – 30	-4.5% – 104.5%	2.25 – 3.75	20.8
B-CLwoSO Bicyclist crossing from left without sight obstruction	Frontal impact, close corner					0
B-CLwoSO Bicyclist crossing from left without sight obstruction	Frontal impact, distant corner					0
B-CLwoSO Bicyclist crossing from left without sight obstruction	Side impact	25 – 50	6 – 30	-4.5% – 104.5%	2.25 – 3.75	10.6

6.1.3 Summary and Discussion

In this analysis, scenarios are considered as AES scenarios if accident avoidance using AEB is impossible and accident avoidance using AES is possible. Accident avoidance is identified using a simulation study based on synthetically generated accident trajectories with full-factorial parameter variations. Only cases without sight obstruction were considered. The relevant Field-of-Effect for the Demo 3 AES development includes both accidentology relevance in terms of ego and VRU velocities as well as technical feasibility in terms of sensor FoV and perception and prediction uncertainties.

The AES accident clusters were further split into three impact location clusters:

1. Frontal impact, close corner

2. Frontal impact, distant corner

3. Side impact

The results show limited avoidance shares for the pedestrian cases with frontal impact location and a quite big avoidance share for the side impact cases. For the bicyclist cases, avoidance shares for the frontal impacts can be neglected, whereas the side impact cases show a significant avoidance share.

All frontal impact clusters show impact locations distributing narrowly around the edge of the ego vehicle. The side impact clusters show impact locations mainly distributing around the front half of the ego vehicle.

Ego velocities always distribute to the maximum value, as AES avoidance potential, especially compared to AEB avoidance potential increases with higher velocities. The inverse effect occurs for the VRU velocities, where the AES avoidance potential increases with lower VRU velocities, as less lateral displacement is required for complete accident avoidance.

These AES accident clusters serve as the basis for the physical testing case selection, which is described in the following section.

6.2 Physical testing campaign

6.2.1 Test campaign setup

A real-world testing campaign of the developed Demo 3 AES system was performed at the IDIADA proving ground facilities in Santa Oliva, Spain, using the BOSCH Demo 3 vehicle as well as state-of-the-art VRU dummy test systems. A detailed description of the developed Demo 3 system can be found in the deliverable reports D3.3 [25] and D3.6 [21]. The general purpose of the test campaign was the generation of the accident avoidance rate statistics under real-world conditions for a low number of test scenarios but with a rather high number of repetitions per scenario. These repetitions per scenario are needed due to the scattering VRU detection performance, leading to different trigger timing for the avoidance system and

hence to different accident avoidance outcomes. Figure 52 shows an impression from the test campaign.

Figure 52. Impression from Demo 3 physical testing.

The following scenarios were tested using both AES and AEB, with approximately 10 runs per system setting (AEB or AES). The scenarios were selected based on the Demo 3 scenario selection method described in the previous section. The lane width for all scenarios was set to 3.5m and the AES maneuver was developed in conformity with the UNECE R79 ESF regulation [26] which only allows in-lane evasion maneuvers. Figure 53 contains a visualization of the tested scenarios, including the definition of the impact location.

a) **P-CRwoSO**, frontal, close corner, ego vehicle speed vEgo = 50 kph, pedestrian speed vPed = 6 kph, lat. impact location = 0 (Pedestrian crossing from right, leading to a frontal impact on the right edge of the vehicle's front)

b) **P-CRwoSO,** side, ego vehicle speed vEgo = 50 kph, pedestrian speed vPed = 6 kph, long. impact location = 0.3 (Pedestrian crossing from right, leading to a side impact on the first third of the vehicle's side)

c) **P-CRwSO**, frontal, close corner, ego vehicle speed vEgo = 50 kph, pedestrian speed vPed = 6 kph, lat. impact location = 0 (Pedestrian crossing from right, leading to a frontal impact on the right edge of the vehicle's front)

d) **P-CRwSO,** side, ego vehicle speed vEgo = 50 kph, pedestrian speed vPed = 6 kph, long. impact location = 0.3 (Pedestrian crossing from right, leading to a side impact on the first third of the vehicle's side)
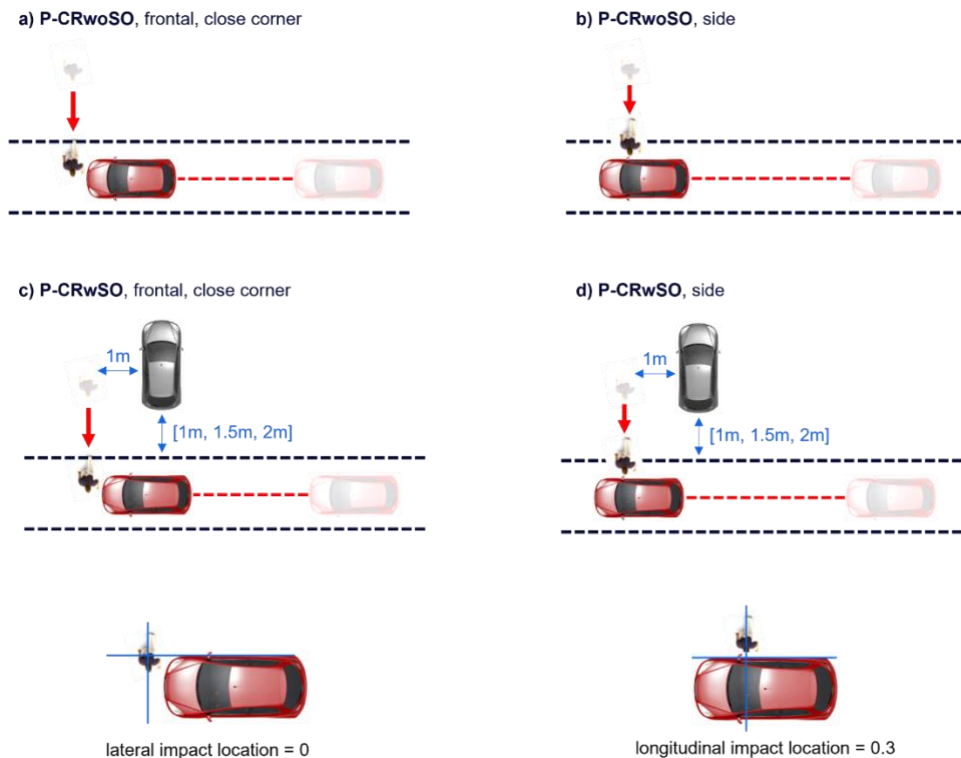
Figure 53. Tested crossing pedestrian scenarios.

To generate the late object detection that makes the AES necessary for a complete avoidance manoeuvre, all of the scenario parameter combinations for the cases with sight obstruction were tested with different obstruction settings, where the obstruction was placed in such a way that 1m, 1.5m and 2m of lateral distance between the obstruction and the outer edge of the vehicle's lane remained.

Both pedestrian speed and impact location parameters were not varied during the test campaign, as the performance was satisfying even with the worst-case parametrization as described above. As the changes mainly result in a change in detection timing, their effect is expected to be estimated in post-processing as well.

6.2.2 Test campaign evaluation

In the following, an evaluation of the frontal collision cases of the physical testing campaign is presented (**P-CRwoSO**, frontal, close corner and **P-CRwSO**, frontal, close corner). The side collision cases are not included, as due to timing constraints not enough runs could be performed to generate significant results. Note that the side collision cases are not included in the virtual simulations as well, as it is expected that their occurance probability in real world accidents is rather low.

Figure 54 shows both AES (green) and AEB (red) avoidance rates for the different sight obstruction settings. The exact number of corresponding runs is given at the top end of each bar. Note that the number of repetitions varies for the different obstruction settings.
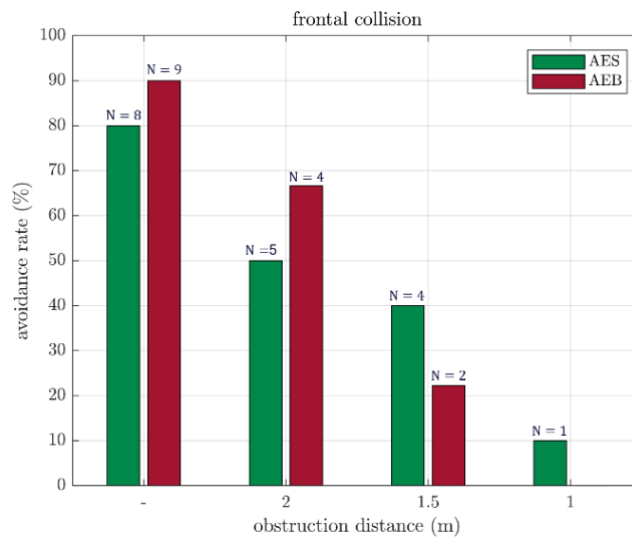
Figure 54. AES (green) und AEB (red) accident avoidance rates for all obstruction variants in the frontal collision case.

The figure shows a higher AEB avoidance rate compared to the AES avoidance rate for cases without sight obstruction and for 2m sight obstruction distance. For the closer obstruction distance of 1.5m, leading to a later trigger time for the systems, the AES avoidance rate exceeds the AEB avoidance rate. For 1m obstruction distance, only one single AES intervention leads to a completely avoided accident. In general, both AEB and AES avoidance rates decrease with closer obstruction settings.

In all not avoided AES cases the crash constellation changes from a frontal collision to a side collision. Note that the VRU dummy speed remained constant at all times. The left graph of Figure 55 shows the percentage of these cases for the different sight obstruction settings. In the right graph, the distribution of the side impact locations is shown, with zero refering to the frontmost part of the vehicle's side. These results show that in the majority of the cases, the impact location is changed to be on the rear half of the vehicle's side.
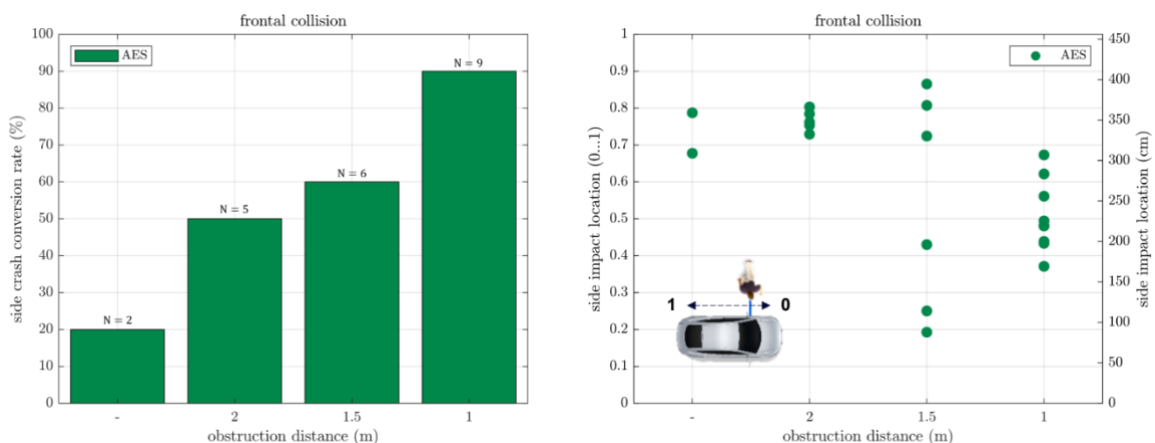
Figure 55. AES side crash conversion rate (left) and distribution of side impact locations (right, 0 = front) for all obstruction variants in the in the not avoided frontal collision cases.

In all not avoided AEB cases the collision speed is reduced. The left graph of Figure 56 shows the percentage of these cases for the different sight obstruction settings. In the right graph, the distribution of the remaining collision speeds after the intervention is shown. These results show that in the majority of the cases, a significant collision speed reduction can be achieved.
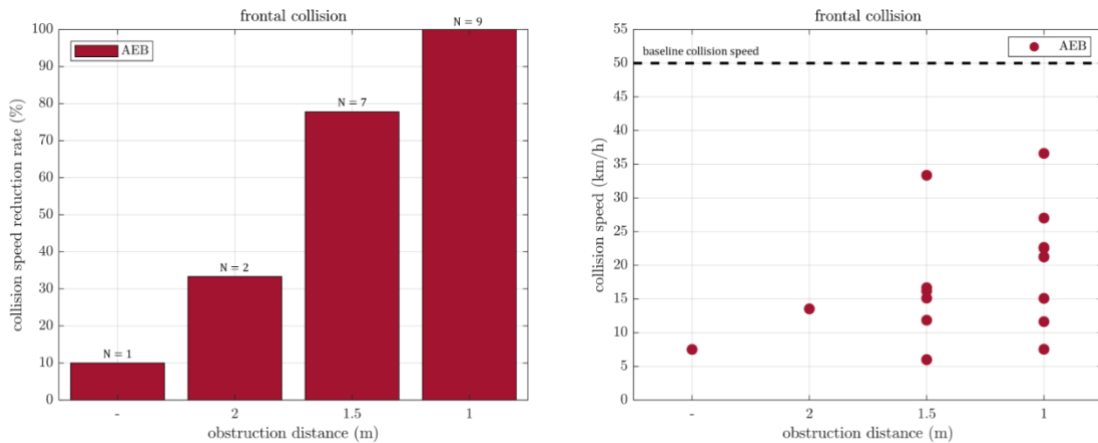
Figure 56. AEB collision speed reduction rate (left) and distribution of collision speeds (right) for all obstruction variants in the in the not avoided frontal collision cases.

Figure 57 shows the distribution of the trigger times for AES (left, green) and AEB (right, red). Note that the Demo 3 trigger logic is implemented in a way that both systems are allowed to trigger as soon as a potential collision based on the predicted VRU position is detected (details see deliverable report D3.6 [21]). The graphs show the delay in triggering the functions due to the closer obstruction settings.
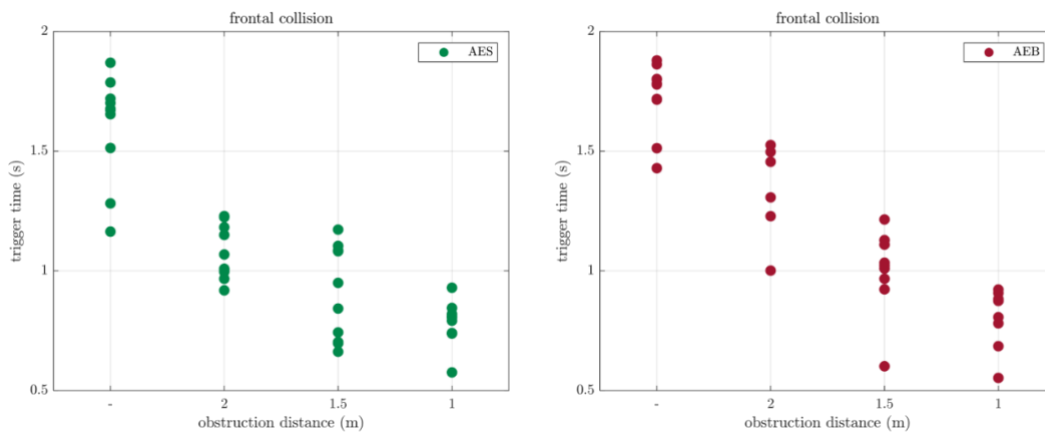
Figure 57. AES (green) und AEB (red) trigger time distribution for all obstruction variants in the frontal collision case.

In the following, example cases are shown for both AEB (Figure 58) und AES (Figure 59) interventions for an obstruction distance of 1.5m.
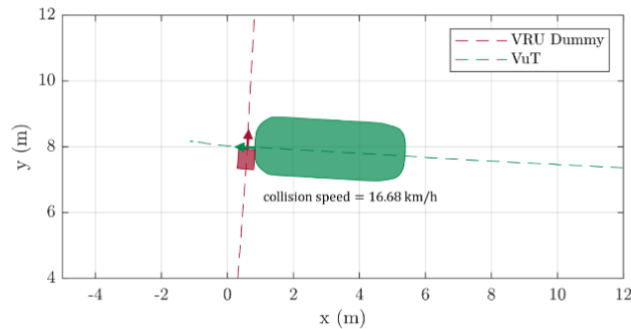
Figure 58. P-CRwSO AEB example case with 1.5m lateral obstruction distance, leading to a crash with collision speed v_{coll} = 16.68 km/h.

In the AEB case, the collision can not be avoided and the intervention leads to a remaining collision speed of 16.68 km/h.
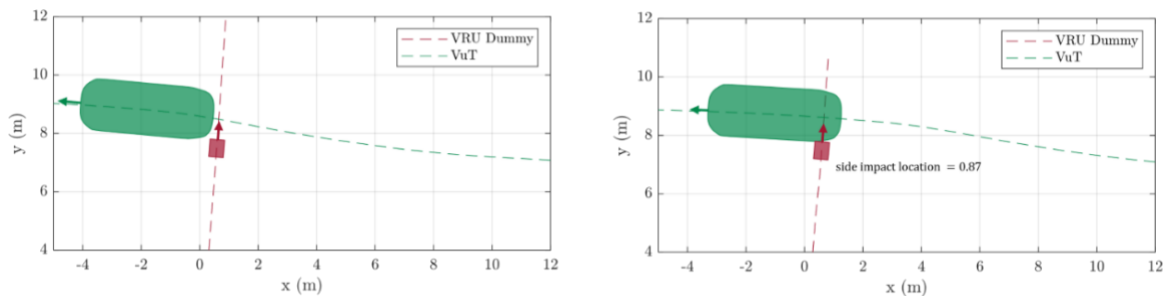
Figure 59. Two P-CRwSO AES example case with 1.5m lateral obstruction distance, leading to full accident avoidance (left) und to a crash (right) with side impact location xsil = 0.87.

For AES, two examplary cases are displayed. The collision in the case shown on the left part of Figure 59 can be completely avoided, while the collision can not be avoided in the case shown on the right part of the figure and the intervention leads to a side collision with an impact location of 0.87.

6.2.3 Discussion

The physical testing campaign yields real-world evidence that in crossing pedestrian scenarios with close sight obstruction, AES can generate an additional accident avoidance potential compared to state-of-the-art AEB systems. In cases where AES fails to avoid the accident, the collision impact location is changed to be on the side of the vehicle, with the majority of the cases showing impact locations at the rear half of the vehicle's side. As the current state of research lacks the knowledge of how this change in crash constellation effects the resulting accident severity, no final statement can be given in this regard. However, side impact locations behind the A-pillar may result in a reduced accident severity. Additionally, side crashes at the rear part of the vehicle may also be avoided by the pedestrian, which has the ability to abruptly stop his movement after a passing vehicle is detected. For a final assessment of the AES safety benefit, these two effects would have to be compared to the AEB velocity reduction in cases where no full accident avoidance is possible. For an initial estimation of how the changed impact loaction might affect the expected accident severity, Figure 60 and Figure 62 show the distribution of accident severities clustered in the categories minor, severe and fatal for different regions of both frontal and side car vs. pedestrian accidents, extracted from the GIDAS database and weighted to German national level.
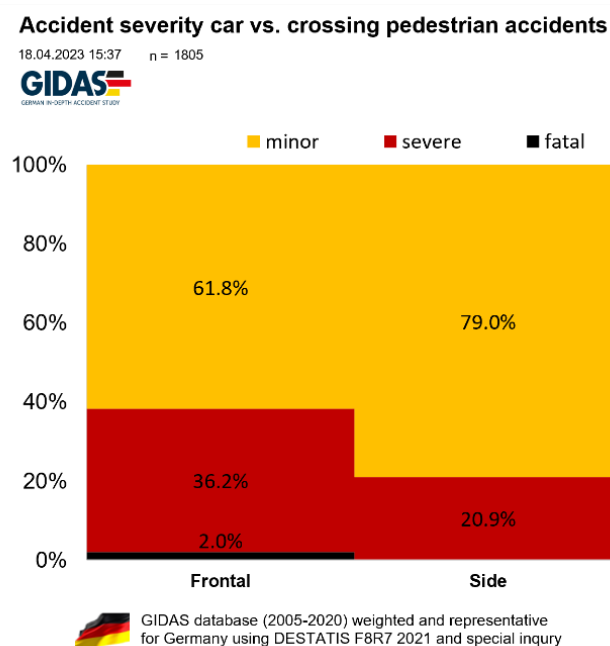
Figure 60. Distribution of accident severities clustered in the categories minor, severe and fatal for frontal and side car vs. pedestrian accidents.
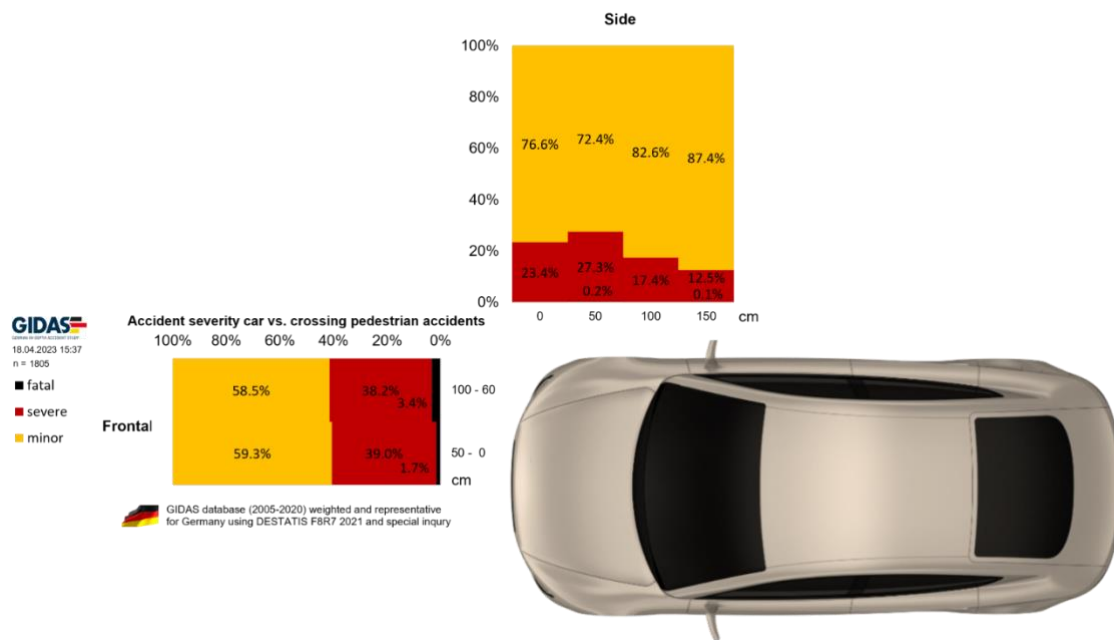
Figure 61. Distribution of accident severities clustered in the categories minor, severe and fatal for different regions of both frontal and side car vs. pedestrian accidents.

These results show that statistically, side crashes result in a lower number of severe accidents than frontal crashes (20.9% compared to 36.2%) and the number of fatal accidents is reduced to 0%, compared to 2% in frontal crashes. Furthermore, for side crashes that happen behind the first 50cm of the vehicle front, the number of severe accidents further reduce. Note that the database does not contain any usable data for side crashes happening behind 150cm of the vehicle front, which might be an indication that crashes where the pedestrian walks into the rear half of the vehicle's side are very unlikely to happen.

Furthermore, the results show that with delayed trigger timing, the AES accident avoidance potential compared to state-of-the-art AEB accident avoidance potential increases. One possible reason for this delay in the trigger timing are sight obstructions, as considered in the test campaign. However, in real-world accident situations it is expected that several reasons may lead to a delayed trigger timing, e.g. less ideal conditions for the perception system (light, weather, many objects, …) or VRUs suddenly changing direction to cross the road. These effects were idealized in the test campaign with good lighting and weather conditions, an empty test track and constant VRU speeds. Therefore, it is expected that in real-world conditions, where trigger timing may be further delayed for the described reasons, the AES accident avoidance potential compared to state-of-the-art AEB accident avoidance potential may further increase.

7. Demo 4 REAL-TIME SAFETY WARNINGS to VRUs' smart devices via enhanced communication among vehicles, infrastructure and a dedicated APP

Demo 4 in SAFE-UP project implements communication of V2X messages, in order to enhance the perception of traffic actors about their surroundings, with main objective to detect possible collision situations between vehicles and VRUs and timely present a warning to the user, so that he can react to avoid the accident, or in the case of the vehicle to also trigger an automated function like the vehicle's AEB system. Demo 4 is dealing with three kind of human traffic participants: drivers of vehicles, riders of bicycles (cyclists) and pedestrians. These are the intended recipients of warnings emitted by the "safety application" within each corresponding individual system.

7.1 Scenarios selected

The scenarios selected focused first on crashes with high KSI relevance, in urban areas and related to VRU's, especially non-designated pedestrian crossings and cyclist crossings. Besides this, since the developed system aims not only at providing timely warnings but also at triggering an active safety system (e.g. AEB), scenarios that are aimed by these systems by state-of-the-art technology (SOTA), were considered. Besides these general considerations, the main inputs considered for the scenario selection have been:

1. The accidentology results performed in SAFE-UP within D2.6 (Bálint, et al., 2021), which provides an overview of the accident data figures in terms of relevant passenger car to VRU collisions associated with serious injuries and fatalities (KSI). The recommendations for scenarios related to C-ITS solutions have been considered.

2. The SOTA of active safety system with VRU detection. For this, the (Euro NCAP, 2020) protocol which addresses not only the activation of AEB VRU systems but also the warnings provided to drivers is considered.

3. C-ITS technology relevance, considering situations where communication technology may have a safety benefit potential, such as the cases where there are obstructions that hinder the VRU visibility by a vehicle.

Based on the above inputs, the method followed to identify Demo 4 relevant scenario is following the steps shown under Figure 62.
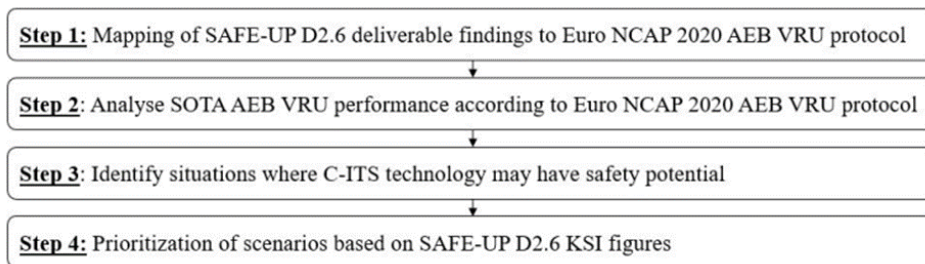
Figure 62.Steps followed for detailed scenario selection of SAFE-UP Demo 4

Within the proposed method, the Euro NCAP 2020 AEB VRU protocol which was the latest protocol at the time of the Demo 4 selection, has been used as reference, not only for the mapping of relevant accident scenarios from the accident data (Step 1), but also to understand what the performance level of a 5-star rated vehicle is like (Step 2). In this second step it was analysed whether the vehicle could avoid, mitigate, or not avoid the collision with the VRU. Only for the Step 1, the recently available Euro NCAP 2023 AEB VRU protocol was considered for the mapping of accident scenarios.

Towards the selection of scenarios, the situations which could be relevant for C-ITS technology were identified, such as when there are limitations from a perception point of view due to obstructions or field of view limitations, as these would represent limitations of SOTA AEB VRU systems (Step 3). Finally, a prioritization of scenarios based on KSI figures was considered since SAFE-Up has a target to meet 10% reduction of injuries and fatalities in road accidents (Step 4).

Following the 4 steps mentioned in the method, in Figures 63 and 64 the selected scenarios are shown for both Passenger car to pedestrian and Passenger car to cyclist scenarios

Scenario ID	Abbreviation	Step 1	Step 2	Step 3	Injury Coverage (%KSI)	Initial Speed (Km/h) PC	P	Proposed Speed (Km/h) PC	P	Test cases
Demo_4_01	P-CRwSO	CPNC (2020)	Mitigation	C-ITS	18.8	26-45		25-45	8	5
Demo_4_02	P-CRwSO	CPNC (2020)	Mitigation	C-ITS	18.8	26-45		35-65	5	7
Demo_4_03	P-CLwSO	N/A	N/A	C-ITS	14	28-45		30-45	8	4
Demo_4_04	P-CLwSO	N/A	N/A	C-ITS	14	28-45		35-65	5	3
Demo_4_05	P-PCTurnLo	CPTA (2020)	No activation	C-ITS	9.3	10-28		10-30	5	5
Demo_4_06	P-PCTurnLo	CPTA (2020)	No activation	C-ITS	9.3	10-28		10-30	8	5
Demo_4_07	P-PCTurnRo	CPTA (2020)	No activation	C-ITS	2.2	11-25		10-25	5	4
Demo_4_08	P-PCTurnRo	CPTA (2020)	No activation	C-ITS	2.2	11-25		10-25	8	4

Figure 63 Passenger car to pedestrian scenarios

Scenario ID	Abbreviation	Step 1	Step 2	Step 3	Injury Coverage (%KSI)	Initial Speed (Km/h) PC	C	Proposed Speed (Km/h) PC	C	Test cases
Demo_4_09	B-CR(+Obs)	CBNAO (2020)	No activation	C-ITS	37,8	5-30	10-18	15-30	15-20	8
Demo_4_10	B-CL(+Obs)	N/A	N/A	C-ITS	25,5	7-32	12-20	15-30	20	4
Demo_4_11	B-CR	CBNA (2020)	No activation	C-ITS	37,8	5-30	10-18	10-25	15-20	8
Demo_4_12	B-CL	CBFA (2020)	No activation	C-ITS	25,5	7-32	12-20	10-30	20	5
Demo_4_13	B-PCTurnRs	N/A	N/A	C-ITS	7,5	10-30	14-20	10-30	15-20	10
Demo_4_14	B-PCTurnLs	N/A	N/A	C-ITS	10	11-29	12-21	10-30	15-20	10

Figure 64: Passenger car to cyclist scenarios

Further information on the selection method and the results can be found both in SAFE-UP Deliverable D3.4 [8] From the scenario selection, IDIADA implemented a detailed characterisation of the scenarios to have a clear procedure towards the physical testing,

which is available in D3.7 [14]. A summary of the selected scenarios for Demo 4 is available in the following sections.

7.1.1 Demo_4_01 & Demo_4_02: Approaching a pedestrian crossing from nearside

Figure 65 show the diagram of the scenarios Demo_4_01 and Demo_4_02, which represent a situation where an approaching pedestrian is crossing the road from the vehicle's nearside (right side) with obstruction in form of parked vehicles.

Figure 65. Demo_4_01&02 scenario diagrams

Table 20 shows the relevant parameters of the Demo_4_01 and Demo_4_02 scenarios

Table 20. Demo_4_01 & Demo_4_02 testing parameters

Scenario	Euro NCAP-based scenario	VRU type	VUT speeds (kph)	VRU speeds (kph)
Demo_4_01	CPNA	Pedestrian	25-45 (every 5 kph)	8
Demo_4_02	CPNA	Pedestrian	35-65 (every 5 kph)	5

7.1.2 Demo_4_05 & Demo_4_06: Approaching a crossing pedestrian walking from farside while turning to the farside

Demo_4_05 and Demo_4_06 represent a turning situation where a pedestrian is crossing the road from the farside while a vehicle is turning towards the same road, as show in Figure 66.
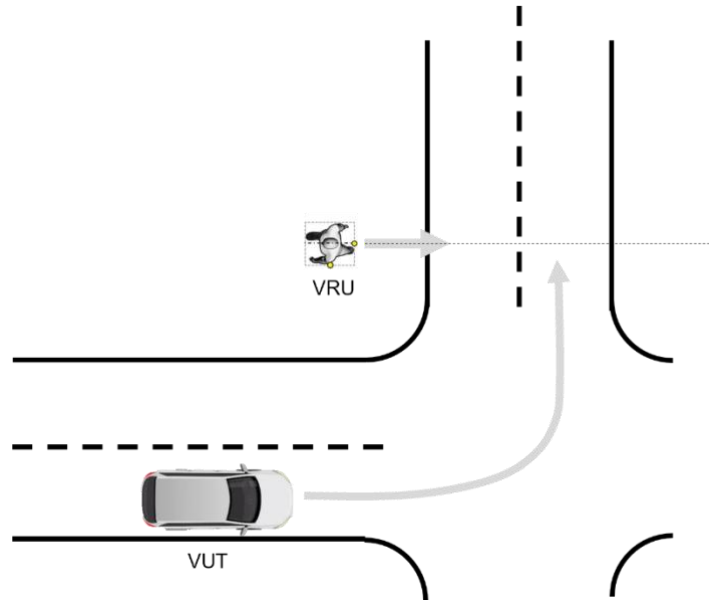
Figure 66. Demo_4_05&06 scenario diagrams

Table 21 shows the relevant parameters of the Demo_4_05 and Demo_4_06 scenarios

Table 21. Demo_4_05 & Demo_4_06 testing parameters

Scenario	Euro NCAP-based scenario	VRU type	VUT speeds (kph)	VRU speeds (kph)
Demo_4_05	CPTA	Pedestrian	10-30 (every 5 kph)	5
Demo_4_06	CPTA	Pedestrian	10-30 (every 5 kph)	8

7.1.3 1.1.3 Demo_4_08: Approaching a bicyclist crossing from nearside obstructed

Figure 67 shows the diagram of the Demo_4_08 scenario, which is a crossing situation involving a bicyclist and a passenger car, where the VRU is crossing from the nearside.

Figure 67, Demo_4_08 scenario diagram

Table 22 presents relevant parameters of the Demo_4_08 scenario

Table 22. Demo_4_08 testing parameters

Scenario	Euro NCAP-based scenario	VRU type	VUT speeds (kph)	VRU speeds (kph)
Demo_4_08	CBNAO	Cyclist	15-30 (every 5 kph)	15-20 (every 5 kph)

7.1.4 Demo_4_09: Approaching an obstructed bicyclist crossing from farside

Demo_4_09 is the inverse of Demo_4_08 scenario, where a bicyclist is crossing the road from the farside while a vehicle is approaching, as shown in Figure 68

Figure 68. Demo_4_09 scenario diagram

Table 23 shows the relevant parameters of the Demo_4_09 scenario

Table 23. Demo_4_09 testing parameters

Scenario	Euro NCAP-based scenario	VRU type	VUT speeds (kph)	VRU speeds (kph)
Demo_4_09	CBFAO	Cyclist	15-30 (every 5 kph)	20

7.1.5 Demo_4_13: Approaching a crossing bicyclist moving from farside while turning to the farside

Demo_4_13, like Demo_4_05 and Demo_5_06, is a turning scenario. In this case, a bicyclist is crossing from the farside while the vehicle is turning to the same road on the farside, as shown in Figure 69.
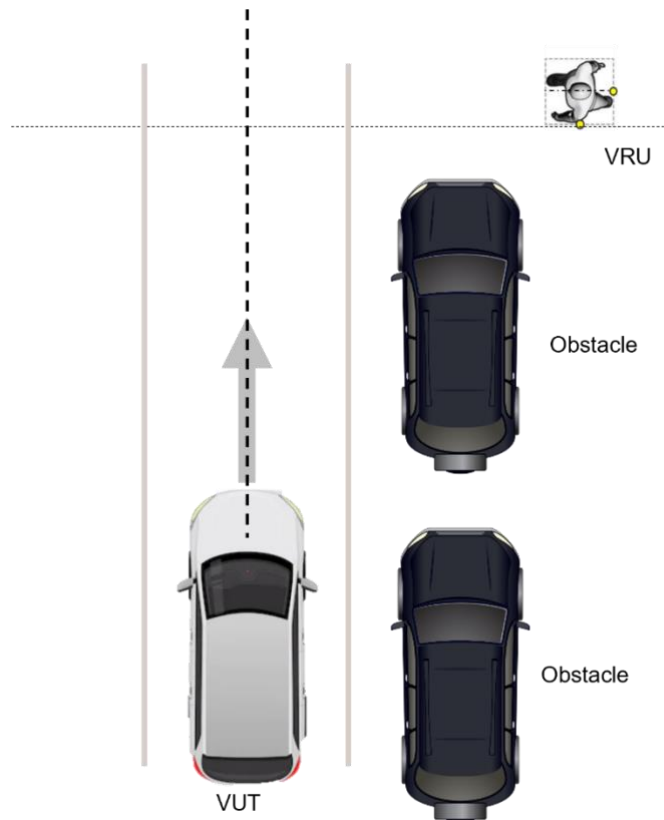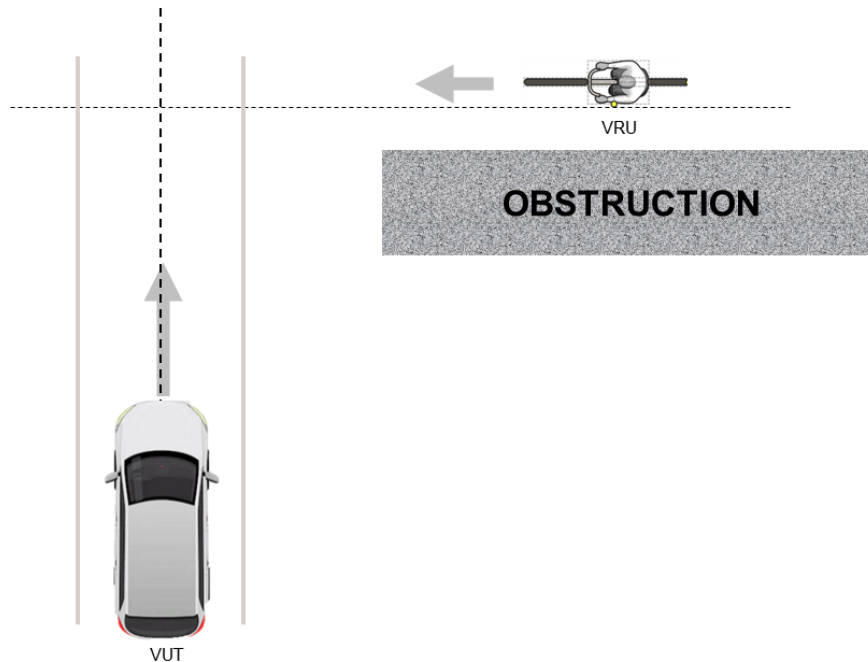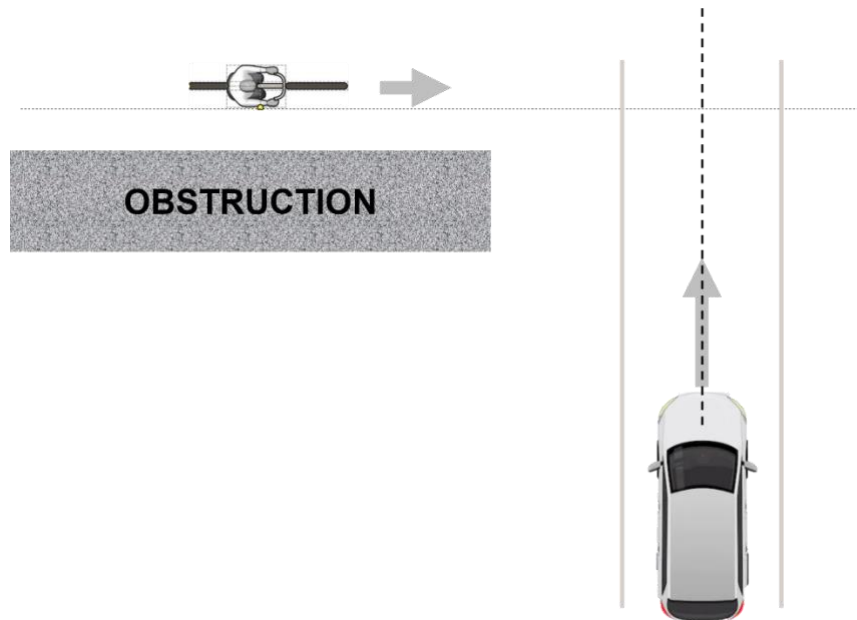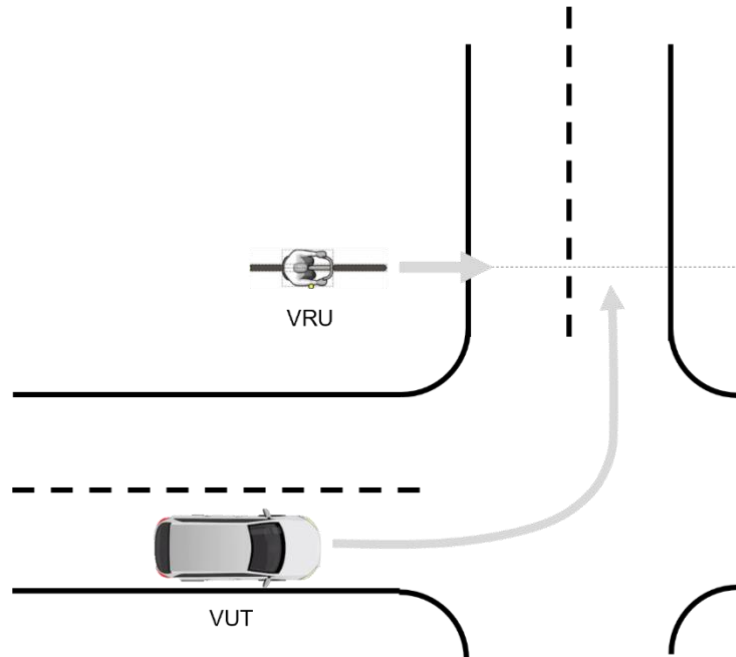

Figure 69. Demo_4_13 scenario diagram

Table 24 shows the relevant parameters of the Demo_4_13 scenario

Table 24. Demo_4_13 testing parameters

Scenario	Euro NCAP-based scenario	VRU type	VUT speeds (kph)	VRU speeds (kph)
Demo_4_13	CBTA	Cyclist	15-30 (every 5 kph)	15-20 (every 5 kph)

7.2 Testing / Challenges

7.2.1 Introduction

A modern vehicle, equipped with on-board sensors like cameras, lidars, radars etc, is able to monitor its surroundings for possible objects in its route path, that could cause a collision. In this case, the position of any "obstacle" is determined relatively to the detecting sensor's position and the accuracy of this detection depends on the sensor's hardware and software capabilities and quality. Obviously, in the real world there can be obstacles or environmental conditions, that limit the effective range of the on-board sensors and therefore reducing their perception capabilities. By communicating with other traffic participants and exchanging awareness messages with them, the perception range can be increased and be directly related to the communication range of the used RF transceiver. The main difference though with the on-board sensors is that the vehicle, or every other connected traffic participant that receives these messages, are now relying in information produced by sensors installed on the transmitting station. The communicated position is now an absolute position and the precision of it, depends on the capabilities of the GNSS receiver installed on the transmitting station. Any poor positioning solution either due to bad GNSS coverage in the area of interest, or due to the use of older, low end GNSS receiver, will lead to connectivity perception deterioration.

For safety critical applications in automotive, like collision warnings and actions or countermeasures for collision avoidance, the accuracy of assessments for self geo positioning and kinematic parameters is crucial. The transmission of such awareness information with low confidence in accuracy can lead to the service failing in its objective either by not detecting near future collisions, or by producing too many false positive results. In transport industry safety critical applications as well as autonomous driving do need high accuracy positioning services that will most likely include hybrid solutions like fusion with IMUs and GNSS corrections, like for example RTK. Also, enhancement services by the current constellations, like the High Accuracy Positioning Services (HAS) that are scheduled to be offered in full in the near future (2024) by Galileo, seem extremely promising since it targets positioning performance of 20 cm. All these enhancements can certainly increase the confidence levels of an ITS station's assessment about it's own position and movement parameters.

The main focus of Demo 4 in SAFE-UP was the evaluation of V2X communications playing the role of an "extra" sensor from the vehicle's perspective and an enhancement of human situational awareness from the VRU's perspective. Due to safety limitations during in-project testing, a real human VRU and a real vehicle never co-existed in any test case scenario. The vast majority of tests were conducted with a vehicle and a dummy pedestrian playing the role of VRU. There was also some limited testing that involved a human cyclist and a virtual vehicle (vehicle's OBU transmitted the awareness messages of a predefined path that intersected with the cyclist's path). Also, project's limited resources rendered the pedestrian's VRU device too valuable to risk its destruction in a possible collision, so only the GNSS antenna was installed in the dummy's platform. A "safe" compartment should ideally be constructed in the dummy platform for the placement of the VRU V2X device in

order to fully exploit the fusion of GNSS and IMU sensor outputs that can be present in any modern localization modules.

The way a VRU perceives an oncoming collision warning and the time that is needed for correct perception and avoidance reaction, is extremely important and directly related to the optimal TTC that initially triggers this warning. Extensive testing should be conducted in the future for various scenarios and with VRUs with different perception and reaction profiles (children, elderly etc.). Since safety issues will always exist in such testing, augmented or mixed reality procedures should also be considered in future.

A factor that also needs to be addressed when we are considering V2X connectivity for VRUs is the availability of such communication devices specially tailored for their needs. For the case of cyclists, wheelchair and any kind of micromobility user, the direction can be pretty straightforward. Devices like the OBUs installed on connected vehicles, with special adjustments in dimensions, weight and sensor interfacing, can be produced and properly installed on the bicycle's, or scooter's bodies. In the case of pedestrians however, that already use a personal device for their modern communication needs, any V2X solution should be somehow embedded in it and operate (automatic or on-demand) when the user is having the role of a pedestrian in traffic environments.

The following sections describe in detail specific challenges overcome during Demo 4 testing.

7.2.2 Larger obstacles for the obstructed cyclist scenarios

Based on the GIDAS-PCM analysis for the Demo 4 scenarios from D3.7 [14], the most common obstruction for car-to-cyclist scenarios are structural circumstances (e.g., walls, buildings, etc.). It was agreed that a larger obstacle different than the passenger car should be used for the Demo 4 cyclist scenarios.

This way, the obstructed cyclist scenarios (*Demo_4_08: Approaching a bicyclist crossing from nearside obstructed* and *Demo_4_09: Approaching an obstructed bicyclist crossing from farside*) with dummies have been performed with using larger vehicles (i.e., 2 vans) with dimensions shown in Figure 70.

Figure 70. Dimensions of the large obstruction used for the Demo 4 cyclists scenarios

Therefore, the final Demo_4_08 and Demo_4_09 diagrams look like Figure 71 and Figure 72. The scenario parameters are not altered and can be found in D3.7 [14].
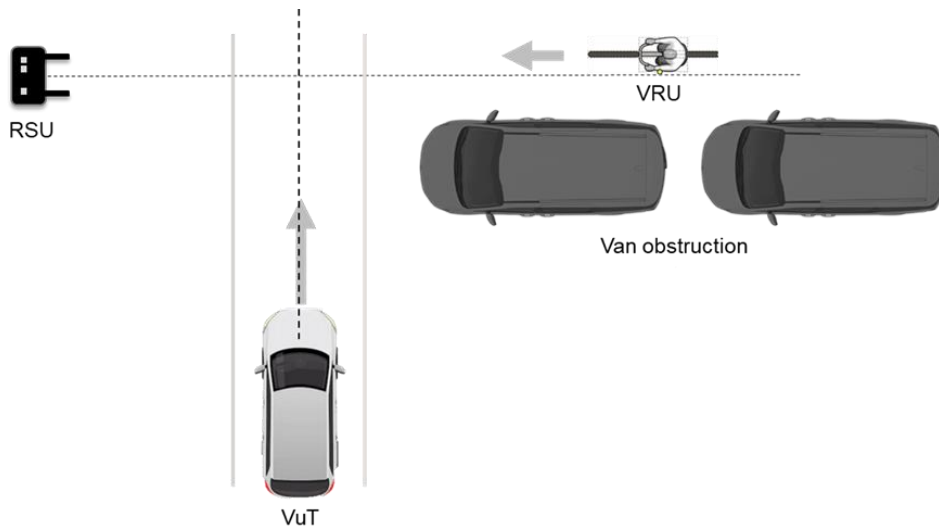
Figure 71. Demo_4_08 with large obstruction
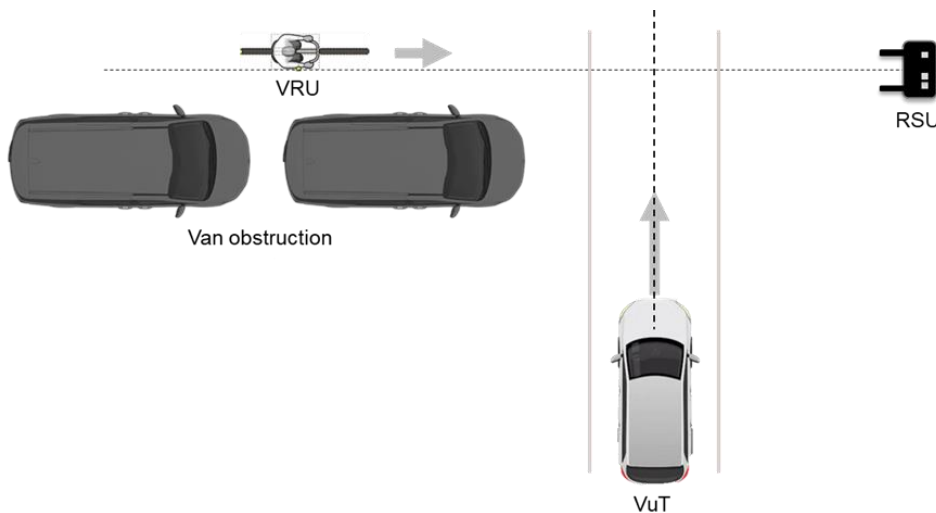
Figure 72. Demo_4_09 with large obstruction

However, the GIDAS-PCM analysis shows that most car-to-cyclist scenarios involve even larger obstacles, like walls or buildings. Therefore, it could be advisable to represent Euro NCAP car-to-cyclist tests with more realistic obstacles than two large vehicles.

7.2.3 VRU V2X device's location for Euro NCAP scenarios

For the testing on the test tracks, the dummies take the role of the VRUs in the scenarios. As a result, the VRU device (described in D3.4 [8] and D3.7 [14]) must be attached to the dummies' platforms during the execution of the scenario, in order to be able to transmit the CAM messages as long as the dummy is moving with the correct location information.

However, during the preparation phase, IDIADA's testing team highlighted the chances of having hits in certain scenarios, especially at high speeds. It was therefore highlighted that this could jeopardise the integrity and safety of the VRU device, since when the dummies are hit, they are thrown several meters away, as shown in Figure 73.

Figure 73. Picture of a scenario ending with crash

The main reason why the VRU device should be installed on-board the dummy platform is due to the need to capture the exact location at every moment. Therefore, IDIADA and CERTH worked in an off-board solution in which only the GNSS antenna of the VRU device is attached to the dummy, while the rest of the device is placed in a safe location without any damage risk.

The following diagram shows the approach developed to solve this safety issue. It consists of a 11m flexible cable which connects the VRU device with the GNSS antenna attached to the dummies.
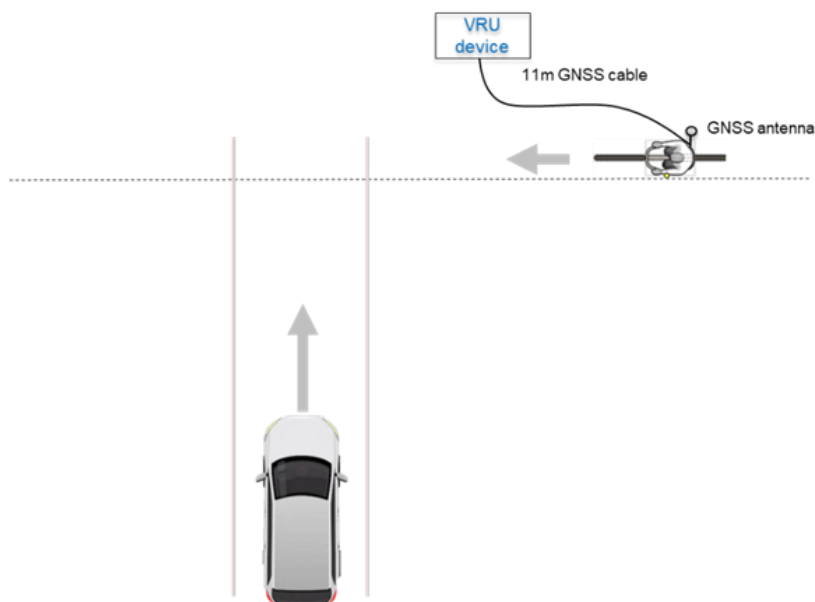
Figure 74. Diagram showing VRU V2X device location

The current off-board solution for SAFE-UP uses the Demo 4 VRU V2X pedestrian device (specifications available in D3.7 [14]), which is a portable but fragile device which was designed for pedestrians, but not to be integrated into the current NCAP equipment and support high-speed impacts usually happening in Euro NCAP tests.

Despite this solution worked for the SAFE-UP tests, V2X Euro NCAP scenarios would require an integrated V2X device into the platform for dummies. This integrated solution has been developed within SECUR project [15], but it was not commercially available during SAFE-UP lifetime.

An alternative would also be that the positioning and dynamics information of the dummy platform during the scenario are sent by an external V2X device, on behalf of the dummy. This similar approach has been followed for the virtual vehicle solution used in the real cyclist testing (details can be found in D3.7 [14]), as a similar approach has been designed within SECUR project [15] as well.

However, this solution does not provide a realistic fading and destructive effects on the signal of the V2X communications due to the obstructions. As any other communication technology, objects between the transmitter and the receiver affect the signal quality, which would not be experienced if using an external V2X device not integrated in the dummy platform.

7.2.4 Crash avoidance scenarios and V2X

There are two critical requirements that V2X-based scenarios needs to fulfil:

7.2.4.1 Low latency

Current V2X technologies (ITS-G5 and C-V2X) offer good latency values, as analysed in [16], which are around 100 milliseconds in the worst-case conditions. However, V2X latency is very dependent on the number of users, which would not be a concern for Euro NCAP testing, due to the low number of V2X stations involved, but that would mean that realistic situations (e.g., city centres, crowded intersections, etc.) may bring different results.

Moreover, safety-critical scenarios require a maximum latency of 50ms, which could potentially be too low for certain technologies (e.g., LTE-V2X) and would require that newer communication technologies should be used (e.g., 5G-V2X).

7.2.4.2 Positioning accuracy and sensitivity

The Demo 4 scenarios are safety-critical and based on sharing accurate positioning information between the actors (vehicle, RSU and VRU). The CAM messages sent between the entities, which contain the required minimum information for these crash-avoidance type scenarios like coordinates, speed, and heading (see D3.4 [8] for the complete full list of data), are basic messages defined by the ETSI ITS standard (ETSI EN 302 637-2 [17] which are mandatory to be sent by all V2X stations.

Thus, using CAM messages is a safe way to guarantee the compatibility between the V2X devices in the scenarios.

However, since these kinds of message contain positioning information, the accuracy of the data must be ensured. The VUT is expected to use highly accurate GNSS systems, some of them based on RTK technology, but the VRU devices are usually simpler, and its positioning depends on general GNSS systems (e.g., Galileo, GPS, GLONASS) which cannot guarantee two critical requirements:

7.2.4.3 Accuracy of few cm (~3cm)

Euro NCAP scenarios are meant to be executed with high-precision equipment which allows fine assessments. The positioning of the entities is a critical system which need to be compliant with the highest standards in terms of accuracy and reliability. Currently, non-V2X scenarios from Euro NCAP are executed with equipment provided by Tier 1s that complies with such standards, which leads to the need to have the same accurate systems for the positioning of the VRUs when V2X technology is required for safety-critical scenarios.

7.2.4.4 Response times on slow movement

Due to the initial location of the dummy platforms in certain scenarios, in which they are quite near the impact point and their trajectory consists of a few meters, the standard GNSS systems does not work reliably. They usually have troubles when stationary or moving at slow speeds but work well when the entity is already moving at certain medium-high speed. Highly accurate and sensitive positioning systems are required to ensure repeatable and consistent scenarios by providing accurate data in all scenarios and conditions.

7.3 Guidelines Results

7.3.1 Introduction

SAFE-Up Demo 4 aimed at developing an on-user active safety system, which could increase vulnerable road users (VRU's) safety enhanced by communications. Communication technology now works on two different approaches, one being DSRC (Dedicated Short-Range Communication) and the other one which is based on cellular wireless mobile telecommunications technology [1]. The communications can take place between vehicles (V2V), with infrastructure (V2I), with pedestrians (V2P) and to the cloud (V2C) [1]. The main applications of this technology aim to address aspects such as improved road safety and traffic efficiency among others [2] while it still has some challenges to address, such as latency, reliability, and security, which makes it a technology under development.

Roadmaps for this technology has been drafted both by the European Commission and by the Car 2 Car Communication Consortium, which is a consortium gathering industry and research partners aiming to achieve vision zero with the contribution of communication

technology [4]. The roadmaps use different terms between them but they both consider a stepwise implementation of the technology with regards to road safety.

- Step 1: Related to providing safety related information and awareness driving. Some examples include in-vehicle speed limits, road works warning and local hazard notification.

- Step 2: Sensing driving, which includes advanced warnings and VRU's protection.

At the same time, Euro NCAP has included V2X in its 2030 roadmap and aims at capitalizing in industry approaches in systems that improve driver information, raise situational awareness, and warn of imminent hazards [5]. Similarly, to the roadmaps defined by the European Commission and the Car 2 Car Communication Consortium, Euro NCAP aims at stepwise approach, focusing first on technology which is existing in the market such as local hazard [6] but considering further safety applications based on technology maturity and evolution.

When it comes to SAFE-Up Demo 4, the proposed system aimed at tackling VRU's protection, which is related to the above-mentioned Step 2 in the proposed roadmaps. Some recommendations have been made on the need to research areas in this field [7] which include among others the need to identify high-risk situations regarding pedestrians and places and the definition of triggering conditions for delivery of VRU warnings. Both aspects have been addressed by SAFE-Up Demo 4 [8][9]. However, it must be considered that Demo 4 is not aiming to deliver a ready to use product, but it focuses in developing a prototype with which the safety potential of communication technology can be explored. There are still several challenges that need to be addressed before this technology is introduced in the market and therefore before it is considered for any upcoming consumer assessment protocol, such as Euro NCAP. Among these challenges, below a quick summary is listed but there could be others as mentioned under [7].

- The accuracy of the positioning of VRUs and vehicles

- The need to integrate necessary signals following standard communication procedures

- The fact that this technology has been assessed in a controlled environment, so aspects such as false activations or warning perception and acceptance by either driver or VRU is not assessed.

Besides the above-mentioned limitations, it must be considered that V2x technology relies on a network of connected devices and infrastructure, which may not be available in all areas. For reference, Japan since 2015 has been aiming to deploy this technology but within 6 years it could equip 113 intersections in 8 prefectures, showing the need for public road authorities' involvement [10]. This shall also be considered in EU, where a platform for harmonised deployment from Member States already exists, named C-ROADS [11].

7.3.2 Test results and Demo 4 scenario relevance

Regarding the concept of SAFE-Up Demo 4 proposed solution, it has been conceived as a safety measure, with several functionalities, considering both connected and non-connected VRUs.

- <u>Warning to driver</u>: For drivers, timely warnings would be issued, when pedestrians are crossing the roads or cyclist appearing when least expected

- <u>Warning to road users</u> (for connected VRUs only): For connected VRUs, warnings would be issued to a connected device when they approach a vehicle and there is imminent risk of collision.

- <u>Activation of active safety system</u>: The vehicle active safety system would activate based on the information received via communication systems rather than from the sensors that the vehicle may be equipped with, making V2X a support feature of the active safety systems.

Based on the fact that during the testing performed, no warning reaction could be assessed, there is no proposal for consideration at this time, since this human reaction behaviour should be carefully considered before making any proposal for assessment. Therefore, the potential safety effect of the proposed technology focuses on the activation of active safety system and its crash avoidance potential.

The proposed scenarios, as mentioned in section 7.1 are related to situations where there is a limitation in the field of view of the driver, which makes it challenging for sensors to perceive and recognise potential VRUs in the surrounding environment.

The results showed that:

- The state-of-the-art active safety systems already show a good performance in the proposed test scenarios, but in some cases the systems reach its limits and even if they avoid the collision, there distance at stop is too small. With V2X, it could be seen that this distance is increased thanks to the early information provided by communication technology. All results are available in D5.3.

- Turning scenarios are quite challenging in terms of execution, since the proposed speeds go beyond the ones defined in current Euro NCAP VRU scenarios. This makes the trajectory definition more complex, and this trajectory is having a strong influence on the underlying state of the art active safety system, making it difficult to reach a conclusion on these scenarios.

- During testing, it was observed that since the communication technology relies on the earlier messages being delivered, at higher speeds such messages could be delivered earlier, although the effectiveness of the active safety system or warnings at higher speeds would face other challenges that need to be carefully addressed.

- For the bicyclist crossing scenarios, the position of the obstruction was based on current Euro NCAP VRU protocol [12] and the obstruction element could consider a different position to have a closer representation of urban environments where communication technology could be considered. Figure 75 shows the considered bicyclist crossing scenario from right, where D_L and D_x represent the distance between the obstruction and the vehicle under test path and the distance between the obstruction and the bicyclist, respectively. D_L value is 3.55m while D_x is 4.8m.
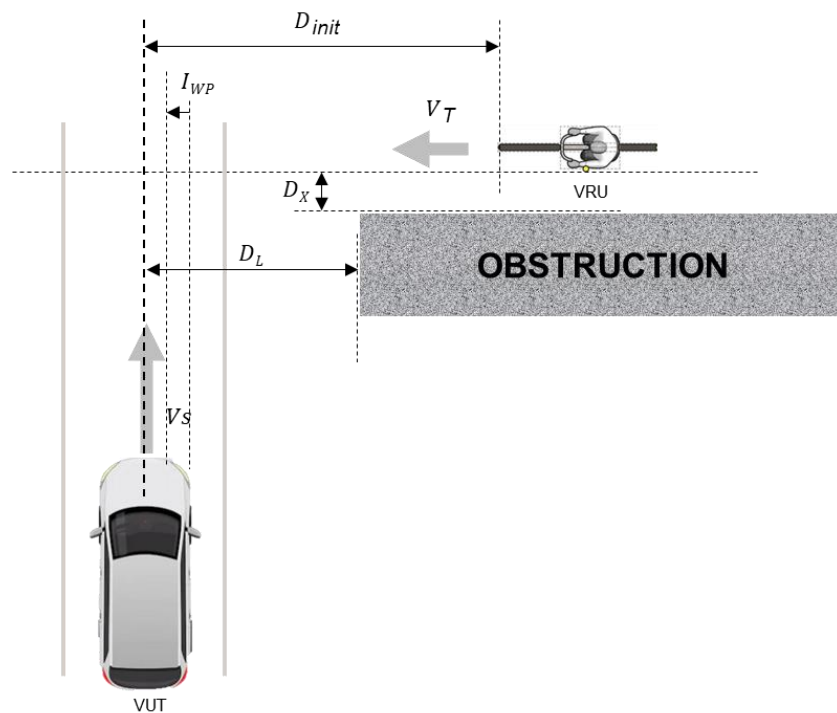
Figure 75. Demo_4_08 scenario parametrization

In summary, from the physical test, it was found during the SAFE-Up Demo 4 testing that turning scenarios are quite challenging from an execution point of view due to the lack of repeatability found during testing. Therefore, if scenarios were to be considered, the ones related to obstruction elements would be more relevant, both for pedestrian and cyclist. Further investigation would be required regarding the position and size of the obstructions.

8. Conclusions

8.1 Demo 1 Occupant MONITORING combined with ADAPTIVE RESTRAINT system for new seating positions.

The development of restraint systems in vehicles has traditionally focused on upright seating positions dictated by legal and consumer crash testing protocols. However, with the emergence of autonomous vehicles (AVs), where the driver becomes a passenger, there is a need to consider alternative seating positions such as reclined or rearward shifted. Current passive safety systems are limited by legislation, which does not account for reclined seating positions.

As future AV journeys are expected to involve non-driving activities, the interior design and seating positions will likely change. To address this, an occupant monitoring system (OMS) can detect different seating positions and occupants' anthropometries, providing valuable information to adapt the restraint system's parameters, including airbag pressure, tape lengths, pre-tensioner firing times, and load-limiter forces. The SAFE-UP project's WP4 team extensively studied various restraint system layouts using virtual environments, evaluating their effectiveness.

One particular layout, "Adaptive actuators" (System Layout 2), was selected for implementation in the physical environment.

The OMS developed within SAFE-UP project utilizes sensors and person recognition modules to infer occupant characteristics and seating positions. It considers the variability in gender diversity, stature, and mass to ensure the system can generalize and minimize bias. Seated posture is a critical factor for adaptation, determining whether the airbag should be deployed or suppressed based on the occupant's proximity to the airbag.

Human pose estimation, typically based on computer vision, is employed to determine body keypoints and spatial relationships. This information helps compute distances to the airbag and other restraint systems for adaptation. Additionally, the state of the seat belt is considered to enhance safety during a crash event.

In highly automated vehicles, where occupants engage in non-driving tasks, additional information such as the presence of objects between the airbag and the occupant's hands becomes crucial for adaptation. To cover a wide range of scenarios and reduce bias, the SAFE-UP project conducted extensive data collection, including anthropometry groups, seat configurations, body movements, and various activities.

The integration of OMS and adaptive actuators in the restraint system represents a significant advancement in vehicle safety. It enables the system to adapt to individual passengers' anthropometry and posture, ensuring optimal protection based on real-time data. This research contributes to improving the safety of autonomous vehicles and paves the way for future advancements in restraint systems tailored to a wider range of seating positions in AVs.

Throughout the SAFE-UP project, the implementation of an occupant monitoring system (OMS) with an adaptive restraint system was not realized, leaving room for ongoing research and development in this area.

8.2 Demo 2 In-vehicle system for enhanced VRU DETECTION in bad weather conditions.

In preparation for the Demo 2 activities, use cases for car-to-VRU crashes in adverse weather conditions have been identified. Fog was found to be less relevant as it is present in 0-1 % of crashes including VRUs, but precipitation was found to be relevant and use cases with a larger-than-average prevalence of precipitation like rain, snow, hail or sleet were identified. Conflicts with the highest absolute number of crashes with precipitation for pedestrians and bicyclists were selected as the most important test cases. These are the crossing scenario from left without sight obstruction for the pedestrian (AWC-P1: CLwoSO) and the crossing scenario from right for the bicyclist (AWC-B1: B-CR). Hence, test specifications including the VUT speed, the target speed, the VUT path, the target path, as well as the impact location were defined. In addition to those common test specifications, for those scenarios under adverse weather conditions also the friction coefficient, the rain amount, and the rain area size were specified.

The results of the conducted static measurement campaigns for Demo 2 development allow a quantification of the adverse weather influence on the investigated sensors. The weather effect impacts the sensors' performance, and the different characteristics of the sensors are noticeable. The resulting weather-dependent FoV models were used in simulations to assess the influence of different adverse weather conditions. Therefore, scenarios and velocity configurations were selected based on accident statistics and simulations with adapted FoVs and friction coefficients were performed, where generic AEB and AES functions were triggered. Only in the longitudinal scenarios with a high ego velocity (79 kph) a decision was made to select an AES intervention over an AEB intervention. In simulations of certain scenarios and speed configurations accidents occurred due to visual obstruction, decreased sensor performance, and especially reduced friction. Further evaluation is necessary if more performant, state-of-the-art intervention functions also hold a potential for earlier triggering when considering the friction coefficient.

With the third measurement campaign for Demo 2 data was generated to compare the simulative results, where FoV models based on static testing are integrated, with dynamic detection performances in adverse weather conditions. Overall, the detection performance in the dynamic measurement was considerably lower than expected from the results of the simulations. Due to no detection degradation between 0 mm/h and 16 mm/h at the vehicle velocity configuration of 15/16 kph, but an obvious detection degradation between 0 mm/h and 16 mm/h at the vehicle velocity configuration of 35/32 kph, it is assumed that the influence of the rain rate on sensors should not be evaluated independent of the vehicle velocity. However, this effect can also stem to some extent from other limitations, which are summarized in Chapter 5.4. Future work should focus on developing waterproof test equipment and improved rain systems for further dynamic testing and methods for reliable

friction estimation. If progress has been made on those topics, further investigation is necessary for generating realistic sensor models and for virtual testing possibilities.

8.3 Demo 3 Vehicle integrated BRAKING & SWERVING FUNCTIONS to avoid collisions with other vehicles and VRUs.

Both the simulation study results (section 6.1) and the physical testing campaign results (section 6.2) show that AES can provide an additional safety benefit compared to state-of-the-art AEB systems in car vs. crossing VRU accident cases, while considering limitations from the UNECE R79 ESF regulation [26], which only allows in-lane evasion manoeuvres, a limited intervention intensity to ensure controllability by the driver, and VRU perception and prediction uncertainties. Further details of how these limitations are considered in the analysis can be found in the deliverable reports D3.3 [25] and D3.6 [21].

In general, the main advantage of the AES system compared to the AEB system lies in the avoidance of accident cases where the target object becomes visible at a very late point in time, and the crash impact location is given in a way that an in-lane avoidance maneuver is feasible. For the crossing VRU accident cases this leads to an additional safety benefit in cases where:

- the impact location is on the edge of the vehicle's front (impact location = 0 according to definition in section 6.2.1, leading to half of the VRU width overlapping with the vehicle's front) or on the side of the vehicle,

- the VRU velocity is low (~ < 6 km/h),

- the accident can only be detected at a very late point in time, due to:

   o Sight obstructions

   o VRU changing direction to cross the road very abruptly

   o Not ideal environmental conditions (weather, light, ...)

These conditions can be interpreted as general global guidelines for the definition of AES test scenarios, if the AES system is intended to generate an additional safety benefit compared to the AEB system, and given the precondition that an AES system will not be fired if a complete accident avoidance can be achieved with the AEB system.

However, as already discussed in section 6.2, both AEB and AES systems might fail to achieve complete accident avoidance due to perception and prediction uncertainties. In case of the AEB the accident severity reduction effect based on the reduced collision speed can be estimated with existing injury risk functions for frontal impacts. In comparison to that, the AES system might change the impact location from a frontal collision to a side collision. In order to assess the effect of this change on the expected accident severity outcome, injury risk functions for side crash accidents are needed. The effect of the AEB collision speed reduction would then have to be compared against the AES collision impact location change for a final decision of to system to be fired. These side crash injury risk functions are not

available in current state of research. Therefore, future work is needed to provide this knowledge in order to be able to safely deploy AES functionalities.

8.4 Demo 4 Vehicle integrated BRAKING & SWERVING FUNCTIONS to avoid collisions with other vehicles and VRUs.

The safety potential of communication technology could be analysed within SAFE-Up Demo 4, although the assessment could only focus on the activation of active safety systems and not on the provision of timely warnings since the human reaction to these warnings could not be evaluated and should be part of future work.

The test results from SAFE-Up Demo 4 [18] show that communication technology has potential to improve road safety, on obstruction related scenarios where an increased distance at stop to the target could be seen.

However, there are still several challenges that still need to be addressed to improve the maturity level of this technology to make it ready for market introduction, especially when it comes to positioning accuracy, signal integration trough standard procedures and reliability of information. Additionally, Euro NCAP, together with the help of industry shall closely monitor the effectiveness of V2X technology in reducing road accidents, in combination of existing active safety systems. As mentioned before, more data is required to understand its potential benefits. HMI and control systems could be considered for future assessments. Drivers will be provided with real-time information that could be used to help them taking better decisions and avoid accidents. Those studies should also consider user acceptance of the technology, especially when it comes to warnings, since past research has already shown that false system activation results in lower acceptance of the technology [13].

To sum up, considering technology will mature over time, and current State-Of-The-Art focuses on previously mentioned Step 1 approaches (information awareness for local hazard warning), it would be more realistic to consider advanced warnings as a second Step, similarly to what is envisaged in the EC and Car 2 Car consortium roadmaps, leaving system interventions to a further point in time and depending on market penetration.

In terms of timing and Euro NCAP protocol updates, this would mean a first implementation from 2026 based on information awareness for local hazard warning and 2029 for more advanced warnings such as what has been evaluated within SAFE-Up Demo 4. Further system interventions would then relate to later protocol updates.

References

[1] Securing Vehicle-to-Everything (V2X) Communication Platforms Monowar Hasan, Sibin Mohan, Takayuki Shimizu, and Hongsheng Lu

[2] Wang J, Shao Y, Ge Y, Yu R. A Survey of Vehicle to Everything (V2X) Testing. Sensors (Basel). 2019 Jan 15;19(2):334. doi: 10.3390/s19020334. PMID: 30650658; PMCID: PMC6359058.

[3] European Commission. C-ITS Platform. 2017. https://transport.ec.europa.eu/system/files/2017-09/2017-09-c-its-platform-final-report.pdf

[4] Car 2 Car Consortium- Roadmap 2020 https://www.car-2-car.org/fileadmin/downloads/PDFs/roadmap/Roadmap_2020_figure.pdf

[5] Euro NCAP. Vision 2030. https://cdn.euroncap.com/media/74468/euro-ncap-roadmap-vision-2030.pdf

[6] Volkswagen. Car2X. https://www.volkswagen-newsroom.com/en/stories/car2x-in-the-new-golf-a-technological-milestone-5919

7 5GAA. Accelerate the understanding and adoption of VRU protection services enabled by C-V2X. https://5gaa.org/content/uploads/2023/02/5gaa-p-220057-accelerate-the-understanding-and-adoption-of-vru-protection-services-enabled-by-c-v2x.pdf

[8] S. Nikolaou, J. Castells, J. Lorente Mallada, I. Gragkopoulos and I. Tsetsinas, D3.4 Demo 4 (system for on-time warning provisions to VRUs and drivers in critical conditions), SAFE-UP EU Project (861570), 2021.

[9] TRA Demo 4 publication: TRA editors have informed that the public reference won't be available until September.

[10] TOYOTA. V2X for Cooperative Transportation. https://www.toyota.co.jp/its/en/2021/v2x_deployment/

[11] C-ROADS. The C-Roads Platform. https://www.c-roads.eu/fileadmin/user_upload/media/Dokumente/C-Roads_Brochure_2021_final_2.pdf

[12] EURO NCAP. TEST PROTOCOL - AEB/LSS VRU systems . 2023. https://cdn.euroncap.com/media/75436/euro-ncap-aeb-lss-vru-test-protocol-v43.pdf

[13] J. Navarro, J. Deniel, E. Yousfi, C. Jallais, M. Bueno, A. Fort, Influence of lane departure warnings onset and reliability on car drivers' behaviors, Applied Ergonomics, Volume 59, Part A, 2017, Pages 123-131,https://doi.org/10.1016/j.apergo.2016.08.010.

[14] S. Nikolaou, J. Castells, J. Lorente Mallada, I. Gragkopoulos and I. Tsetsinas, "D3.7 Demo 4 (system for on-time warning provisions to VRUs and drivers in critical conditions)," SAFE-UP EU Project (861570), 2022.

[15] L. CORNEC, D. LEDAIN, A. PICK, L. KEMPTON, L. MENIS, ERDEM, N. PULLER y J. RAMMLER, «Deliverable 4.1 - Connected testing tools and environment. SECUR project,» 2023. [En línea]. Available: https://www.utac.com/wp-content/uploads/2023/04/SECUR-D4.1-Connected-testing-tools-and-environment-specifications-v2.pdf.

[16] V. Mannoni, V. Berg, S. Sesia y E. Perraud, «A Comparison of the V2X Communication Systems: ITS-G5 and C-V2X - IEEE Vehicular Technology Conference (VTC),» 2019. [En línea]. Available: https://hal-cea.archives-ouvertes.fr/cea-02183828/file/V2X_VTC19_CameraReady_VM.pdf.

[17] ETSI, «ETSI EN 302 637-2. Intelligent Transport Systems (ITS); Vehicular Communications; Basic Set of Applications; Part 2: Specification of Cooperative Awareness Basic Service,» 2014. [En línea]. Available: https://www.etsi.org/deliver/etsi_en/302600_302699/30263702/01.03.02_60/en_30263702v010302p.pdf.

[18] SAFE-UP. D5.3 Active safety system assessment results. 2023

[19] Balint, A., Labenski, V., Köbe, M., Vogl, C., Stoll, J., Schories, L., … Schindler, R. (2021). D2.6 Use Case Definitions and Initial Safety-Critical Scenarios.

[20] Löffler, C., Vogl, C., Labenski, V., Weihmayr, D., Gloger, T., Schwaderer, T., . . . Koebe, M. (2022). D3.5 Demo 2 Vehicle demonstrator for object detection in adverse weather conditions update.

[21] Löffler, C., Gloger, T., Smit, R., Vogl, C., Tolksdorf, L., Munoz Sanchez, M., . . . Stoll, J. (2022). D3.6 Vehicle demonstrator for trajectory planning and control for combined automatic emergency braking and steering manoeuvres including system for VRU detection, motion planning and trajectory control to enhance real world performance.

[22] Euro NCAP. (2022). Euro NCAP - Test protocol - AEB/LSS VRU systems - Implementation 2023. https://cdn.euroncap.com/media/67888/euro-ncap-aeb-lss-vru-test-protocol-v41.pdf

[23] Park, J., Jeong, H., Jang, I., Hwang, S. (2015). Torque Distribution Algorithm for an Independently Driven Electric Vehicle Using a Fuzzy Control Method

[24] Pohle, M., Erbsmehl, C. (2021). Methodology for addessing the criticality for all driving scenarios

[25] Löffler, C., Gloger. D3.3 Vehicle demonstrator for trajectory planning and control for combined automatic emergency braking and steering manoeuvres including system for VRU detection, motion planning and trajectory control to enhance real world performance.

[26] UNECE. (2018). Regulation No 79 of the Economic Commission for Europe of the United Nations (UN/ECE) — Uniform provisions concerning the approval of vehicles with regard to steering equipment [2018/1947]. UN/ECE Regulation. Opgehaald van http://data.europa.eu/eli/reg/2018/1947/oj

[27] German In-Depth Accident Study. (sd). Opgehaald van https://www.gidas.org

[100] Fryar CD, Gu Q, Ogden CL, Flegal KM. 2016. Anthropometric reference data for children and adults: United States, 2011-2014. National Center for Health Statistics. Vital Health Stat. 3(39):9–15.

[101] Zimmer A, Silva J, Perretto M, Östling M. Deliverable Report 4.3 – Algorithm Development SAFE-UP European Project Horizon 2020. April of 2021.

[102] Östling M. 2021. Deliverable Repot 4.2 – Architecture of passive safety systems. SAFE-UP European Project Horizon 2020, link to publication